Time-Varying Identification of Intrinsic and Reflex Joint Stiffness

Heidi Irene Giesbrecht
Degree of Master of Engineering

Department of Biomedical Engineering
McGill University, Montreal

January, 2007

A thesis submitted to McGill University
in partial fulfilment of the requirements of the degree of
Master of Engineering.

Library and
Archives Canada

Published Heritage
Branch

395 Wellington Street
Ottawa ON K1A 0N4
Canada

Bibliothèque et
Archives Canada

Direction du
Patrimoine de l'édition

395, rue Wellington
Ottawa ON K1A 0N4
Canada

Your file Votre référence
ISBN: 978-0-494-32588-9
Our file Notre référence
ISBN: 978-0-494-32588-9

NOTICE:
The author has granted a non-exclusive license allowing Library and Archives Canada to reproduce, publish, archive, preserve, conserve, communicate to the public by telecommunication or on the Internet, loan, distribute and sell theses worldwide, for commercial or non-commercial purposes, in microform, paper, electronic and/or any other formats.

The author retains copyright ownership and moral rights in this thesis. Neither the thesis nor substantial extracts from it may be printed or otherwise reproduced without the author's permission.

AVIS:
L'auteur a accordé une licence non exclusive permettant à la Bibliothèque et Archives Canada de reproduire, publier, archiver, sauvegarder, conserver, transmettre au public par télécommunication ou par l'Internet, prêter, distribuer et vendre des thèses partout dans le monde, à des fins commerciales ou autres, sur support microforme, papier, électronique et/ou autres formats.

L'auteur conserve la propriété du droit d'auteur et des droits moraux qui protège cette thèse. Ni la thèse ni des extraits substantiels de celle-ci ne doivent être imprimés ou autrement reproduits sans son autorisation.

In compliance with the Canadian Privacy Act some supporting forms may have been removed from this thesis.

While these forms may be included in the document page count, their removal does not represent any loss of content from the thesis.

Conformément à la loi canadienne sur la protection de la vie privée, quelques formulaires secondaires ont été enlevés de cette thèse.

Bien que ces formulaires aient inclus dans la pagination, il n'y aura aucun contenu manquant.

Canada

Abstract

Dynamic joint stiffness is an important property of the neuromuscular system used to control movement and stability of the body. Joint stiffness may be thought of as a combination of two physiological components: an intrinsic component encompassing the mechanical properties of the joint, muscle, and tissues, and a reflex component arising from muscle activation in response to stretch. The functional role of joint stiffness and reflex stiffness, in particular, during movement remains relatively unknown. Current stationary methods for system identification are not applicable, since the system properties are time-varying. This thesis examined time-varying, intrinsic and reflex dynamics of the human ankle joint during movement. A parallel-cascade algorithm was used in conjunction with ensemble techniques to identify joint dynamics as time-varying systems. The algorithm was validated using both simulated and experimental data. Experimental results suggest that reflexes are tonically inhibited, but modulate phasically to adapt to the functional requirements of a movement.

Résumé

La raideur dynamique des articulations est une importante caractéristique du système neuromusculaire qui est utilisé pour contrôler les mouvements et la stabilité du corps. Cette raideur des articulations est une combinaison de deux composantes physiologiques : une composante intrinsèque incluant les propriétés mécaniques de l'articulation, des muscles et des tissus, et une composante réflexe qui est le résultat de l'activation du muscle par son étirement. Les rôles de la raideur des articulations et particulièrement de la raideur réflexe pendant le mouvement restent plus ou moins inconnus. Les méthodes stationnaires courantes pour l'identification de ces systèmes ne conviennent pas puisque les propriétés du système sont instationnaires. Cette thèse a examiné les composantes instationnaires intrinsèques et le réflexe de l'articulation d'une cheville humaine en mouvement. Un algorithme « parallel-cascade » a été utilisé en conjonction avec un ensemble technique pour identifier les mouvements de l'articulation comme un système instationnaire. Cet algorithme fut validé en utilisant des données expérimentales et simulées. Les résultats expérimentaux suggèrent que les réflexes sont inhibés « tonically » et que la modulation physique s'adapte aux demandes fonctionnelles requises pour le mouvement.

Acknowledgements

I would first like to thank my supervisor, Dr. Robert Kearney—his guidance, knowledge and patience gave me the freedom to explore my own ideas and the wisdom to stay on course. Thank you for all the times I came stumbling into your office with a new question.

I would like to thank Mackenzie for initiating this project and offering her insight at the beginning stages of my research. Special thanks to my lab colleague Daniel, who often shed light on seemingly unsolvable problems. Also, thank you Baher and Yong for your supportive words and shared laughs. My gratitude is given to Dr. Ross Wagner for offering his time and expertise to our lab, without you we would all be Lost. I would like to extend my sincere appreciation to the Department of Biomedical Engineering and in particular, Pina Sorrini for her assistance in all things great and small.

Thank you to my family and friends for their love and support, especially during the trying times of this endeavor. Mila, *merci beaucoup!* Mom and dad, you have always encouraged me to open new doors, thank you for believing me capable of great things. Karina, thank you for reminding me to take time in life for laughter. And finally, thank you to my husband, Alex whose endless encouragement is the unwritten chapter of this thesis.

This work was supported by funding provided by the Natural Sciences and Engineering Research Council of Canada (NSERC) and the Canadian Institutes of Health Research (CIHR).

Contribution of Authors

The TVPC algorithm described in Chapter 4 was developed by my predecessor, Mackenzie Baker as the topic of her thesis. The ensemble methods used in the algorithm were developed by Dr. M. Lortie and Dr. R. Kearney. I contributed toward improving this algorithm by modifying the way in which three items are computed: intrinsic compliance, reflex gain, and total torque. The simulation scheme was also developed by Mackenzie, although I made substantial modifications to improve the simulations for realistic conditions. I devised the stationary experimental paradigm to validate the TVPC algorithm's ability to predict intrinsic and reflex dynamics using real data and carried out the experiments. My lab colleague, Daniel Ludvig and Dr. Ross Wagner were helpful in troubleshooting many experimental hurdles I encountered. Finally, I wrote the manuscript with substantial feedback from my supervisor, Dr. Kearney.

I also devised the experimental paradigm for Chapters 5 and 6 with the guidance and suggestions of Daniel and Dr. Kearney. I performed the experiments and then prepared the manuscripts with the assistance of my supervisor.

Table of Contents

List of Figures

List of Tables

1 Introduction

A polished ballet dancer will move with such control and grace that it is easy to forget that the origin of these movements involves the coordinated action of rigid bone, muscle and nerves. Even the smallest movements involve complex interactions between the dancer's brain and body. The combination of the nervous system and muscles working together to control movement is known as the neuromuscular system. The neuromuscular system receives information from multiple sources, including motor commands from the brain (instructing the dancer to *plié* or rise *en pointe*) and feedback from the peripheral sensory systems (signaling the amount of tension or stretch in the muscles). This information is integrated to form a motor program, which guides the dancer's movement and posture.

The study of neuromuscular control will provide a greater understanding of able-bodied as well as impaired movement. Research in this field can advance a variety of clinical and industrial challenges, including methods of rehabilitation, the design of prosthetics, robotics and man-machine interfaces.

1.1 DYNAMIC JOINT STIFFNESS

The mechanical behaviour of a joint can be described by a quantity known as dynamic stiffness. Dynamic joint stiffness quantifies the relationship between the position of a joint and the torques acting about it. It is an important feature of the motor control system that provides movement and stability of the body. Joint stiffness may be thought of as a combination of two physiological components [1]:

1. An intrinsic component, arising from the mechanical properties of the joint, active muscle and passive, visco-elastic tissues surrounding the joint.
2. A reflex component, resulting from the muscle activation in response to a stretch (stretch reflex).

The role of joint stiffness and particularly, the role of reflex stiffness in posture and movement remain relatively unknown. One of the major difficulties in determining the functional significance of stretch reflexes is distinguishing reflex activity from the intrinsic properties of the joint and muscle. Our lab developed a parallel-cascade, nonlinear system identification algorithm to separate intrinsic and reflex contributions to dynamic ankle stiffness [2]. Angular position and torque are related via two parallel pathways, where the intrinsic pathway is modelled as a linear dynamic element and the reflex pathway is modelled as a static non-linearity in series with a linear dynamic element. The technique was used to examine both able-bodied and spastic, spinal cord injured (SCI) subjects during a variety of postural conditions [1, 3, 4].

1.2 SYSTEM IDENTIFICATION DURING MOVEMENT

More complex methods are required to examine a joint during movement. The techniques developed to examine joint dynamics during postural conditions are not applicable, since the system dynamics change with the movement. It is known that intrinsic and reflex stiffness change, however, these changes are difficult to characterize because they occur rapidly and therefore require time-varying identification techniques. Our lab developed separate time-varying techniques to identify intrinsic and reflex dynamics during rapid movements [5-7]. These techniques use an ensemble of input-output data acquired during experiments in which a subject's ankle is rotated by an electrohydraulic actuator. Estimates of intrinsic and reflex stiffness are generated by cross-correlating the input and output at each time point across the ensemble to produce an instantaneous description of the system dynamics. Recently, the time-varying techniques were combined with the parallel-cascade algorithm to permit the simultaneous analysis of intrinsic and reflex mechanisms during rapid imposed movements about the ankle joint [8]. Preliminary steps were taken to validate the algorithm and show its ability to work under simulated and experimental conditions.

The overall goal of this thesis was to use the time-varying, parallel-cascade (TVPC) algorithm to examine the functional role of joint stiffness and stretch reflexes during movement. The first objective was to improve the existing implementation of the TVPC algorithm for the analysis of intrinsic and reflex dynamics. The second objective was to validate the algorithm's performance under realistic conditions by conducting both a simulation and experimental study. The simulation study used parametric approximations for intrinsic and reflex dynamics to simulate time-varying systems. Pseudo-random binary sequences (PRBS) were used as the input ensemble and convolved with the simulated systems to generate an ensemble of output torque. TVPC identification was performed on the input-output data to produce system estimates; these estimates were compared with the simulated systems. The experimental study was conducted under stationary conditions where the subject's ankle was continuously perturbed with a PRBS about a fixed operation position. Time-varying estimates of intrinsic and reflex dynamics were averaged and compared with those computed using an established time-invariant algorithm. The final objective was to explore the time-varying properties of a subject's ankle during two imposed movements: (1) a gait cycle similar to 1.5 km/hr walking speed, and (2) a cyclic, smooth-ramp sequence, in which the subject's ankle underwent a rapid stretch of the triceps surae, followed by a pause, then a return stretch of the tibialis anterior, followed by a pause.

1.3 THESIS OUTLINE

This thesis is composed of seven chapters. Following this introductory chapter, is a background chapter that describes the peripheral neuromuscular system, including motor neurons, skeletal muscle physiology, the peripheral sensory systems and stretch reflexes. An extensive review of previous studies in dynamic joint stiffness is also included in this chapter as well as a review of the system identification methods used to analyze ankle joint dynamics. Chapter 3 examines our experimental methods, describing in detail the electrohydraulic actuator, sensors for detecting position, torque and EMG, experimental control and data acquisition. Chapter 4 is in the form of a manuscript, which presents the time-varying, parallel-cascade algorithm and summarizes the results from simulation and stationary experimental studies. Chapters 5 and 6 are also in manuscript form. These chapters apply the TVPC algorithm to examine joint dynamics during two imposed movements: a gait cycle and a cyclic, smooth-ramp. The modulation of stretch reflexes is examined in particular detail and compared with similar movement studies. The final chapter gives a brief summary of the conclusions reached from each of the manuscripts and offers suggestions for future work.

2 Background

2.1 ANATOMY OF THE ANKLE JOINT

The talocrural joint, commonly known as the ankle joint, is a complex mechanism consisting of bone, cartilage, muscle, and passive tissues (tendons and ligaments). Figure 1 illustrates the anterior and posterior musculature of the ankle joint and lower leg. Three major bones comprise the joint: the distal ends of the tibia and fibula, and the trochlea of the talus. The distal ends of the tibia and fibula, known as the medial and lateral malleolus respectively, articulate with the trochlea of the talus to form a ginglymus, or hinge-joint. The joint is free to move in a single plane, resulting in plantar flexion and dorsiflexion. Plantar flexion occurs when the toes are pointed away from the body. This is accomplished by contracting the triceps surae muscle group consisting of the gastrocnemius and soleus. The gastrocnemius muscle originates at the femoral condyles and the soleus originates at the proximal end of the fibula and a portion of the medial tibia; both insert on the calcaneus bone of the foot via the achilles tendon. Dorsiflexion involves bringing the foot toward the anterior surface of the leg, which is accomplished by contracting the tibialis anterior muscle. This muscle originates at the lateral condyle of the tibia and inserts at the medial and plantar surface of the first metatarsal. Two groups of ligaments support the talocrural joint: the lateral collateral and medial collateral ligaments.

In addition to plantar and dorsiflexion, the foot is capable of moving in the transverse plane by the action of the subtalar joint. This is a synovial joint comprised of the heel (calcaneus) and the talus, which are connected by the talocalcaneal interosseous ligament. Movement of the subtalar joint produces heel inversion and eversion movements. Because the gastrocnemius and soleus attach distal to the talus, contraction of these muscles also produces motion of the subtalar joint.

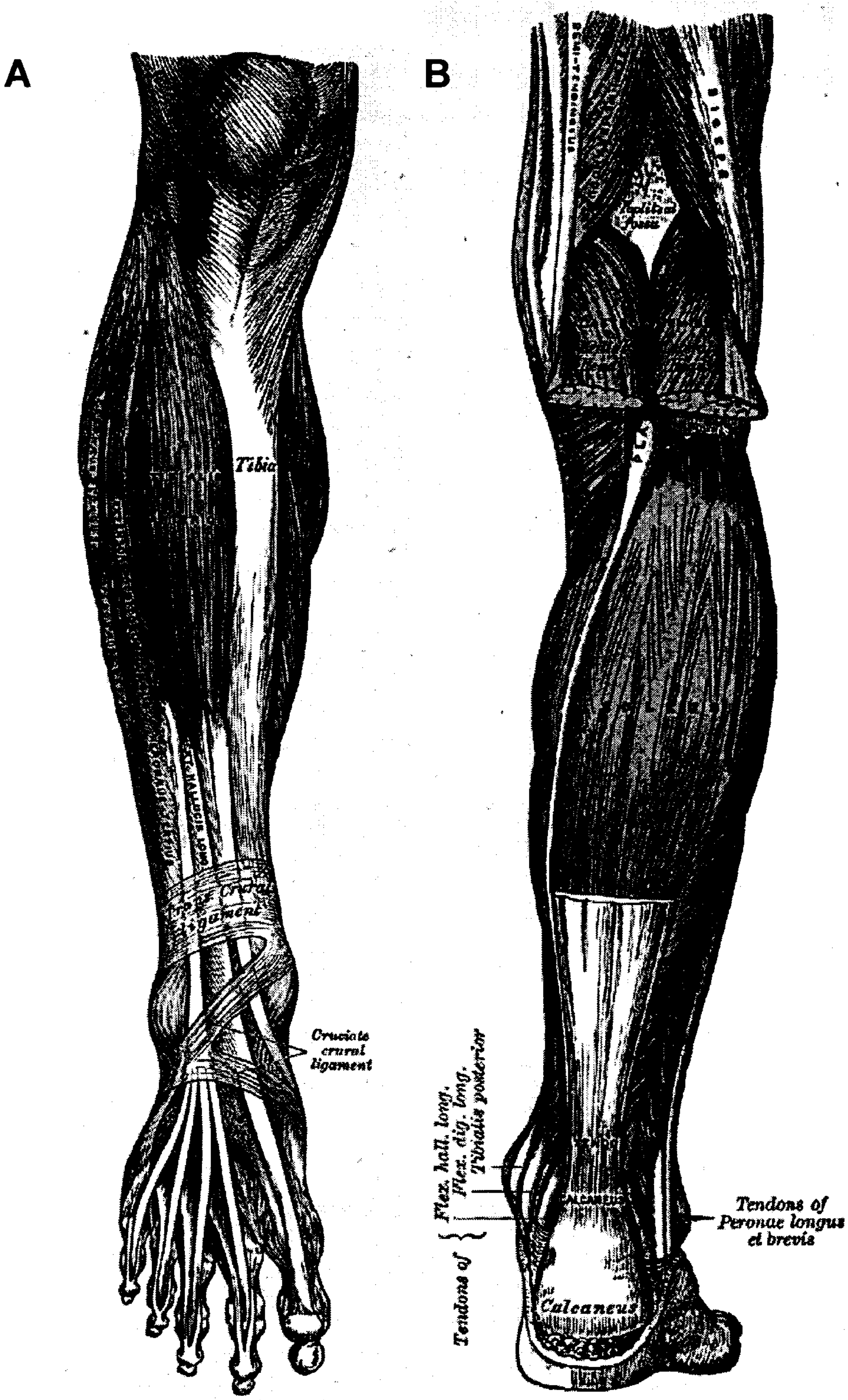

Figure 1: (A) Anterior and (B) posterior muscles of the lower leg and ankle. The gastrocnemius and soleus comprise the triceps surae, which causes plantar flexion, while the tibialis anterior causes dorsiflexion. Adapted from [9].

2.2 FUNCTION OF THE ANKLE JOINT

The ankle participates in movement and stability of the body through the action of dorsi- and plantar flexion. Running, walking and quite standing all require co-activating or alternating contractions of the triceps surae and tibialis anterior muscle groups. Running and walking are initiated by allowing the body's center of gravity to fall forward into an unstable position and then propelling one foot forward to provide support. Quiet standing is maintained by small, precise contractions of the leg muscles that are mediated by feedback from the visual, vestibular and neuromuscular systems.

2.2.1 Gait

During gait, dorsiflexion causes the foot to contact the ground at heel-strike and subsequently ensures a stable ankle position during midstance, when the lower limb supports the weight of the torso. Plantar flexion then elevates the heel, causing the toes to contact the ground. This motion provides the propulsive force that lifts the leg off the ground and initiates swing during the toe-off portion of gait. Dorsiflexion then ensures that the foot clears the ground during the swing phase. The complete range of motion (ROM) of the ankle joint varies in different individuals, but typically extends from 50° plantar flexion to 20° dorsiflexion. The ROM used during gait is typically one-third to one-half of the full ROM [10].

2.3 PERIPHERAL NEUROMUSCULAR SYSTEM

The nervous system may be divided into two parts: the central nervous system (CNS), composed of the brain and spinal cord and the peripheral nervous system (PNS), consisting of the nerves that extend between the brain or spinal cord and the body's muscles, glands and sense organs [11]. The peripheral nervous system can be further subdivided into efferent and afferent divisions. Afferent neurons carry information from sensory organs to the CNS, while efferent neurons carry information from the CNS to muscles or glands. Efferent neurons are classified as autonomic or somatic. Autonomic neurons innervate smooth and cardiac muscle, glands, and the gastrointestinal tract. Neurons of the somatic division are motor neurons that innervate skeletal muscle. All motor neurons are excitatory, meaning they stimulate muscle tissue to contract; muscle relaxation is accomplished by inhibiting motor neurons.

2.3.1 Motor Neurons and Motor Units

Skeletal muscle is activated by somatic efferent nerves referred to as motor neurons (Figure 2-A). The cell bodies of these neurons are located in the brainstem or ventral horn of the spinal cord, but their axons can extend well beyond one meter [12]. The motor neuron is referred to as the "final common pathway" of the central nervous system since all central commands and sensory feedback converge at this junction to control muscle contraction. Each muscle fibre is controlled by only one motor neuron, but each motor neuron typically innervates many muscle fibres. The motor neuron and muscle fibres it innervates are referred to as a motor unit (Figure 2-B). The collection of motor neurons that control a given muscle make up its motor neuron pool [11]. The following section describes in more detail the chemical events required to initiate muscle contractions by motor neurons.

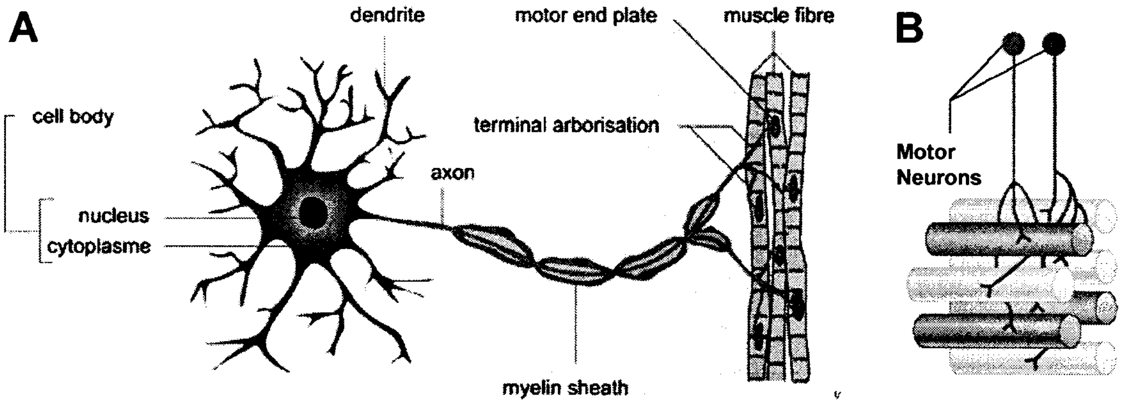

Figure 2: (A) Motor neuron and (B) motor units. Each muscle fibre is controlled by only one motor neuron, but a single motor neuron typically innervates many muscle fibres. Adapted from [13] and [11].

2.3.2 Neuromuscular Junction

When an excitation signal travels along a motor neuron, all the associated muscle fibres are stimulated to contract. This signal is referred to as an action potential (AP). Action potentials propagate along motor neurons at high velocities due to the large diameter, myelinated axons of motor neurons. The terminal end of a motor neuron is composed of vesicles that contain a neurotransmitter called acetylcholine (ACh). The region of the muscle fibre that lies directly below the axon terminal is referred to as the motor end plate and the junction between the axon terminal and motor end plate is called the neuromuscular junction (shown in Figure 3). The process by which an AP propagates along a motor neuron and subsequently activates the muscle fibres involves a sequence of chemical events summarized as follows: when an AP arrives at the axon terminal, it depolarizes the plasma membrane of the neuron; this opens voltage-sensitive channels that allow calcium ions to diffuse into the axon terminal from the extracellular fluid surrounding the neuron. The calcium ions bind to proteins that cause ACh containing vesicles to release into the neuromuscular junction. ACh diffuses to the motor end plate where it binds with receptors that open ion channels at the motor end plate. This allows sodium and potassium ions to flow rapidly through the channels resulting in an electro-chemical gradient across the plasma membrane. The electro-chemical gradient produces a local depolarization of the motor end plate (referred to as an end-plate potential, or EPP). A single EPP is normally sufficient to depolarize the entire fibre membrane, enough to initiate an action potential that propagates in both directions over the surface of the muscle fibre causing the muscle to contract [11].

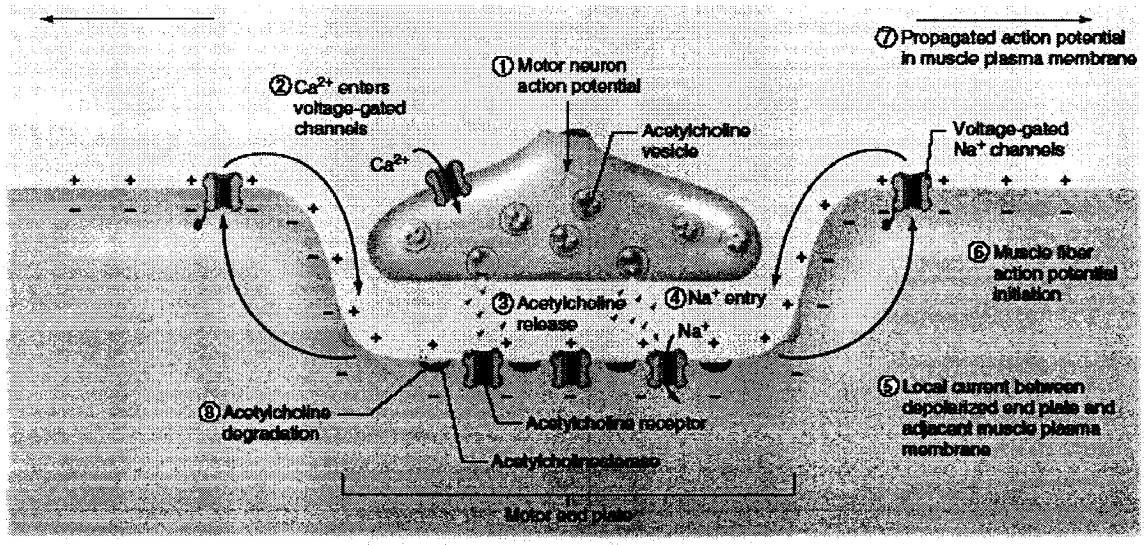

Figure 3: Neuromuscular junction depicting the electro-chemical events leading a contraction of a muscle fibre. Adapted from [11].

2.3.3 Skeletal Muscle Physiology

A single skeletal muscle cell, or muscle fibre, ranges in diameter from 10-100μm. The fibres are organized in cylindrical bundles, joined together by connective tissue, to form a muscle. Muscles are then linked to bone via tendons (bundles of collagen fibres). An illustrated cross-section of the biceps muscle is shown in Figure 4. Some muscle fibres extend the entire length of the muscle (up to 20cm), but typically fibres are shorter and oriented at an angle to the muscle axis. A single muscle fibre consists of cylindrically arranged myofibrils (1-2μm diameter), which have a distinct striated pattern perpendicular to the muscle axis. This pattern is due to the arrangement of thick and thin filament bundles within a myofibril. The thick filaments are roughly 15nm in diameter and primarily consist of the contractile protein myosin. Myosin molecules have a long tail portion and two globular heads which contain binding sites for the thin filament contractile protein, actin. The thin filaments are half the diameter of thick filaments and primarily consist of actin, but have additional proteins troponin and tropomyosin [11].

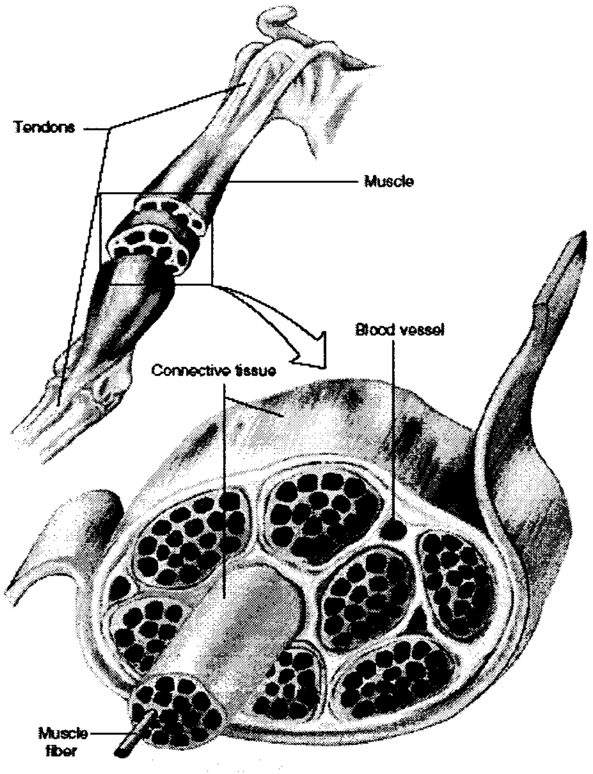

Figure 4: Skeletal muscle fibres arranged as cylindrical bundles bound together by connective tissue. Muscle is linked to bone via collagen fibres known as tendons. Adapted from [11].

A sarcomere is the repeating pattern of a myofibril that is the basic functional unit of skeletal muscle. Each sarcomere contains two sets of thin and one thick filament. The thick filaments are located in the middle of the unit to form the dark A band (refer to Figure 5). Thin filaments run parallel and overlap the thick filaments; the sections that do not overlap the thick filaments form the light I band. Thin filaments of two adjacent sarcomeres are anchored together by interconnecting proteins at the Z line, which marks the division of two sarcomeres. The overlapping sections of thin and thick filaments are linked by the globular heads of myosin, referred to as cross-bridges. The cross-bridges extend toward the thin filaments ready to bind to actin; however, at rest the thin filament protein, troponin, holds tropomyosin in a configuration such that it blocks the binding sites on actin. As we will see in the next section, a chemical change in calcium concentration is required to initiate myosin-actin binding [11, 12].

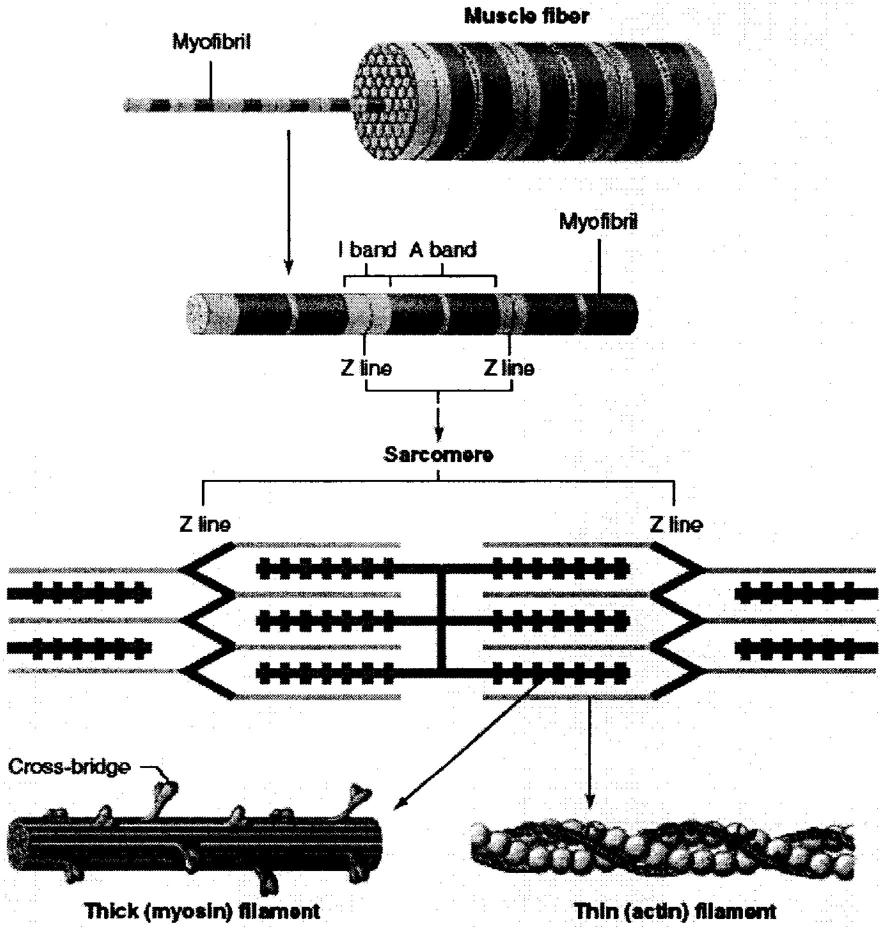

Figure 5: Muscle fibres form a distinct striated pattern as a result of the alternating thin and think filaments in myofibrils. A sarcomere is the basic functional unit of a muscle fibre. Adapted from [11].

2.3.3.1 Sliding-Filament Mechanism

The ability of a muscle to generate force depends on the interaction between thick and thin filaments, known as the sliding-filament mechanism. When a muscle contracts, the cross-bridges on myosin bind to actin and move in an arc-like motion to slide the thin filament relative to the thick filament. The cross-bridges successively bind to neighbouring sites on actin and pull the filament toward the center of the sarcomere. During this process, both the thin and thick filaments retain their original length, but the relative distance between the Z lines decreases as illustrated in Figure 6.

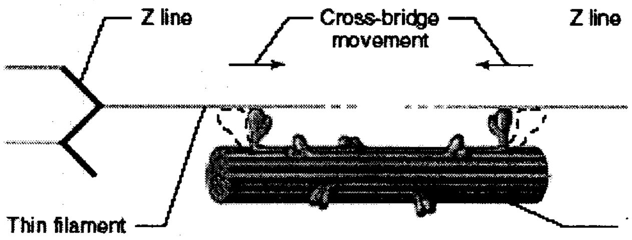

Figure 6: The sliding-filament mechanism describes the process by which muscles generate force. Successive cross-bridge binding pulls the thin filaments relative to the thick, resulting in a contraction of the muscle fibre. Z lines move closer together, while the filaments retain their original shape. Adapted from [11].

Each cross-bridge cycle in this mechanism can be summarized as a sequence of four events [12]:

1. The cycle begins as an action potential (AP) propagates along a motor neuron and reaches a muscle fibre. This causes a membrane excitation that rapidly elevates the concentration of calcium in the fibre cytoplasm. Calcium then binds to the thin filament protein troponin, which produces a conformational change that drags tropomyosin away to expose the myosin binding sites on actin. The rise in calcium in response to a single AP is normally enough to saturate troponin and expose all actin binding sites available for cross-bridging. Energized cross-bridges on myosin then bind to the thin filament actin.
2. This spontaneously initiates the second stage, or power stroke, of the cycle where the potential energy stored in the cross-bridges results in a translational movement of the cross-bridges and adjoining thin filament. At this stage, myosin is tightly bound to actin and the link must be broken in order for the cross-bridge to re-energize and the cycle repeat.

3. In the third stage, ATP binds to myosin which breaks the link between the cross-bridges and actin.
4. The final step re-energizes the cross-bridges by ATP hydrolysis, which also reorients the myosin heads in preparation for the next cross-bridge cycle. Relaxation of the muscle occurs when the calcium-ion concentration decreases, which turns off the contractile cross-bridge cycle. However, this process takes time since the calcium ions must be pumped back into the resting reservoir, and thus relaxation is slower than activation.

2.3.4 Skeletal Muscle Contraction Mechanics

Muscles produce tension in response to a load; to generate movement, the tension in the muscle must exceed the load imposed on it. If a muscle generates tension but does not shorten or lengthen, the contraction is said to be isometric or constant length. Similarly, if the load remains constant while the muscle shortens, the contraction is said to be isotonic or constant tension. Lengthening contractions are called eccentric and only occur when the load on the muscle exceeds the tension generated by the cross-bridges within the muscle fibres. The overall tension produced by a muscle is a function of several variables: (1) the initial length of the muscle fibres, (2) the frequency at which the fibres are stimulated, and (3) the number of fibres actively contracting. In the following sections we will see how each of these variables affects muscle tension [11].

2.3.4.1 Length-Tension Relation

A muscle is capable of producing the largest isometric tension when the fibres within the muscle are at the optimal length, l_o. Typically, when muscles are relaxed the fibres are near l_o. The relationship between fibre length and tension can be explained by recalling the sliding filament mechanism (refer to Figure 7). Shortening and lengthening involve sliding thin filaments past thick ones. Stretching a fibre past $1.75l_o$ results in zero overlap between the filaments; consequently, the cross-bridges can not bind with actin and tension can not be generated within the muscle. Alternatively, the greatest amount of overlap between filaments occurs at l_o, resulting in maximal tension in the muscle. However, shortening past l_o once again reduces tension because thin filaments from opposite ends of the sarcomere tend to overlap and interfere with cross-bridge binding. In the extreme case of very short lengths, the Z lines of adjacent sarcomeres collide with the thick filaments, resisting further shortening [11].

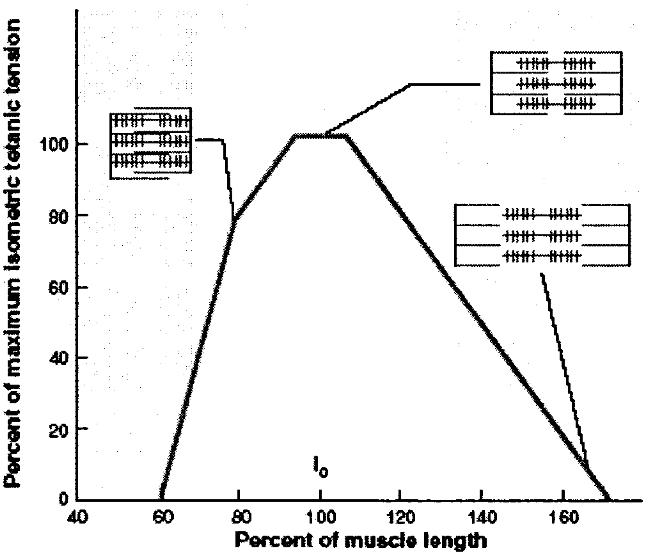

Figure 7: Length-tension relation for generating muscle force. Maximal force is generated when the thin and thick filaments have the most overlap (l_0). At long muscle lengths, there is no overlap between the filaments; at short lengths, adjacent thin filaments interfere with cross-bridge binding. Adapted from [11].

2.3.4.2 Summation (Rate-encoding)

Muscle fibres contract as a result of excitation by action potentials travelling along motor neurons. The response of a muscle fibre to a single action potential is referred to as a twitch and can last up to 100ms. Successive action potentials arriving during the twitch response increase the overall tension developed in the muscle fibre. This process, known as summation, will increase tension until a sustained contraction known as fused tetanus is achieved as illustrated in Figure 8. Fused tetanus is typically three to five times greater than the tension from a single twitch. The physicochemical explanation for summation relates to the number of cross-bridges bound to actin: as AP firing rate increases, the concentration of calcium in the fibre remains elevated, which maximizes the cross-bridges available to bind to actin. At lower stimulation frequencies, the successive action potentials result in smaller, oscillating contractions called unfused tetanus. Therefore it is possible to adjust the amount of tension in the muscle by adjusting the firing frequency of action potentials. This process is known as rate-encoding [11, 12].

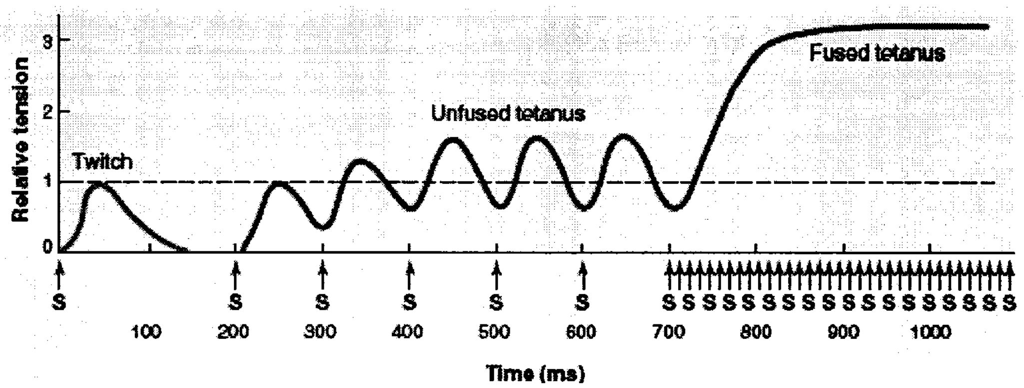

Figure 8: Rate-encoding action potentials can lead to unfused tetanus (low frequency firing) or fused tetanus (high frequency firing). The response to a single AP is known as a twitch. Adapted from [11].

2.3.4.3 Recruitment

Muscle force depends on the tension developed in each fibre (discussed above) as well as the number of fibres contracting at a given time. The number of contracting fibres further varies with the number of active motor units and their respective size. Small motor units have a small motor neuron and are composed of only a few muscle fibres. Their threshold for activation is also lower than a large motor unit with many associated fibres. Motor units are selectively activated according to the size principle (Figure 9): the smallest motor units are recruited first, followed by progressively larger units as the demand for muscle force increases. By activating small motor units first, the muscle tension can be increased in small steps and fine precision achieved (e.g. writing or typing). In fact, recruitment is the primary means of varying tension and velocity in muscles, since the maximum tension achieved by a tetanic contraction is only three to five times that of a twitch contraction [11].

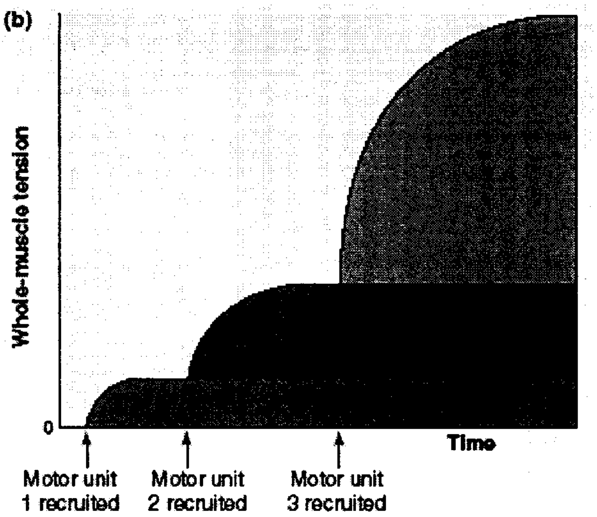

Figure 9: Successive recruitment of motor units is the primary means of adjusting muscle tension. Small motor units that generate small amounts of tension are activated first, followed by larger ones. Adapted from [11].

2.3.5 Peripheral Sensory Receptors

At this point, we have closely examined one division of the peripheral nervous system referred to as the efferent pathway; this pathway delivers motor commands from the CNS to the muscle fibres via motor neurons. The other component of the PNS, referred to as the afferent pathway, carries information about the external and homeostatic environment to the CNS from the various sensory modalities within the body. The ability to sense our body position in space and its parts relative to one another is termed proprioception and is unlike the exteroception senses (i.e. sight, taste, touch, smell, hearing, and balance) that advise us of the outside world. Proprioceptors provide feedback solely on the internal status of the body by way of afferent neurons that monitor length and tension of skeletal muscle, tendons and movement of joints. This information is delivered to the CNS where neurons in the middle levels of the brain integrate with command signals to create a motor program. In essence, the sensory information provides feedback to the command centres, which contributes to an awareness of limb and body position. The two primary sensory organs of the neuromuscular system are muscle spindles and Golgi tendon organs (GTO) [11, 12].

2.3.5.1 Muscle Spindles (Length-monitoring)

Muscle spindles are encapsulated sensory organs located in muscle tissue that range from 4 to 10mm in length [12]. The spindles consist of three primary components shown in Figure 10: (1) peripheral sensory endings, called stretch receptors, which sense change in muscle length and velocity, (2) afferent nerve fibres, which direct information from the receptors to the CNS, and (3) intrafusal muscle fibres upon which the nerve fibres wrap around in a helical fashion. The intrafusal fibres only function as a conduit for the stretch receptors and are separate from the skeletal muscle fibres that generate force and movement, called extrafusal fibres. The intrafusal fibres are arranged in parallel with the extrafusal fibres. There are three types of intrafusal fibres, each with a unique set of mechanical and contractile properties: dynamic nuclear bag, static nuclear bag and nuclear chain fibres [12].

Muscle spindles monitor the length and velocity of a muscle by means of two kinds of sensory nerves: primary afferents (Group Ia) and secondary afferents (Group II). The primary afferents wrap around all three types of intrafusal fibres, whereas secondary afferents wrap around only static nuclear bag and nuclear chain fibres. Primary and secondary afferents exhibit similar high-pass dynamic characteristics with an identical 2 Hz break frequency; however, the absolute sensitivity of the secondary afferent is an order of magnitude lower [14]. In other words, at low frequencies both afferents react to the static change in muscle length and at higher frequencies the response increases with velocity. In addition, Group Ia afferents are more sensitive to acceleration at high frequencies and small length changes.

Group II fibres synapse with motor neurons via interneurons, whereas Group Ia fibres synapse directly with the alpha motor neurons to activate extrafusal fibres as in the case of the stretch reflex (Section 2.3.6). The muscle spindles are aligned parallel to the extrafusal fibres, so a stretch of the muscle also pulls on the intrafusal fibres; this activates the receptor endings. But what happens to the intrafusal fibres when the muscle shortens? In this case, fusimotor innervation maintains the spindle sensitivity by offsetting the spindle fibres, which enables the spindles to encode decreases in muscle length.

Fusimotor innervation involves efferent fibres called gamma motor neurons, which carry signals from the CNS (spinal cord) to innervate the spindle's intrafusal fibres. Gamma motor neurons stimulate the two ends of the intrafusal fibres to shorten and thus maintain tension in the central region where the receptors are located. Research suggests that intrafusal fibres are co-contracted with extrafusal fibres to ensure information about muscle length is continuously available; this process is referred to as alpha-gamma coactivation [11].

Fusimotor innervation alters the sensitivity of the muscle spindles in two ways: (1) dynamic gamma activity enhances the firing of Group Ia afferents in response to stretch velocity by activating dynamic nuclear bag fibres, and (2) static gamma activity enhances the steady-state discharge of both Group Ia and II afferents by activating both nuclear bag and chain fibres [14]. In effect, gamma activity adjusts the dynamic characteristics (either gain or offset) of the spindle afferents by selectively innervating different intrafusal fibres.

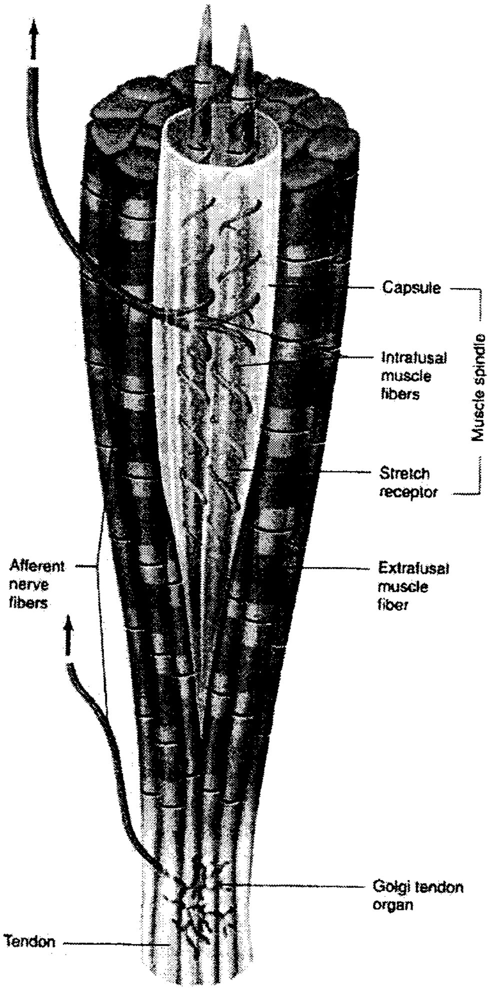

Figure 10: Muscle spindles and Golgi tendon organs. Spindle afferents wrap around intrafusal muscle fibres and lie in parallel with the extrafusal fibres. Spindle receptors sense changes in length and velocity. Golgi tendon organs are located at the muscle-tendon junction and lie in series with the extrafusal fibres to monitor the tension in the muscle. Adapted from [11].

2.3.5.2 Golgi Tendon Organs (Tension-monitoring)

Golgi tendon organs are small sensory capsules about 1mm long and 0.1mm in diameter that are located in the junction between muscle and tendon fibres [12]. Tendon organs are arranged in series with the extrafusal muscle fibres and primarily detect changes in muscle tension. Golgi tendon receptors are more sensitive to active rather than passive muscle tension due to the series arrangement of the tendon organs [14]. Figure 10 illustrates the arrangement of GTOs in relation to the intrafusal and extrafusal muscle fibres.

Golgi tendon organs are composed of collagen fibres, afferent nerves and sensory receptors. Collagen fibres, arising from the muscle tendon, branch into a network of fine fascicles in which the sensory receptors are entwined; the entire structure is encapsulated by a shell of connective tissue and innervated by a single Group Ib afferent fibre. When tension is generated within the muscle as a result of muscle contraction, the tendon organ is stretched. This distorts the collagen fibres and consequently activates the receptor endings. The afferent nerve (Group Ib) then transmits action potentials to the CNS, which in turn causes inhibition of the contracting muscle via interneurons in the spinal cord. The activation of GTOs also has the effect of stimulating motor neurons of the antagonistic muscles [11].

The different functional roles of muscle spindles and GTOs provide the CNS with information about muscle length, velocity and tension in order to modify ongoing motor programs. The sensory systems also aids in protecting the body against movements that could potentially cause harm. This topic is further explained in the following section dealing with peripheral reflexes.

2.3.6 Peripheral Reflexes

Almost all motor behaviour involves both voluntary and involuntary actions. Reflexes are involuntary actions that aid in movement, posture and act as protective mechanisms. For example, the withdrawal reflex is the body's response to a painful stimulus on a limb. If you were to accidentally step on a thumb tack, the reflex mechanism would activate motor neurons of the flexor leg muscles to pull away from the stimulus, while simultaneously inhibiting the extensor muscles to aid in this process. The crossed-extensor reflex would then activate extensor motor neurons and inhibit flexors of the opposite leg so the body would remain stable while retracting from the stimulus [11]. This reflex pathway involves many interconnecting synapses as well as interneurons for inhibition. One fundamental reflex pertaining to movement, called the stretch reflex, involves only one synapse, which we will examine here in more detail.

2.3.6.1 Stretch Reflex

The stretch reflex is an important mechanism used by the body to maintain posture, balance and aid movement. The reflex arc is monosynaptic meaning there is a direct connection between the afferent signal from the muscle spindle and the motor neuron that innervates the same muscle. All other reflexes are poly-synaptic, requiring at least one interneuron between the afferent and efferent pathway.

The traditional knee-jerk is an excellent example of the stretch reflex in action. As the examiner taps the patellar tendon, the tendon stretches and so does the connecting quadriceps muscle. This activates the stretch receptors of the quadriceps, which sends action potentials along the afferent nerve fibre. The signal travels directly to the spinal cord where it synapses with motor neurons. This activates motor units of the quadriceps, resulting in a contraction and extension of the lower leg. A delay is present due to the time it takes for action potentials to propagate along the afferent-efferent pathway; in the case of the gastrocnemius-soleus, the reflex delay is approximately 40 ms [15]. The stretch reflex arc is represented as Path A of Figure 11 below. In Path B, afferent nerve fibres branch off to synapse with interneurons, which inhibit motor neurons controlling antagonistic muscles. The purpose of this is to prevent the antagonistic muscles from interfering with the reflex response. The process of activating one muscle group and simultaneously inhibiting the opposing muscles, called reciprocal innervation, occurs in many movements. Path C of Figure 11 illustrates synergistic activation of muscles that would assist with the intended motion. Path D shows how branches of the afferent neuron go to the brainstem to synapse with interneurons that convey information about muscle length to the motor control areas of brain [11].

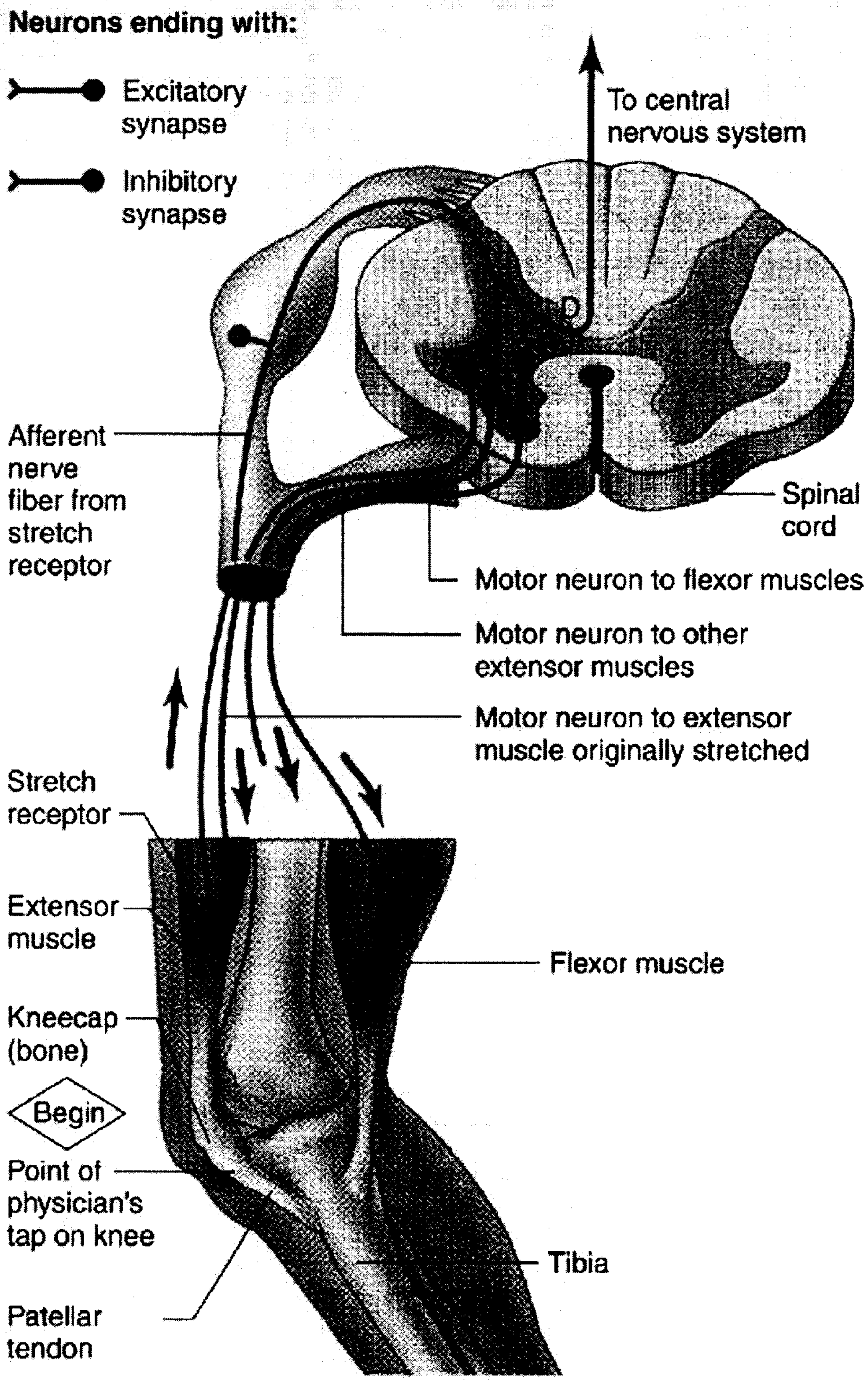

Figure 11: Path A illustrates the monosynaptic stretch reflex, which conveys information from muscle spindles directly to motor neurons of the same muscle. **Path B** and **C** represent reciprocal inhibition and synergistic activation, respectively. **Path D** illustrates the connection to the brainstem. Adapted from [11].

2.3.6.2 Electromyography (EMG)

EMG is a technique used to monitor the electrical activity associated with muscle contraction. It is often used in motor control studies as a measurement of voluntary muscle activation or the stretch reflex response. Muscle activity is easily detected using EMG by applying an electrode to the skin surface. As the muscle contracts, a wave of action potentials propagate along the muscle fibre membrane through the action of membrane depolarization. The spatial-temporal summation of these action potentials gives rise to a voltage signal measurable at the skin surface.

Alternatively, it is possible to measure the activity from a single motor unit using an invasive, indwelling electrode. The combination of all muscle fibre action potentials corresponding to a single motor unit is termed motor unit action potential (MUAP). The amplitude and shape of an MUAP is a function of the geometrical properties of the motor unit, muscle tissue and electrode [16]. A typical muscle contraction involves multiple motor units (i.e. MUAPs), each firing asynchronously.

The EMG signal can be analyzed in the time or frequency domain. Frequency analysis commonly uses Fast Fourier transform techniques to obtain the power density spectrum of the signal. Time domain analysis examines the response, by ensemble averaging the rectified EMG signal. For example, in an EMG trace the stretch reflex appears as a burst of activity at a latency equal to the reflex delay. The magnitude of the stretch reflex is determined by first aligning several responses to stretch onset, then computing the ensemble average amplitude between 40 and 400 ms [16].

In general, EMG is a valuable means of examining reflexes, but can not be used to evaluate the mechanical significance of stretch reflexes since a universal relationship between EMG and muscle force remains unknown [17].

2.4 DYNAMIC JOINT STIFFNESS

The study of dynamics examines motion under the action of forces. This branch of mechanics may be used to evaluate the functional behaviour of a joint by computing its dynamic stiffness. Dynamic joint stiffness quantifies the relationship between the position of a joint and the torques acting about it. It is an important characteristic of the motor control system used to determine the forces required to execute a voluntary movement or alternatively, to govern the displacement resulting from an external perturbation [18]. The design of limb prostheses, orthoses, and development of man-machine interfaces will all benefit from a clear understanding of the function and origin of joint stiffness. Furthermore, it will provide a quantitative means to evaluate the progression and rehabilitation of neuromuscular diseases. Joint stiffness can be thought of as a combination of two physiological components [1]:

1. An intrinsic component, arising from the mechanical properties of the joint, active muscle and passive, visco-elastic tissues surrounding the joint.
2. A reflex component, resulting from the muscle activation in response to a stretch (stretch reflex).

The role of joint stiffness and particularly, the role of reflex stiffness in posture and movement is an ongoing topic of debate [19, 20]. Researchers over the past several decades have postulated a variety of theories as to the functional significance of joint stiffness. One theory maintains that a central pattern generator (CPG) controls the timing and sequence of muscle activation [21, 22]; in this sense, variations in joint stiffness occur as a result of movement. Alternatively, researchers believe that descending pathways regulate peripheral mechanisms as the primary means of executing movement [23, 24]; in other words, joint stiffness is actively modulated to control movement. The true nature of motor control is more likely a combination of these two contrasting philosophies.

The following section explores previous research in joint dynamics. Section 2.5 then examines the specific system identification methods used to identify time-varying, intrinsic and reflex stiffness.

2.4.1 Studies in Joint Dynamics

Reflexes and intrinsic properties depend on a variety of independent conditions. Early research in joint dynamics examined how stationary operating points affected the behaviour of total joint stiffness. This was done by treating torques due to passive joint properties, muscle mechanics, and stretch reflex activity as one dynamic quantity. Studies found that the physiological properties of the joint and associated structures depended on both mean joint angle and level of tonic muscle activation. In one experiment, subjects were required to maintain various levels of tonic activation, while their ankle was perturbed with stochastic position changes about a constant angular position. Researchers computed the dynamic relation between position and torque and found that joint compliance was described well by a linear, under-damped, second-order transfer function having inertial, viscous and elastic elements. They found that estimates of the inertial parameter were independent of muscle activity and mean position, but viscous and elastic terms increased with tonic torque [18, 25], perturbation amplitude [26] and mean deviation from neutral position [25].

2.4.1.1 Stretch Reflexes

Many groups have attempted to isolate the behaviour of the stretch reflex using various methods such as EMG recordings [15], surgical deafferentation [27, 28], nerve blocks [29, 30], or electrical stimulation [19, 31]. Investigators quickly discovered that reflexes not only have dynamics, but also display highly nonlinear rate sensitivity [15, 27, 32]. Kearney *et al.* found that the relation between half-wave rectified velocity and triceps surae (TS) EMG accounted for significantly more variance than a pure linear model [15]. This was confirmed in a later study, where non-linear system identification techniques were applied to compute the first- and second-order Wiener kernels; results suggested a Hammerstein structure, consisting of a static nonlinearity (SNL) followed by a dynamic linear system, better described stretch reflex dynamics [33]. The SNL was found to closely resemble a half-wave rectifier and the linear dynamics were characterized by a pure delay and low-pass filter.

In general, the stretch reflex response depends nonlinearly on the amplitude and bandwidth of the input displacement [2, 34]. Indeed a study conducted by our lab determined that perturbation velocity was an important variable in suppressing reflexes. Figure 12 shows that reflex torque and reflex EMG both decreased as the mean absolute velocity (MAV) of random perturbations increased; this was true for amplitude and bandwidth modulated input sequences at matched MAV. Reflex suppression during high frequency, vibratory inputs is likely due to presynaptic inhibition of the muscle spindle afferents, which impedes the transmission to motor neurons [34]. Therefore, when using random perturbations to identify reflex dynamics, care must be taken to ensure that the chosen inputs do not inhibit reflexes.

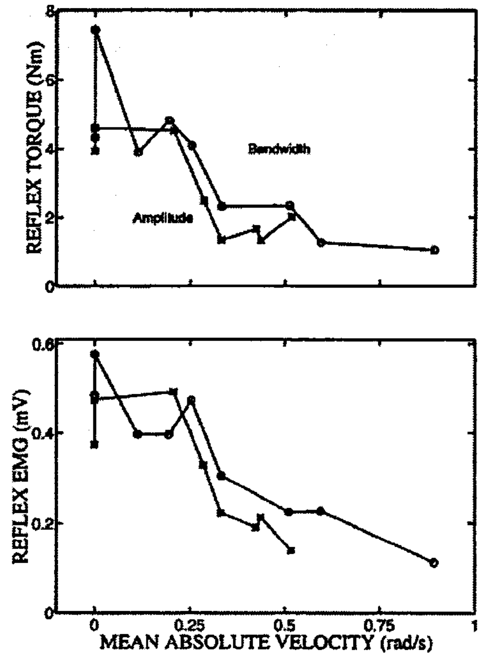

Figure 12: Reflex EMG and reflex torque diminish as mean absolute velocity (MAV) of the position sequence increases. Adapted from [34].

The reflex response also strongly depends on mean ankle position. TS reflex magnitude was found to increase as the ankle was progressively dorsiflexed with peak reflexes occurring near maximum dorsiflexion [35, 36]. Zhang *et al.* similarly determined that stretch reflex gain was higher during muscle stretch than shortening [37]. It was suggested that position induced mechanisms, such as modulation of afferent inputs to motor neurons, fusimotor drive or perturbation transmission to muscle spindles likely accounted for these changes in the reflex response.

Kearney *et al.* found that the magnitude of stretch reflexes depended on muscle activation level in addition to position or perturbation characteristics [15]. Reflex gain was computed by integrating the impulse response function (see Section 2.5.1) between half-wave rectified velocity and TS EMG. The gain was found to increase with tonic muscle activation. Other researchers found that the stretch reflex was regulated even during isometric muscle contractions, indicating that as the CNS increases or decreases muscle force it might simultaneously regulate the sensitivity of the stretch reflex by presynaptic inhibition of the Ia afferent terminals and/or modulation of muscle spindle sensitivity [38]. Alternatively, increasing the activation of muscles also increases the fraction of motor neurons above threshold to be activated by the stretch receptors, a phenomenon known as "automatic gain control" [39].

2.4.1.2 Stretch Reflexes and Movement

In general, movement kinetics have been found to strongly modulate the stretch reflex response. Studies suggest that reflexes are task-, phase-, and context-dependent [20]. One study suggests that as much as 30-60% of EMG produced by ankle extensors during normal walking could arise reflexively [40]. Many researchers have employed the Hoffman, or H-reflex to study how reflexes are modulated during passive and voluntary movements. The H-reflex is evoked by direct electrical stimulation of the Ia afferent fibres, which excites the motor neuron pool giving rise to a monosynaptic reflex response [41]. This reflex arc reflects the excitability of the motor neuron pool, whereas the stretch reflex combines motor neuron excitability with muscle receptor sensitivity. The H-reflex was found to vary in amplitude throughout walking [41-43], beam balancing [44], running [39], and cycling [45-47]. The reflex response was generally smaller during movement than at matched stationary positions. Capaday *et al.* determined that the reflex response amplitude was adjusted appropriately to each phase of the step cycle for locomotion [42]: reflexes were depressed during the swing phase of gait when they would inhibit forward motion by opposing ankle flexion and progressively increased throughout the stance phase of gait to facilitate the forward propulsion necessary to lift the limb off the ground. Findings were similar during a running experiment, but with further reflex suppression [39]. They argued that the source of modulation was not simply a consequence of alpha motor neuron excitation level, but also depended on central mechanisms to modify reflex sensitivity and threshold such as presynaptic inhibition. Furthermore, Brooke *et al.* found no significant difference in reflex modulation between passive and active movements, indicating that somatosensory information may be used within the spinal circuit and CNS to drive reflex gain [48-50]. Andersen *et al.* additionally proposed that the afferent input from muscle spindles not only acts as a compensatory reflex, but actually contributes to locomotion [51].

In general, the stretch reflex and H-reflex have similar temporal profiles, but it is difficult to match operating points between the two responses; the sources of modulation may differ because the H-reflex does not depend on peripheral effects such as fusimotor excitation [42]. Kearney *et al.* examined the stretch reflex response during an imposed gait movement by applying pulse disturbances at various locations throughout the cycle. Reflex torques and EMG were significantly lower during movement than at matched stationary positions throughout the walking cycle. They found that the reflex EMG was low at time of heel contact, increased progressively throughout the stance phase, rapidly decreased as the ankle began to plantarflex, and remained low throughout the simulated swing phase [52]. Reflex torque followed a similar trend, but pulses applied at the peak of dorsiflexion evoked almost no reflex torque despite generating the largest EMG response. Figure 13-A and B illustrate these results. A major conclusion from this study is that muscle mechanics play a key role in determining the functional importance of the stretch reflex during movement.

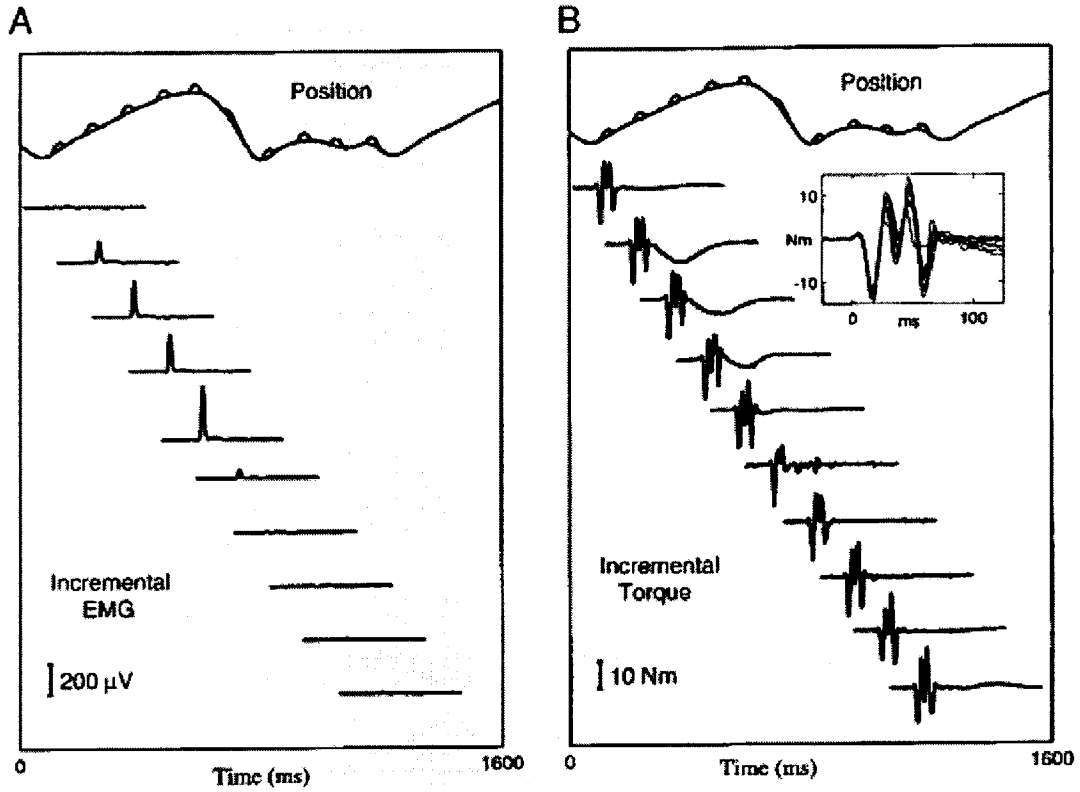

Figure 13: (A) Reflex EMG and (B) reflex torque during an imposed gait cycle. Pulse disturbances were periodically imposed at various locations throughout the cycle to elicit the reflex response during movement. Reflex EMG was maximal at peak dorsiflexion, but reflex torque was nearly zero at this position. Adapted from [52].

2.4.1.3 Intrinsic and Reflex Mechanisms

A continuing controversy exists in distinguishing the mechanical consequences of reflex activity from the intrinsic properties of the joint and muscle [2]. Simultaneous analysis of intrinsic and reflex mechanisms is required to fully describe joint dynamics; system identification techniques that separate intrinsic and reflex components offer a superior approach to the study of dynamic joint stiffness. Kearney *et al.* developed a method to identify intrinsic and reflex stiffness using a parallel cascade method (see Section 2.5.3). They found that reflex mechanisms were most important at frequencies between 5-10 Hz, while intrinsic dynamics dominated at higher frequencies [2]. Studies also confirmed that intrinsic stiffness increased monotonically with contraction level, while reflex stiffness was maximal at low contraction levels. Intrinsic and reflex stiffness both increased as the ankle was dorsiflexed. Overall it was concluded that reflex mechanisms made their largest, relative contribution near neutral position at low levels of activity [1].

2.4.1.4 Time-Varying Dynamics

Few studies have examined the time-dependent nature of dynamic joint stiffness during movement. As intrinsic and reflex mechanisms vary, so do the mechanical properties of a joint; stationary identification techniques alone are not capable of describing the time-varying behaviour of these properties. Early studies conducted by Lacquaniti *et al.* examined stiffness properties during a “do not resist”, then “resist” experiment involving the forearm. They discovered that stiffness and viscosity of the joint increased with active resistance, where viscosity changed more slowly than total stiffness [53]. Cyclic voluntary movements were analyzed with a time-varying technique and found to modulate the mechanical properties of the elbow joint; arm stiffness dropped during movement relative to matched stationary conditions [54]. While subjects tracked a moving target, the properties of the elbow joint varied with the speed of voluntary movement; however, mean stiffness was not significantly different from that during posture [55]. Results from a ball catching task suggested that modulations of the reflex response were generated from within the CNS, since joint properties changed before movement onset [56]. Kirsch *et al.* imposed a rapid ramp movement at the ankle joint while subjects maintained various levels of tonic muscle activation. Imposed movement experiments emphasize the role of peripheral mechanisms since voluntary activation levels are held constant during the motion. In this experiment, ensemble time-varying techniques were used to identify joint dynamics using position, torque and EMG measurements. Results suggested that stretch reflex properties were modulated independently of motor neuron pool activation level and the behaviour was largely mediated by peripheral mechanisms [57]. They found that total joint stiffness increased during the latter portion of the movement and the steady-state stiffness was 60% higher after the stretch [58]. In a complementary study, subjects were asked to generate rapid voluntary isometric contractions; this study eliminated the effect of peripheral mechanisms, by maintaining constant muscle length. Stretch reflex gain was significantly modulated during the contractions, with gain increasing with contraction level. These results suggested that reflex gain and motor neuron pool activation level were controlled by common descending paths, which supported the automatic gain control hypothesis for this particular task.

The studies mentioned here examined only total joint or stretch reflex properties during time-varying conditions. Researchers in joint dynamics have yet to decompose total joint stiffness into its respective intrinsic and reflex components during time variant movements.

2.5 SYSTEM IDENTIFICATION

System identification is the process of developing mathematical models of a system's dynamic behaviour through analysis of its inputs and outputs [5]. These techniques are a valuable tool in the study of motor control. System identification models typically fall into one of two categories: parametric or nonparametric. Parametric models are developed from first principles and have the advantage of producing model parameters of physical significance. These models rely on assumptions about the structure and order of the system under investigation. This eases the process of identification, because it reduces the number of unknowns in the system. In many biological systems, however, it is not possible to make such assumptions about model order or structure, since the dynamics are inherently unknown [59]. Furthermore, if the structure chosen is incorrect, then the resulting parameter estimates are meaningless. Nonparametric system identification methods make fewer assumptions about the system, drawing on the input and output data to describe system dynamics. Consequently, nonparametric models are a more effective means of describing systems with unknown dynamics.

2.5.1 Impulse Response Functions

As we shall see in subsequent sections of this chapter, the impulse response function (IRF) is a fundamental tool for system identification. In the context of joint dynamics, an IRF represents the pattern of response which would be evoked by a unit impulse displacement [60]. An impulse response function completely characterizes the dynamics of a linear system. Given a linear, time-invariant system, the output $y(t)$ can be determined as the convolution of the impulse response function $h(\tau)$ with an arbitrary input $u(t)$:

$$y(t) = \int_{-\infty}^{\infty} h(\tau)u(t-\tau)d\tau$$

where τ represents the lag of the impulse response function, $h(\tau)$. Positive lag indices represent system memory, whereas negative lags represent system anticipation. For physically realizable systems, τ ranges between two finite values, τ_1 and $\tau_2 > 0$, where $h(\tau) = 0$ for lags outside this interval.

The time-invariant convolution integral can be extended to the time-varying case by making the IRF a function of both lag and time [5]:

$$y(t) = \int_{-\infty}^{\infty} h(t,\tau)u(t-\tau)d\tau$$

The discrete-time version of the convolution integral with sampling interval Δt is approximated as:

$$y(i,r) = \Delta t \sum_{j=T_1}^{T_2} h(i,j)u(i-j,r)$$

where i is the discrete time index, $T_1 = \tau_1 / \Delta t$, and $T_2 = \tau_2 / \Delta t$. This application of a nonparametric impulse response function assumes that the system is linear. More complex formulations are necessary if the system is nonlinear: quasi-linear models assume that the system is linear about a fixed operating point; functional expansions apply a more general approach to the impulse response function by using kernels in a Volterra or Wiener series expansion; cascade models split the nonlinearity into series or parallel elements, such as Wiener (linear-nonlinear) or Hammerstein (nonlinear-linear) systems [59]. Section 2.5.2 further discusses the Hammerstein system and cascade models used in this thesis.

2.5.2 Time-Varying System Identification

A system is time-varying if its dynamic properties change with time. Studies in motor control have often been restricted to static conditions by examining system dynamics about a fixed operating point; for example, an experiment with small-amplitude angular displacements during constant voluntary muscle contractions is assumed to have properties that are time-invariant [25]. However, most physiological systems have parameters that are time-dependent [54, 55, 58, 61]. For example during walking, muscle forces rapidly change with the gait cycle and the resulting mechanical properties can no longer be analyzed with time-invariant system identification techniques. Both parametric and nonparametric methods have been developed for time-varying system identification. In general, there are four main classes of time-varying methods:

(1) Quasi-stationary methods assume that the system properties do not change over a time period corresponding to the record length. These methods represent the system at fixed operating points, but cannot be used when the operating points change faster than the system dynamics.

(2) Adaptive methods estimate time-dependent parameters of a parametric model using iterative algorithms to minimize the output error associated with the model predictions [5]. These methods converge to a new set of parameters and work well for slow-moving systems, but their estimates are not valid during periods of change. Also, some assumption about the system's structure (e.g. model order) is required *a priori*.

(3) Temporal expansion methods represent time-varying coefficients as system kernels (e.g. Volterra kernels) in a series expansion of time-dependent basis functions. These methods are memory intensive because the number of parameters rapidly grows with memory length and system order. As with adaptive methods, their estimates are not valid during changes in system dynamics. In addition, the form of the time-varying behaviour must be known in advance, which is often not possible in biological systems.

(4) Ensemble methods estimate system dynamics from an ensemble of input and output realizations, each corresponding to the same time-varying behaviour. These methods have the advantage of requiring no *a priori* information about the form of time-variation and can be used when the system dynamics change on a time scale shorter than the dynamics themselves [5]. Indeed variations can be detected at intervals corresponding to the sampling rate. Section 2.5.2.1 further discusses ensemble methods and the implementation used in this thesis.

2.5.2.1 Ensemble Methods

Ensemble methods are a unique approach to time-varying system identification; indeed they have provided robust results for several biological systems [55, 58, 61]. Soechting *et al.* pioneered the ensemble method to study the temporal modulation of myotatic responses of the human elbow [61]. The initial implementation of the algorithm imposed strict requirements on the synchronization between the input sequence and time-varying behaviour. The technique involved time-shifting a single input sequence relative to the time-varying behaviour for each successive trial to produce the required data ensemble. Time-invariant techniques were then applied to the cross-ensemble data at time increments corresponding to the sampling interval. At each time point, the cross-correlation between the input and output corresponded to the instantaneous system dynamics and was represented as an IRF. Consequently, the change in the system dynamics throughout time was portrayed by a surface of IRFs. Despite the severe restrictions on the timing of the input sequence, this approach was successfully applied in several studies. Lacquaniti *et al.* examined changes in limb compliance [62] and the stretch reflex response [56] of the human arm during a ball catching task using the ensemble technique.

Researchers later applied the concept of ensemble analysis to parametric models in an attempt to ease the constraints imposed on the input sequence. An ARMA model form was used by Bennett *et al.* to study the time-varying stiffness characteristics of the elbow during cyclic voluntary movements [54]. The time-varying parameters of the ARMA model were computed by applying an estimation procedure to the ensemble matrix. Xu *et al.* similarly applied a parametric model to examine the mechanical properties of the elbow during target tracking experiments. In this case, the human forearm was modelled as a second order system having inertial, damping, and elastic parameters; ensemble data was used to solve for the parameter estimates [55].

Our lab successfully developed a least-squares method for identifying time-varying system dynamics as IRFs using ensemble data [5]. The nonparametric approach is based on the singular value decomposition (SVD) of the input ensemble. This implementation places few conditions on the input signal, namely it need not be white nor time-locked with the time-varying behaviour [5]. The method relies on an ensemble matrix of input and output data. The columns of the ensemble matrix (illustrated in Figure 14) correspond to trial number and the rows correspond to time. At each time increment, the input is de-convolved with the output to produce an instantaneous description of the system dynamics. System parameters are estimated at fixed time points across the ensemble, rather than computing the usual time-invariant response and averaging across time. The major drawback of this method is the large number of realizations required for the data ensemble; system estimates improve as the number of realizations having consistent time-varying dynamics increases, since averaging is conducted across the ensemble rather than across time.

This ensemble method was successfully used in two motor control studies. The first study examined the time variations in the stretch reflex of the triceps surae during rapid voluntary changes in isometric contractions [63]. The second study imposed a rapid stretch upon the ankle joint during a constant level of voluntary contraction [57]. System dynamics were represented as IRFs relating the input perturbation to TS EMG at each sample time throughout the time variation.

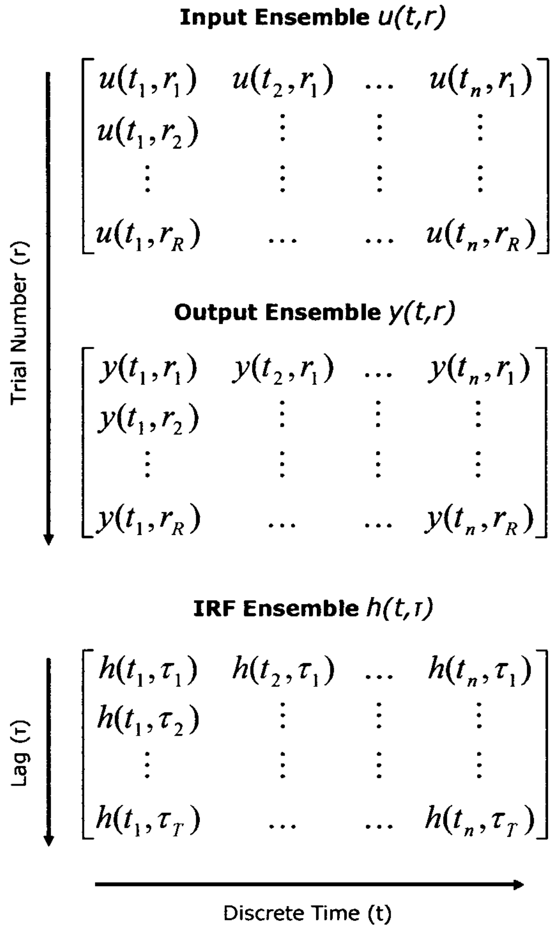

$$\begin{bmatrix} u(t_1,r_1) & u(t_2,r_1) & \cdots & u(t_n,r_1) \\ u(t_1,r_2) & \vdots & \vdots & \vdots \\ \vdots & \vdots & \vdots & \vdots \\ u(t_1,r_R) & \cdots & \cdots & u(t_n,r_R) \end{bmatrix}$$

$$\begin{bmatrix} y(t_1,r_1) & y(t_2,r_1) & \cdots & y(t_n,r_1) \\ y(t_1,r_2) & \vdots & \vdots & \vdots \\ \vdots & \vdots & \vdots & \vdots \\ y(t_1,r_R) & \cdots & \cdots & y(t_n,r_R) \end{bmatrix}$$

$$\begin{bmatrix} h(t_1,\tau_1) & h(t_2,\tau_1) & \cdots & h(t_n,\tau_1) \\ h(t_1,\tau_2) & \vdots & \vdots & \vdots \\ \vdots & \vdots & \vdots & \vdots \\ h(t_1,\tau_T) & \cdots & \cdots & h(t_n,\tau_T) \end{bmatrix}$$

Figure 14: (top) Input ensemble, **(middle)** output ensemble, and **(bottom)** ensemble of time-varying system parameters or impulse response functions. Columns correspond to discrete time, and rows correspond to trial number (input-output matrices) or IRF lag (system parameter matrix).

2.5.2.2 TV Linear Pseudoinverse Approach

An improved technique to identify linear time-varying systems from ensemble data was developed by our lab [6]. The algorithm first expresses the discrete-time convolution equation in terms of the input-output cross-correlation and input auto-correlation functions evaluated over the entire ensemble:

$$\hat{\phi}_{yu}(i,-k) = \Delta t \sum_{j=T_1}^{T_2} h(i,j)\,\hat{\phi}_{uu}(i-k,k-j)$$

where i denotes the discrete time index, and j and k are lag indices. A nonparametric estimate of the weighting function $h(i,j)$ is computed at each sample time by solving the matrix equation relating the correlation functions. An optimized matrix, known as the pseudoinverse, is used in place of the matrix inverse required to solve the matrix equation. In effect the pseudoinverse approach disregards elements that contribute more toward noise than output variance; by removing these terms, the estimates of the dynamics are considerably improved with no adverse effect on the predicted outputs. The pseudoinverse technique has proven more reliable than the previous least-squares method in the presence of coloured inputs and when the output signal-to-noise ratio (SNR) is low [6].

2.5.2.3 TV Hammerstein Systems Approach

Specialized techniques are required for the identification of nonlinear systems. Section 2.5.1 briefly introduced one method known as a cascade model. A Hammerstein system is a cascade model consisting of a static nonlinearity in series with a linear dynamic system. The time-invariant analysis of Hammerstein systems has been used in a variety of biomedical systems [33, 64]. Our lab developed a technique to identify time-varying Hammerstein systems using a correlation method. The identification technique works as follows: an initial estimate of the IRF describing the linear subsystem is obtained at time i from the input-output cross-correlation function and the input auto-correlation function. An iterative algorithm is then used to produce final estimates of the system parameters at time i. The algorithm consists of two steps. In the first step, the estimates of the linear subsystem are fixed and the estimates of the nonlinear subsystem that minimize the sum of squared error (SSE) between the observed and predicted output for the Hammerstein system are found. In the second step, the process is reversed and the nonlinear subsystem is fixed, while the estimates that reduce the SSE for the linear system are found. The iterative process is repeated until the SSE fails to decrease. The entire process is repeated for every sampling time i. The method was proven effective for non-white inputs and low output SNR [7].

2.5.3 Parallel-Cascade Model of Joint Mechanics

Dynamic joint stiffness is composed of two distinct mechanisms, intrinsic and reflex, which together contribute to overall ankle torque. A parallel cascade system identification method was developed by Kearney *et al.* to separate the relative contributions of intrinsic and reflex mechanisms to total joint torque [2]. The cascade structure is shown in the figure below:

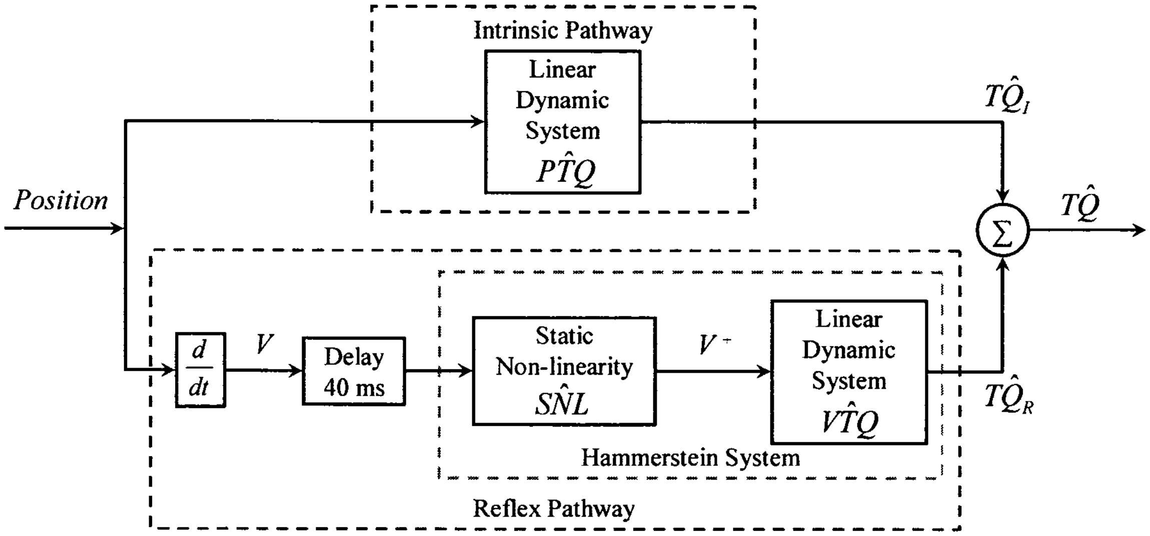

Figure 15: Block diagram showing the parallel-cascade model used to separate intrinsic and reflex contributions to total ankle torque.

The upper pathway represents intrinsic mechanisms and relates the position of the joint to torque via a TV, linear, dynamic element. The lower pathway represents reflex mechanisms and relates the velocity of the joint to torque via a differentiator and delay in series with a Hammerstein system. Each pathway is assumed to contribute linearly to the net torque produced by the joint. The dynamics of the two pathways are identified using an iterative algorithm, which proceeds as follows:

1. Intrinsic stiffness is estimated as a nonparametric IRF, $P\hat{T}Q$, relating position to torque. The length of the IRF is fixed at a value less than the reflex delay to prevent reflex contamination in the intrinsic estimate.
2. $P\hat{T}Q$ is convolved with the position input to predict intrinsic torque, $T\hat{Q}_I$. The intrinsic residual torque is computed as the difference between net torque and predicted intrinsic torque:

$$T\hat{Q}_{IR} = TQ - T\hat{Q}_I$$

3. Reflex dynamics are estimated as a Hammerstein system, relating velocity to intrinsic residual torque, $T\hat{Q}_{IR}$. The reflex dynamics are modelled as a static nonlinearity, $S\hat{N}L$, in series with a nonparametric IRF, $V\hat{T}Q$. A correlation approach is used first to obtain an initial, nonparametric estimate of the linear subsystem. Then an iterative optimization algorithm is used to produce final estimates of the system parameters, by alternating between the linear and nonlinear subsystems.
4. The nonlinear Hammerstein system is used with the differentiated position input (velocity) to generate $T\hat{Q}_R$, and estimate of the reflex torque.
5. The total predicted torque is computed as

$$T\hat{Q} = T\hat{Q}_I + T\hat{Q}_R$$

6. To evaluate the quality of the identification, the percent variance accounted for (%VAF) is computed between the observed and predicted total torque:

$$\%VAF = 100\left(1 - \frac{\mathrm{var}\left(TQ - T\hat{Q}\right)}{\mathrm{var}(TQ)}\right)$$

   where TQ is the observed and $T\hat{Q}$ the predicted torque.
7. The procedure is repeated using reflex residual torque in subsequent iterations to compute $P\hat{T}Q$, effectively increasing the signal to noise ratio. This is repeated until successive iterations fail to improve the %VAF.

The parallel cascade model of joint mechanics has been used in several time-invariant studies conducted by our lab [1-4]. It has also been extended to the time-varying case by incorporating the techniques outlined in Sections 2.5.2.2 and 2.5.2.3 for TV linear and TV Hammerstein system identification. Development of the new TV parallel-cascade identification algorithm was the topic of a previous Master's thesis completed by Mackenzie Baker [8]. Preliminary steps were taken to validate the algorithm and show its ability to work under simulated and experimental conditions. Algorithm improvements, validation and experimental applications are the topic of this thesis.

2.6 THESIS RATIONALE

The role of ankle joint stiffness and particularly, the role of reflex stiffness in posture and movement is an ongoing topic of debate [19, 20]. Studies have shown that joint properties depend on task, phase and intensity of movement compared to matched postural conditions [39, 43, 51, 65]. Therefore, it is not possible to use stationary identification methods to examine the ankle during movement; rather time-varying techniques are required. Furthermore, an algorithm that separates intrinsic and reflex mechanisms is needed to distinguish their respective contributions [2]. The time-varying parallel-cascade (TVPC) algorithm developed by our lab has the ability to analyze and separate intrinsic and reflex dynamics during movement. In addition to research in motor control, this algorithm can be applied to a variety of clinical and industrial circumstances. Spasticity, manifested as increased muscle tone or joint stiffness, is a common symptom of patients suffering from stroke, spinal cord or brain injury. An imbalance in muscle tone can substantially impair motor control, requiring therapeutic intervention. Current methods of rehabilitation (e.g. functional electrical stimulation) rely on qualitative or semi-quantitative methods to assess therapy or recovery, such as the tendon tap or Ashworth scale [66]. Quantitative tools such as the TVPC algorithm will provide an objective means to evaluate movement and/or the efficacy of treatment [3, 4, 67]. Furthermore, the design of robotics [68] and man-machine interfaces will benefit from a clearer understanding of how human joints function.

2.6.1 Thesis Objectives

The primary objectives of this research were the following:

1. Improve the existing implementation of the time-varying parallel-cascade identification algorithm for the analysis of intrinsic and reflex properties.
2. Validate the algorithm's performance under realistic, simulated conditions using a pseudo-random binary sequence perturbation input.
3. Validate the algorithm's performance under stationary, experimental conditions and compare the results with existing time-invariant techniques
4. Explore the dynamic joint properties of the ankle during imposed time-varying movements, such as a gait cycle and periodic input sequence.

3 Experimental Methods

This chapter describes the experimental methods used by our laboratory to study joint dynamics. Figure 16 shows a schematic representation of the experimental apparatus. Subjects lay supine with their ankle attached to an electrohydraulic actuator by means of a custom-made fibreglass boot. Sandbags were placed beneath the knee to provide support and maintain the lower leg at a comfortable, slightly flexed position. A strap was placed over the lower thigh to secure the upper leg and prevent motion at the knee joint. A foot pedal fastened to the fibreglass boot rotated the subject's ankle in the dorsi- and plantarflexion direction. Rotations were controlled by a proportional position servo implemented using xPC Target, a real time digital signal processing (DSP) system. An LCD monitor was mounted above the subject to provide visual feedback information of tonic muscle activation. Position, torque, gastrocnemius EMG and tibialis anterior EMG were digitally sampled along with the input command signal and stored on the host PC. Each of these subsystems will now be described in detail.

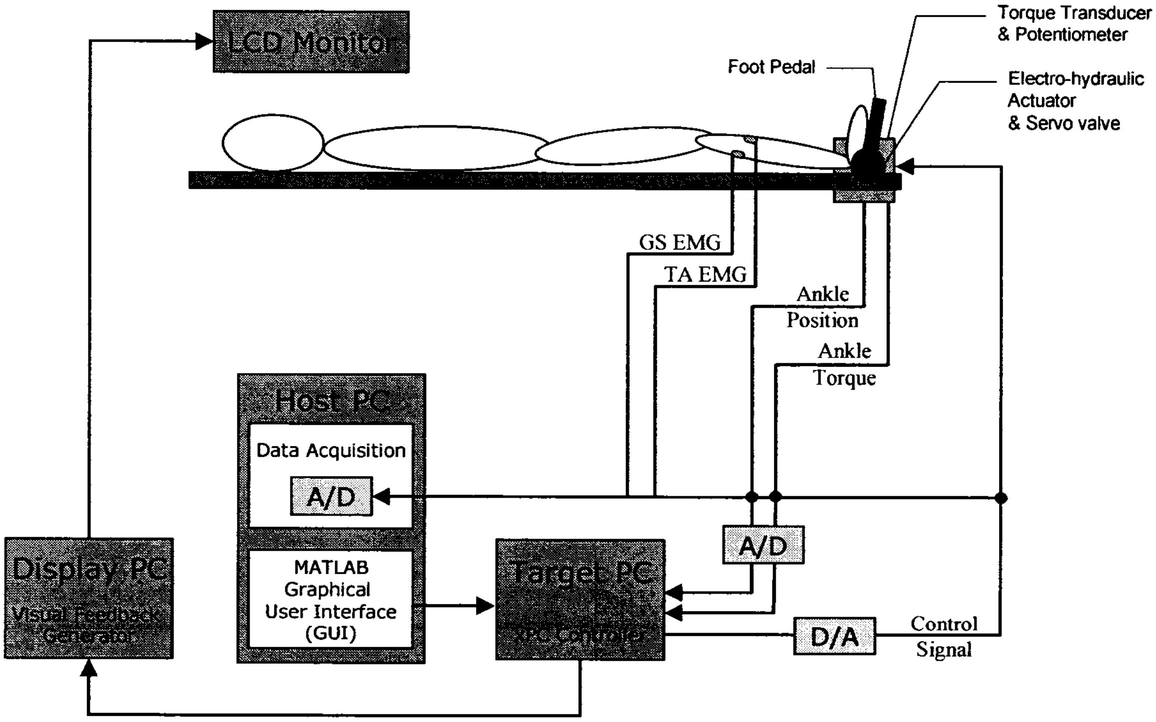

Figure 16: Experimental apparatus illustrating subject placement, hardware configuration and signal transmission. Subjects lay supine while their left ankle was perturbed by an electro-hydraulic actuator. Position, torque and EMG were digitally sampled and used to evaluate joint dynamics.

3.1 ELECTROHYDRAULIC ACTUATOR

The electrohydraulic actuator was a high pressure, reciprocating rotary torque motor (ROTAC 26R-5). Flow to the actuator was controlled by a two-stage electrohydraulic servo valve (MOOG 730-233). The shaft of the actuator was coupled directly to the boot fixation assembly to minimize backlash at the interface between the two mechanisms. The axis of the actuator was aligned with ankle's axis of rotation during boot construction ensuring pure rotation about the ankle joint. Section 3.2.1 outlines how this was accomplished. Figure 17-A and B show the experimental apparatus and a subject attached to the rotating foot pedal.

Figure 17: Electrohydraulic actuator assembly. (A) Close-up of actuator, potentiometer, torque transducer and boot assembly (rotating foot pedal, aluminum posts and fibreglass boot); (B) An example of a subject connected to the hydraulic actuator, illustrating boot fixation, EMG electrodes and thigh strap.

3.1.1 Safety Mechanisms

The electrohydraulic actuator was capable of generating very large and rapid movements at the ankle. Several safety mechanisms were implemented to prevent the actuator from moving beyond the subject's comfortable range of motion (ROM). These included:

1. *Mechanical stops:* Two steel bolts were fixed to the actuator assembly stand as shown in Figure 18-A. The bolts were placed at the plantar flexion and dorsiflexion limits of the test subject. They acted as a mechanical stop that prevented rotating beyond the subject's ROM.

2. *Flow bypass valve:* The actuator was equipped with a hydraulic flow bypass mechanism shown in Figure 18-B. The mechanism consisted of a cam, which activated a bypass valve when the elevated portion of the cam came in contact with the plunger. This cut off the flow of hydraulic fluid and prevented further rotation. The two adjustable plates were rotated relative to each other to define a ROM smaller than the mechanical stops.
3. *Panic button:* As a final precaution, both the subject and experimenter were provided with a panic button. When pressed, the device stopped the flow of hydraulic fluid to the actuator, leaving the foot pedal in a pliable state.

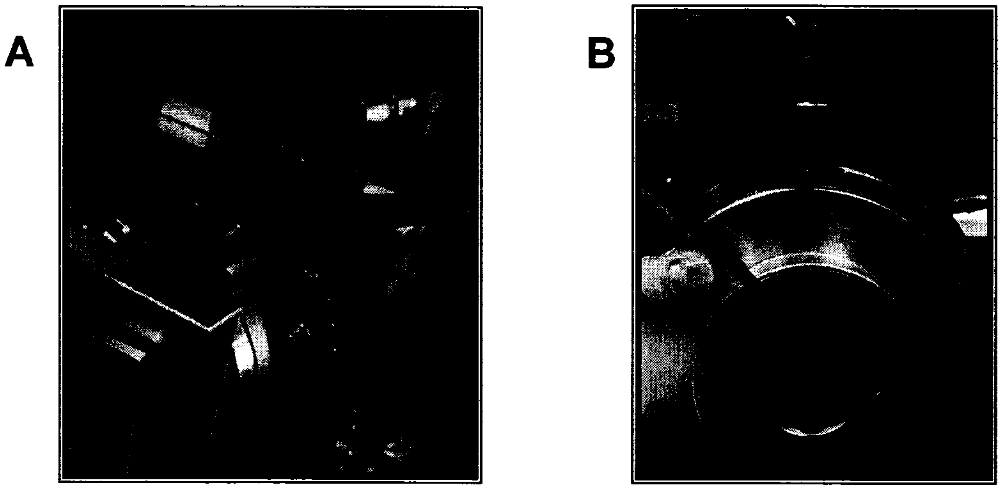

Figure 18: Safety Mechanisms. (A) Steel bolts act as a mechanical stop to prevent motion beyond the subject's comfortable ROM; (B) A flow bypass valve diverts hydraulic fluid from the actuator when the elevated cam comes in contact with the bypass plunger.

3.2 BOOT

A form-fitting, low inertia, rigid interface was required to properly transmit actuator rotations to the subject's ankle without interfering with the overall dynamics of the joint. To accomplish this, a custom-made fibreglass boot was constructed as illustrated in Figure 17-A.

3.2.1 Materials and Construction

Orthopaedic casting tape (Dynacast) was chosen as the material for the boot based on its high strength-to-weight ratio and low density. To construct the boot, several layers of tape were wrapped around the subject's foot while they held their ankle at a 90° angle.

The tape began to set into a stiff form shortly after wrapping was complete. A cast cutter was used to remove the hardened boot from the subject's foot. The boot was then trimmed so the subject could easily slide the boot on and off. As well, the toe portion was cut away to prevent the subject from exerting forces with their toes during experiments. The malleoli—corresponding to the rounded protrusions on the ankle—were marked on the cast to help determine the ankle's axis of rotation. Anthropomorphic studies indicate that the axis of rotation passes through a point 11 mm anterior and 12 mm distal to the lateral malleolus (Figure 19-A) and 1 mm posterior and 16 mm distal to the medial malleolus (Figure 19-B) [69]. Holes were drilled in the boot at these locations marking the centre of rotation. The boot was then placed in a gluing jig, which replicated the electrohydraulic actuator assembly. Aluminum posts were fastened to the sides of the boot using steel-filled epoxy (Devcon). The axis of the motor shaft and the ankle's axis of rotation were aligned at this stage using the jig. A thermoplastic tongue was moulded to the surface of the subject's boot and foot and held in place via a Velcro strap to provide additional rigidity during experiments. The finished boot was fastened to the rotating foot pedal using two steel bolts. A more detailed description of each step in boot construction can be found in the REKLAB manual [70].

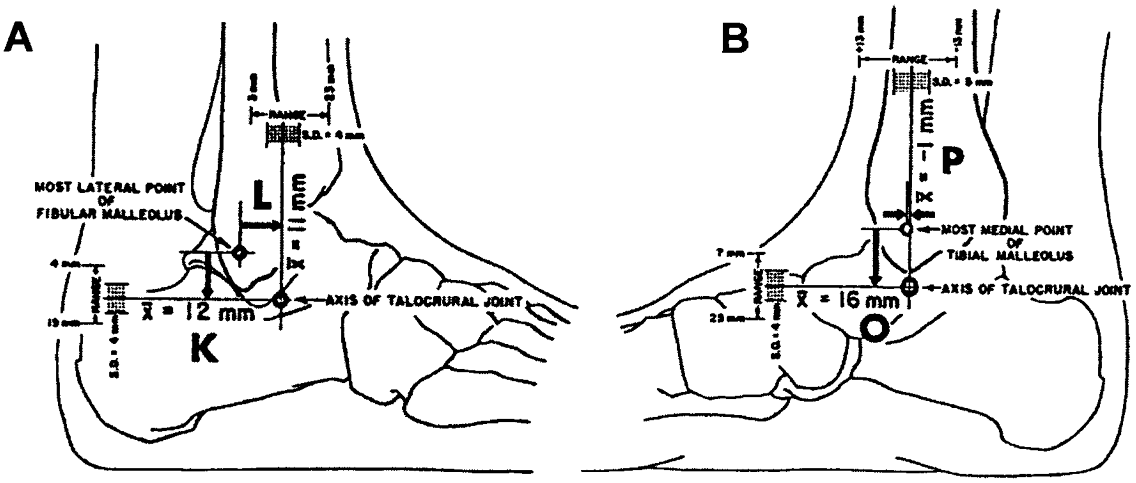

Figure 19: (A) Lateral and (B) medial axis of rotation for a human ankle. Estimate is based on anthropomorphic data using the malleoli as anatomical landmarks. Adapted from [69].

3.3 SENSORS AND SIGNAL CONDITIONING

Analog sensors were used to measure physiological information relating to joint dynamics into useful data for system identification. Signals corresponding to position, torque, and EMG were acquired using the following signal transducers.

3.3.1 Angular Position

A precision potentiometer (BI Technologies, 6273) made of conductive plastic material measured angular position. This single-turn device was configured in a circular geometry. The housing of the potentiometer was fixed to a stationary support on the supine apparatus; the shaft was connected to the lateral bearing shaft on the boot assembly via a flexible helical beam coupling (McMaster-Carr, 6208K51). The all-metal coupling had six cuts to provide the flexibility necessary to account for parallel, angular, and axial misalignment. It was ideal for our motion-control application, since it provided zero backlash despite frequent starts and stops.

The potentiometer consisted of a mechanical contact that swept across the surface of the conductive material to produce an output voltage linearly related to the rotational displacement of the contact. The maximum non-linearity of the potentiometer was ±0.5% over 5.943 rad. A custom-built electronic module conditioned the output of the potentiometer, providing amplification and DC offset to the position signal. The module was calibrated to a sensitivity of 10 V/rad (or 0.1 rad/V). The noise of the position transducer and module was measured using a multimeter (Fluke 80) over a bandwidth of 200 kHz—the root-mean-square (RMS) noise was found to be 1.0 mV (or 0.0001 rad) [71].

3.3.2 Torque

Torque was measured using a general purpose reaction torque sensor (Lebow, 2110-5K) mounted to the medial boot fixation support. The maximum nonlinearity of the transducer was ±0.1% over a range of 565 Nm. The torque transducer was characterized by high resistance to bending moments, minimal friction error and low end sensitivity due to the absence of moving parts. The torsional stiffness of the transducer was 103,941 Nm/rad—by comparison, the stiffness of the human ankle is typically less than 200

Nm/rad. Forces generated by the subject's ankle did not influence the transducer's measurement accuracy since the subject's ankle was significantly more compliant than the transducer. A custom-built electronic module amplified the torque signal and provided a DC offset. The sensitivity of the module was calibrated to 0.05 V/Nm (or 20 Nm/V). The resolution of the transducer and module was measured as previously discussed in Section 3.3.1; the RMS noise level was found to be 2.1 mV (or 0.042 Nm) [71].

3.3.3 Electromyography (EMG)

EMG signals were recorded from the medial gastrocnemius and tibialis anterior muscles using an 8-channel Bagnoli EMG System (Delsys Inc). A schematic of the EMG set-up is shown in Figure 20 illustrating the electrodes, interface and main amplifier units, medical grade power supply and storage PC.

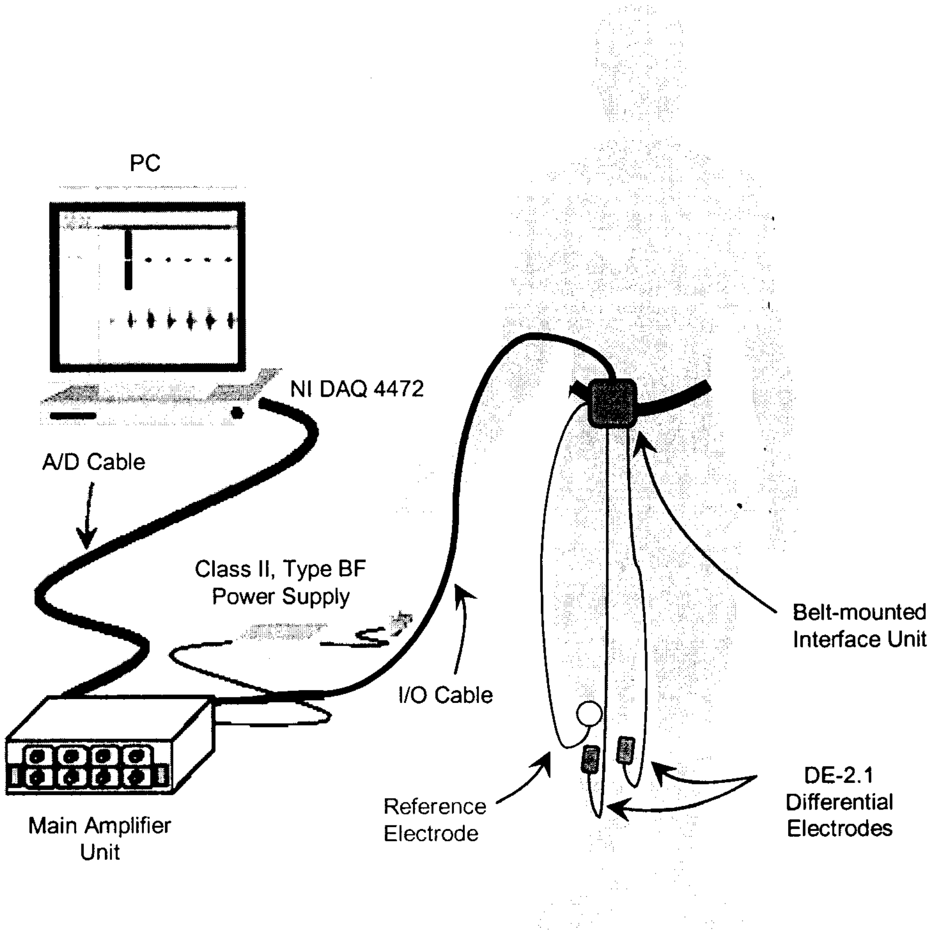

Figure 20: Components of the Bagnoli EMG system. Adapted from [70].

3.3.3.1 Electrodes

Single differential surface electrodes (DE-2.1) shown in Figure 21-A were applied to the skin surface using double-sided tape, directly above the GS and TA muscles. Prior to applying the electrodes, the skin surface was prepped by lightly shaving and rubbing with alcohol. The parallel bars of the electrode sensor were placed perpendicular to the muscle fibre orientation at the centremost location of the muscle.

The Delsys electrodes used an active-electrode design, producing a high signal-to-noise ratio. The electrode housing was made from waterproof polyurethane plastic; the housing was internally shielded to reject ambient electrical noise. The electrode was made from 99.9% pure silver bars, 10 mm in length and 1 mm in diameter—the bars were spaced 10 mm apart from each other as shown in Figure 21-B. The differential design rejected common mode signals such as motion and cable artefacts; the common mode rejection ratio (CMRR) was greater than 90 dB at 60 Hz. To minimize waveshape distortion and signal attenuation the sensor input impedance was greater than $10^{15}\,\Omega$ // 0.2 pF, significantly larger than the EMG source impedance.

The EMG signal was measured as the potential difference between the two parallel bars (v_1 and v_2, respectively). The potentials were measured relative to a neutral location above the patella using a reference electrode. The detected signals were subtracted, resulting in a single-ended output (v_{out}) free of common mode noise. The electrode pre-amplified the output signal with a gain of 10 before sending to the main amplifier unit.

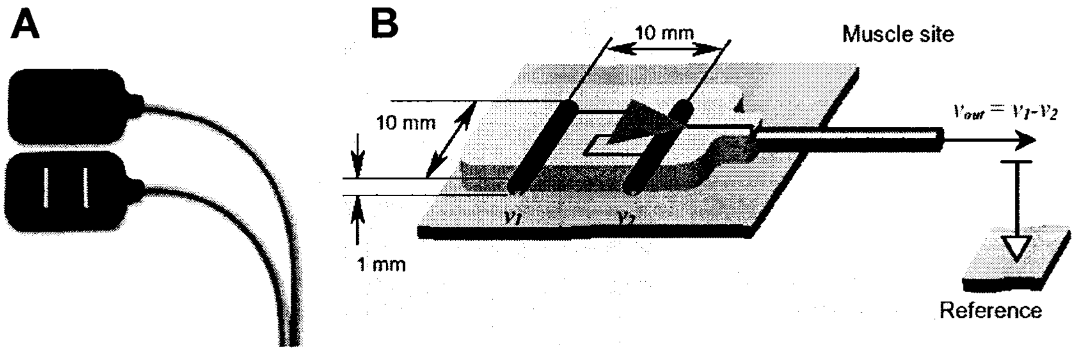

Figure 21: (A) DE-2.1 single differential electrode; (B) Schematic of voltage differential (EMG signal is the result of the potential difference between v_1 and v_2 at the skin surface). Adapted from [70].

3.3.3.2 Main Amplifier and Interface Unit

A lightweight, belt-mounted interface unit hosted the input from the EMG electrodes and reference electrode. The electrode signals were converted with low output impedance to the main amplifier unit via an I/O cable (see Figure 20). The main amplifier unit provided power to the electrodes, conditioned the EMG signals and relayed the signals for data acquisition. The unit filtered the EMG to a bandwidth between 20 and 450 Hz. Each channel had a selectable gain setting of 100, 1000, or 10000. A zero gain setting was also available to view the reference potential. Additionally, each channel was equipped with two signal quality detectors: (1) a line interference detector identified excessive 60 Hz noise, typically due to poor electrode-skin contact; (2) an amplitude saturation detector identified channel clipping due to over-amplified signals. The unit was powered by a medical-grade, isolated power supply with leakage currents less than 10 μA and safety isolated to 3750 V_{RMS}. The supply conformed to UL2601, CSA601, and IEC 60601-1 safety standards.

3.4 EXPERIMENTAL CONTROL

Experimental control tools were developed using MATLAB, Simulink and related software (The Mathworks Inc.). A custom-made graphical user interface (GUI) was programmed for use on a Windows XP workstation, which managed the input properties, model transfer, data acquisition and output inspection.

3.4.1 Servo Control System

Servo control was implemented using xPC Target—a real-time digital signal processing (DSP) system using a host-target structure. The controller model was developed in Simulink on the host machine and compiled into DSP code using the Real-Time Workshop. The control code was loaded via Ethernet to the target computer running a real-time DSP kernel. Feedback signals used by the controller were first anti-alias filtered with an 8-pole, 6-zero, constant-delay, low-pass filter with a 250 Hz cut-off frequency and 80 dB stop band attenuation (Frequency Devices, D68L8D). The signals were then sampled at 1 kHz by the target computer using a 16-bit analog-to-digital (A/D) card (ComputerBoards Inc., PCIM-DAS1602/16). Desired position sequences were digitally generated and loaded to the target computer using the custom-made GUI. The model used proportional position feedback to determine the corresponding control signal, which was output to the actuator using a 16-bit digital-to-analog (D/A) card (ComputerBoards Inc., PCIM-DDA06/16). The Simulink model used for the experiments in this thesis is shown in Appendix B.

3.5 DATA ACQUISITION

Position, torque, EMG and command signals were sampled at 1 kHz by a dynamic signal acquisition card (National Instruments, 4472). The device used oversampling delta-sigma modulating A/D converters to minimize total harmonic distortion (THD) and boost signal-to-noise ratio (SNR). Anti-aliasing was performed by an internal digital brick wall filter with an extremely flat frequency response and sharp roll-off near the cut-off frequency of 486.3 Hz. The rejection ratio for this filter was greater than 110 dB above 546.5 Hz. The sampled data was subsequently stored on the host machine.

3.6 VISUAL FEEDBACK

Some experiments required subjects to maintain a constant level of voluntary muscle activation. Subjects were assisted by an LCD monitor suspended above the supine apparatus displaying a visual feedback cue. The cue represented their level of tonic muscle activity determined by one of two methods: (1) the error signal between a target torque and low-pass filtered torque, or (2) the error signal between a target EMG level and low-pass filtered EMG. The low-pass filter (Bessel filter, 0.4 Hz cut-off frequency) eliminated the cyclic oscillations generated in response to the time-varying motion or stretch reflex. As a result, the feedback signal represented the subject's baseline contraction level. Additionally, the EMG signal underwent a sample-and-hold triggered by stretch onset to further reduce the transient effects due to reflexes. In both cases, the subject was instructed to minimize the error between the target value and actual value by constantly contracting the GS muscle at 5% of maximum voluntary contraction (MVC). The feedback data was computed using the Simulink control model on the target computer and sent to the display machine using a UDP network protocol. Figure 22 shows a sequence of graphical screenshots taken while a subject attempted to carry out the feedback task.

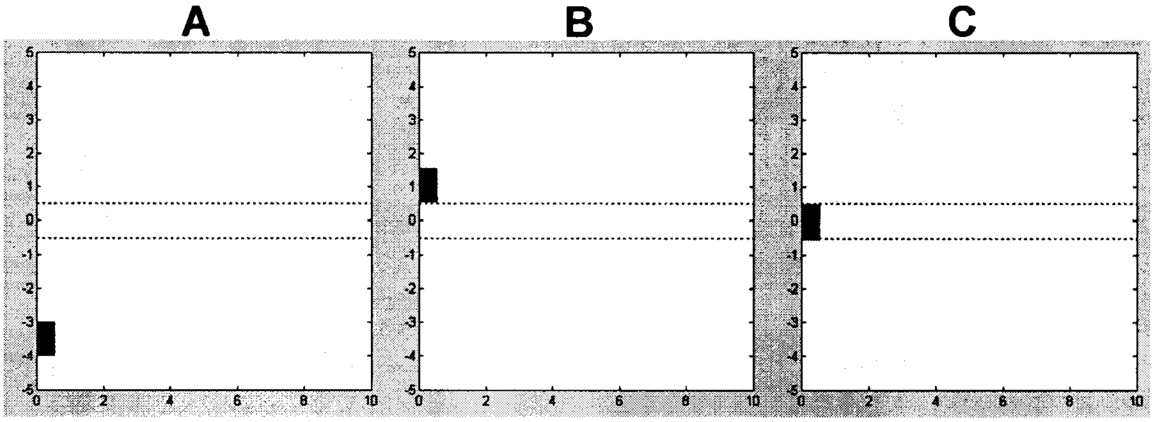

Figure 22: Visual feedback. (A-C) Subject attempted to minimize the error between a target and actual level of contraction. The target level is delimited by the dashed lines and the red square represents the error between the actual and target contraction. The subject was successful in Figure C.

4 Identification of Time-varying Intrinsic and Reflex Joint Stiffness: Simulation and control study

Chapter 4 introduces the time-varying, parallel-cascade method. The iterative algorithm is described in detail with particular attention to how the ensemble, time-varying techniques are incorporated. A simulation study is summarized, which examines the algorithm's ability to track time-varying changes during a rapid ramp change in joint dynamics. Details of an experimental study are then provided, demonstrating the success of the TVPC method with real data.

Identification of Time-varying Intrinsic and Reflex Joint Stiffness: Simulation and control study

**Heidi Giesbrecht, Mackenzie Baker, Daniel Ludvig,
Ross Wagner, Robert E. Kearney**

**Target Journal:
IEEE Transactions on Neural Systems and Rehabilitation Engineering**

4.1 ABSTRACT

We have developed a time-varying, parallel-cascade system identification algorithm to separate joint stiffness into intrinsic and reflex components at each point in time during rapid movements. The components are identified using an iterative algorithm in which intrinsic and reflex dynamics are identified using separate time-varying (TV) techniques based on ensemble methods. An ensemble of input-output records having the same TV behaviour is acquired and used to identify the system dynamics as impulse response functions at time increments corresponding to the sampling interval. Simulation studies showed that the time-varying, parallel-cascade algorithm performed well under realistic conditions with 99.9% VAF between simulated and predicted torque. Additive noise was applied to the output ensemble to demonstrate the algorithm's ability to produce good system estimates even in the presence of low SNR. To evaluate the performance of the algorithm under realistic conditions we applied it to an ensemble of experimental data acquired under stationary conditions. Results demonstrated that the TV estimates converged to those of the established time-invariant algorithm and allowed us to determine how variance of the TV estimates fluctuated with the number of realizations in the ensemble.

4.2 INTRODUCTION

Dynamic joint stiffness quantifies the relationship between the position of the joint and the torque acting about it [18]. It is an important mechanism used by the body to maintain posture and control movement. Joint stiffness can be separated into two pathways: intrinsic and reflex [2]. Intrinsic stiffness encompasses the mechanical properties of the joint, active muscle and passive, visco-elastic tissues. Reflex stiffness arises from muscle activation in response to the stretch reflex. As yet, there is no consensus on how the CNS modulates stiffness or the role of intrinsic and reflex mechanisms in the control of posture and movement [38, 39, 48, 49]. It is known that intrinsic and reflex stiffness change during movement; however, these changes are difficult to characterize because they occur rapidly and therefore require time-varying (TV) identification techniques. We have developed a time-varying, parallel-cascade (TVPC) identification algorithm capable of separating intrinsic and reflex mechanisms during rapid movements. This paper examines the algorithm's performance under simulated and experimental conditions. We compare the experimental results to those found using an established time-invariant (TI) algorithm [2].

4.3 IDENTIFICATION ALGORITHM

Figure 23 illustrates the parallel-cascade model that describes the intrinsic and reflex contributions to joint stiffness. The intrinsic pathway relates position of the joint to torque via a TV linear dynamic element. The reflex pathway relates velocity of the joint to torque via a differentiator, delay and TV Hammerstein system. The Hammerstein system comprises a static non-linear element in series with a linear, dynamic element. The contribution from each pathway is assumed to add linearly to give the total torque produced by the joint.

To identify this TV model, we use an iterative algorithm in which the two pathways are identified using separate TV techniques based on ensemble methods. This requires the acquisition of an ensemble of input-output records having the same time-varying behaviour. The algorithm proceeds as follows (refer to Figure 23):

1. The input auto-correlation and input-output cross-correlation matrix are estimated at each sample time using data across the ensemble. A nonparametric estimate of intrinsic stiffness is estimated as an impulse response function (IRF) by solving the matrix equation relating the auto-correlation and cross-correlation. The length of the IRF is fixed at a value less than the reflex delay to prevent reflex contamination in the intrinsic estimate. Previous methods used least-squares minimization to solve for the IRF [5]; this was improved for noise resistance and coloured inputs by replacing the matrix equation with a pseudoinverse [6]. The pseudoinverse disregards elements that do not contribute significantly toward the output variance. The process is repeated at each sample time to produce a series of intrinsic stiffness estimates, $P\hat{T}Q(t,\tau)$.
2. $P\hat{T}Q(t,\tau)$ is convolved with the position ensemble to predict intrinsic torque, $T\hat{Q}_I(t,N)$. The intrinsic residual torque is computed as:

   $$T\hat{Q}_{IR}(t,N) = TQ(t,N) - T\hat{Q}_I(t,N)$$
3. The static non-linear, $S\hat{N}L(t,V)$, and linear dynamic, $V\hat{T}Q(t,\tau)$, elements of the reflex pathway are estimated using an ensemble method, treating velocity as the input and intrinsic residual torque, $T\hat{Q}_{IR}(t,N)$, as the output [7]. A correlation approach is used first to obtain initial, nonparametric estimates of the linear subsystem. Then an iterative optimization algorithm is used to produce final estimates of the system parameters. This process is repeated at each sample time to produce a series of nonparametric, Hammerstein system estimates.
4. The non-linear Hammerstein system is used with the differentiated, position input ensemble to generate $T\hat{Q}_R(t,N)$, an estimate of the reflex torque.
5. The total predicted torque is computed as:

   $$T\hat{Q}(t,N) = TQ_I(t,N) + T\hat{Q}_R(t,N)$$
6. To evaluate the quality of the identification, the percent variance accounted for (%VAF) is computed between observed and predicted total torque at each time instant, *i*. In general, the %VAF is computed as:

$$\%VAF = 100\left(1 - \frac{\operatorname{var}\left(X_i - \hat{X}_i\right)}{\operatorname{var}\left(X_i\right)}\right)$$

where X is the true value, and $\hat{X}$ is the predicted value.

7. The procedure is repeated using reflex residual torque to compute $P\hat{T}Q(t,\tau)$, in effect increasing the signal to noise ratio. This is done until successive iterations fail to improve the %VAF.

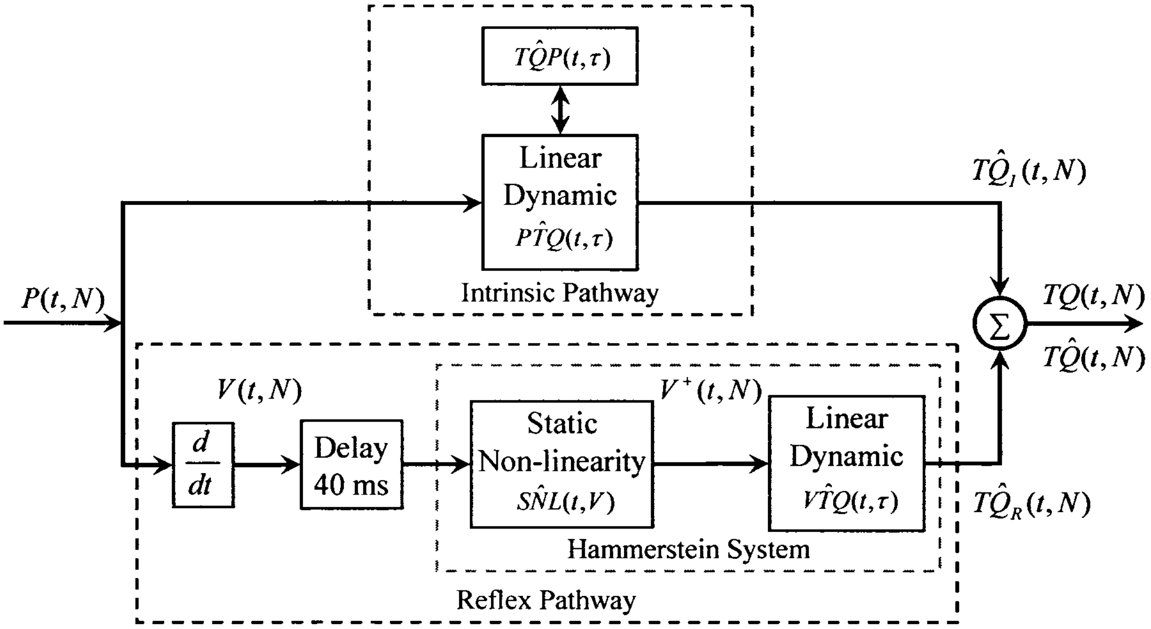

Figure 23. Block diagram showing the time-varying, parallel-cascade model structure used to separate intrinsic and reflex contributions to total ankle torque. Position and torque are a function of time (*t*) and realization (*N*). IRFs are a function of time (*t*) and lag (*τ*).

4.4 SIMULATION STUDY

4.4.1 Methods

We evaluated the identification method using data from simulating a simple model of ankle stiffness. A diagram of the simulation scheme is shown in Figure 24. Second-order parametric models were used to approximate intrinsic and reflex dynamics [2]. Intrinsic stiffness was represented with inertial, *I*, viscous, *B*, and elastic, *K*, elements. Reflex stiffness was represented with gain, *G*, damping, *ζ*, and natural frequency, ω_n elements. The static non-linearity was approximated as a third-order polynomial.

Intrinsic and reflex parameters were varied with time, resulting in TV behaviour of the simulated systems. First *K*, then *G*, and finally *B* underwent a ramp change to half their initial value as illustrated in Figure 27. The simulated coefficients of the third order static non-linearity remained constant in this investigation.

Five hundred, two second pseudo-random binary sequences (PRBS) were generated as the input position ensemble. The input records were convolved with the simulated systems to generate an ensemble of output torque. Figure 25 shows the position input and torque output for several realizations.

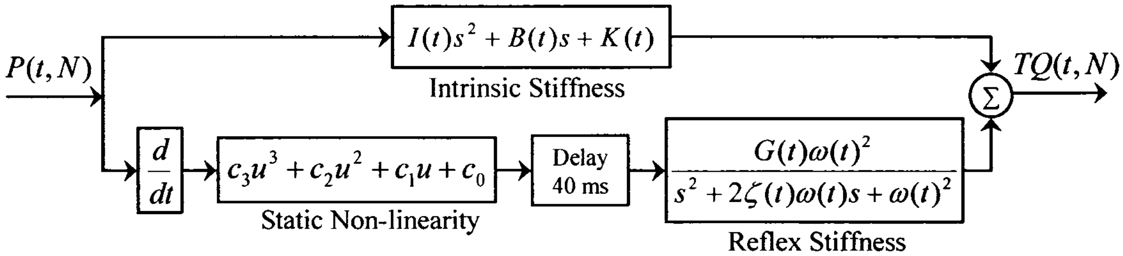

Figure 24: Block diagram showing the simulation scheme used to evaluate the TV parallel-cascade identification algorithm. Intrinsic elasticity (*K*), viscosity (*B*), and reflex gain (*G*) varied with time, while the coefficients of the static non-linearity (c_0, c_1, c_2, c_3) remained constant.

4.4.2 Results

Time-varying, parallel-cascade system identification was performed on the input-output data at a sampling rate of 100 Hz. The identification algorithm yielded excellent results. Several realizations of predicted torque are shown in Figure 25 and overlaid on simulated torque (red traces) to demonstrate near perfect agreement. VAF between simulated and predicted torque was computed at each point in time and the mean value obtained. The mean VAF for intrinsic, reflex and total torque were all greater than 99%. The accuracy and precision of the algorithm was also evaluated by comparing the simulated and estimated systems. At each point in time, the VAF between the simulated and estimated system was computed; VAFs ranged from 97-99.9%.

Figure 26 shows the VAF between simulated total torque and predicted intrinsic and reflex torque as a function of time. These plots illustrate the relative contribution from intrinsic and reflex mechanisms to the total torque. Overlaid on the figure are arrows indicating the range in which simulated parameters *K*, *G* and *B* underwent a ramp change. As intrinsic stiffness decreased, so did the proportion of variance attributed to intrinsic torque, while the VAF for reflex torque increased. Likewise, we see an increase in intrinsic VAF as reflex gain and VAF decreased. Changes in intrinsic viscosity had no visible influence on the torque variance for intrinsic or reflex mechanisms.

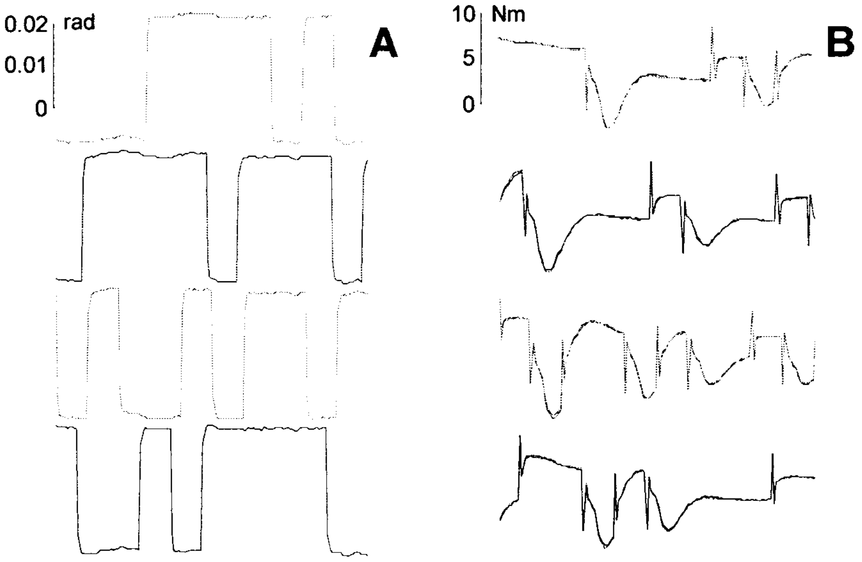

Figure 25: Several realizations of input position (A) and output torque (B) used for system identification in the simulation study. Predicted torques are overlaid on simulated torques (shown in red) to illustrate excellent agreement between the signals.

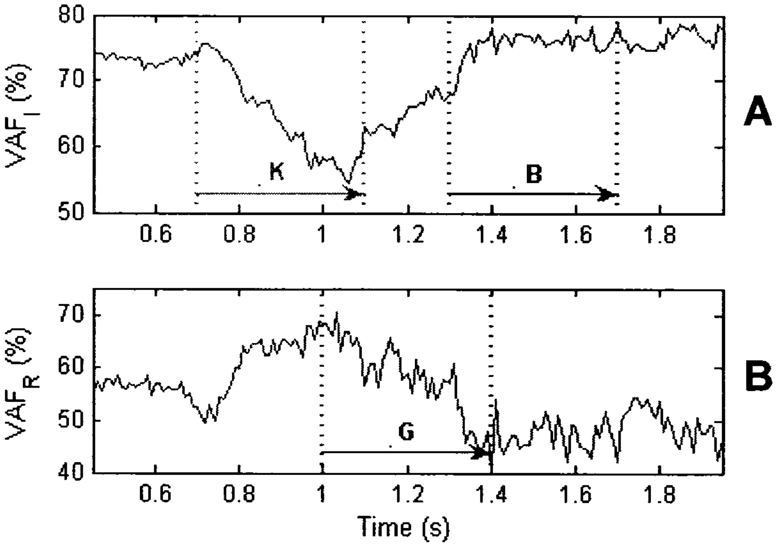

Figure 26: %VAF between predicted total torque and (A) predicted intrinsic torque, (B) predicted reflex torque. This figure illustrates the relative contribution from intrinsic and reflex mechanisms at each point in time. Ramp changes in *K*, *G* and *B* are denoted by arrows on the figure.

4.4.3 Parametric Fits

The parametric equations used to simulate intrinsic and reflex dynamics were also fit to the IRF estimates. The time-varying properties of each system were extracted from these fits. Intrinsic dynamics were parameterized by first inverting intrinsic stiffness, $P\hat{T}Q(t,\tau)$, to obtain compliance, $T\hat{Q}P(t,\tau)$, then applying a Levenberg-Marquardt non-linear, least-square fit algorithm to find the second-order, low-pass system relating torque to position. Intrinsic compliance was fit rather than stiffness, because the IRFs were causal, whereas stiffness IRFs were anti-causal. Reflex stiffness was parameterized using the second-order, low-pass system relating rectified velocity to torque. Figure 27 shows the recovered time-varying parameters for the estimated systems. Recall that *K*, *B*, and *G* underwent a ramp change to half their initial value. It is clear from these results that the identification algorithm correctly tracked the TV properties of the simulated systems with no *a priori* information of the TV behaviour.

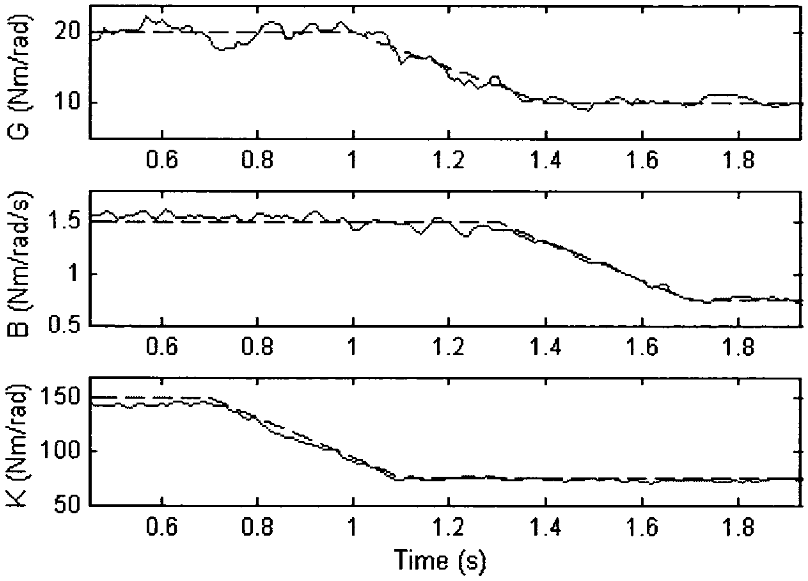

Figure 27: Intrinsic and reflex second-order parameter estimates. Estimated parameters are shown in solid and simulated in dashed. Only those parameters that varied with time are shown: reflex gain (*G*), intrinsic viscosity (*B*), and intrinsic elasticity (*K*).

4.4.4 Additive Noise

To simulate noisy conditions, Gaussian white noise was added to the output signals at various signal-to-noise ratios (SNR). The input signals and noisy output signals were used to identify TV intrinsic and reflex systems. VAF between simulated and predicted total, intrinsic and reflex torque were computed for each level of additive noise. Figure 28 shows the quality of identification as a function of SNR. The identification algorithm returned good system estimates above 10dB SNR, demonstrating that the time-varying, parallel-cascade method is capable of producing very good results even in the presence of significant output noise. These results provide an upper bound for the parallel-cascade algorithm, which typically accounts for 80-90% of the torque variance during stationary studies with an approximate SNR of 19 dB.

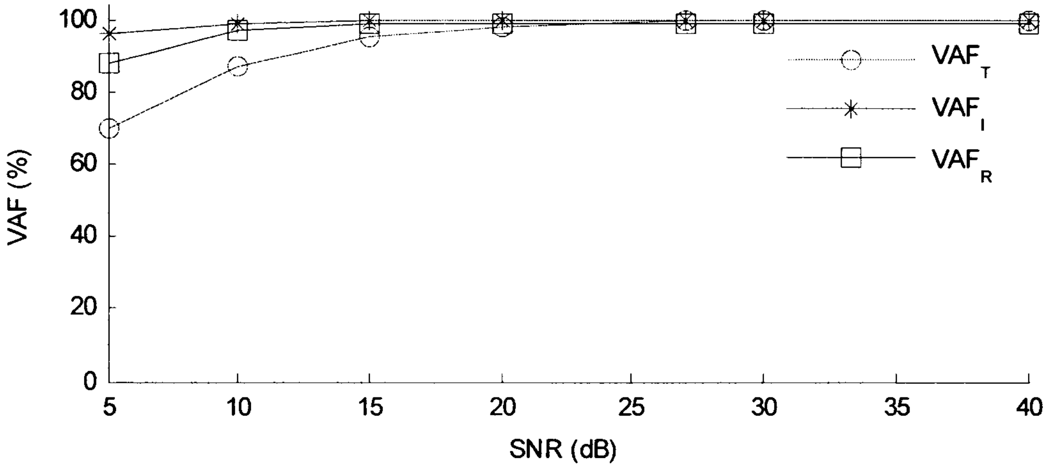

Figure 28: Mean VAF between simulated and predicted torque as a function of SNR. (Red circles) Total torque; (Blue stars) Intrinsic torque; (Black squares) Reflex torque.

4.5 EXPERIMENTAL STUDY

The algorithm was tested with real data to further validate its ability to predict intrinsic and reflex dynamics during experimental conditions. For example, background noise due to variable levels of voluntary activation was expected to adversely affect the quality of identification. To provide a benchmark for the experimental results, we employed a time-invariant paradigm where the dynamic properties of the joint were stationary. This enabled us to compare the TV identification results to that of our established TI algorithm.

4.5.1 Apparatus

Subjects laid supine with their ankle attached to an electro-hydraulic actuator by means of a custom made fibreglass boot. Their leg was immobilized and ankle movement restricted to plantarflexion and dorsiflexion. Perturbations were applied to the subject's ankle and measured with a potentiometer (BI Technologies 6273). Torque produced in response to the perturbations was measured with a torque transducer (Lebow 2110-5K). Position and torque were sampled at 1 kHz using a NI-4472 data acquisition card.

4.5.2 Experimental Paradigm and Post-processing

Three normal male subjects were examined. Subjects were required to provide a constant level of voluntary activation by maintaining a tonic 5 Nm contraction of the gastrocnemius-soleus. Subjects were assisted by a visual feedback displaying low-pass filtered torque.

Small amplitude PRBS perturbations of 0.03 rad peak-to-peak were applied to the subject's ankle about the optimal operating point for reflex activity. System dynamics were assumed to remain constant at perturbations of this magnitude [59]. The perturbations were applied continuously for 5 minute periods, followed by a 1 minute rest period. This was repeated 3-5 times resulting in a total of 15-30 minutes of position and torque data. The data was then decimated to 100 Hz and analyzed in two ways: First, we used a stationary, time-invariant (TI) algorithm. Second, we segmented the data into a series of 3 second trials and treated as if it were an ensemble of responses to a time-varying (TV) condition. The data ensemble for subject TG, CB, and BE consisted of 1011, 1084, and 1050 realizations respectively.

4.5.3 Identified Systems

The time-varying, parallel-cascade algorithm produced a system estimate of intrinsic stiffness, intrinsic compliance, reflex stiffness, and static non-linearity at each 10 ms time increment. Figure 29 shows the 3D portrayal of these estimates for Subject TG. TV IRFs are a function of '*lag*' and '*time*', since the time-varying method tracks system dynamics at each point in time. Similarly, an estimate of the reflex SNL was produced at each time increment. By examining the dynamics along the time axis, we see that the IRFs and SNL are all alike. This was expected since the experiment operated under time-invariant conditions, which means there was no larger movement invoking TV system dynamics. Therefore, the system estimates confirm stationary behaviour.

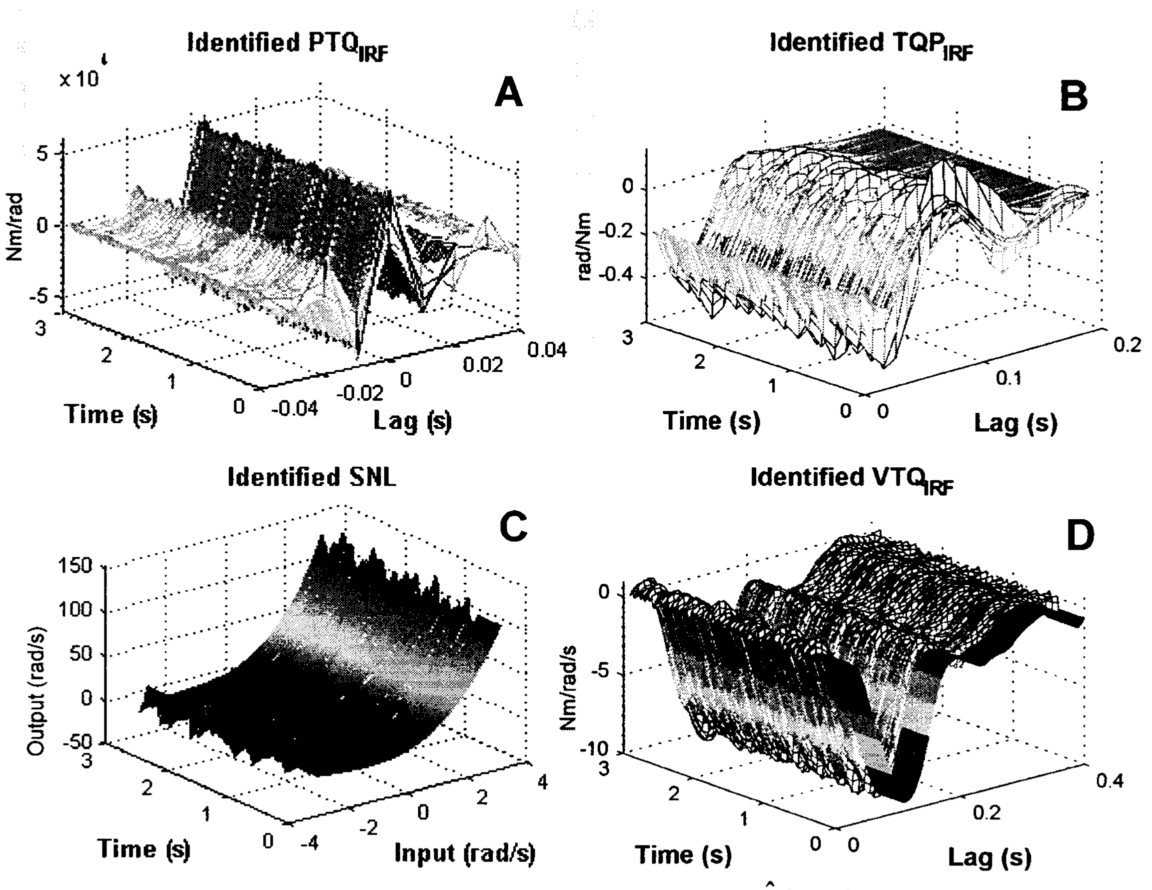

Figure 29: Identified time-varying systems. (A) Intrinsic stiffness, $P\hat{T}Q(t,\tau)$; (B) Intrinsic compliance, $T\hat{Q}P(t,\tau)$; (C) Reflex static non-linearity, $S\hat{N}L(t,V)$; (D) Reflex stiffness, $V\hat{T}Q(t,\tau)$.

4.5.4 Predicted Torque

The VAF between observed and predicted total torque was computed and the mean value obtained. The relative contribution of the intrinsic and reflex pathway to total torque was evaluated as the VAF between total torque and predicted intrinsic and reflex torque, respectively. Table 1 outlines the mean VAF between predicted and observed torque for all three subjects. On average, the intrinsic pathway contributed anywhere from 27 to 62% of the total variance for this type of input displacement. The reflex pathway also contributed anywhere from 29 to 66% of the total variance, indicating there was significant subject-to-subject variability. However, we see from the total torque VAF that the TV algorithm produced good predictions of torque for all three subjects. The output variance unaccounted for may be attributed to modelling error or additional noise sources such as variable levels of voluntary contraction.

Table 1: Mean VAF for Predicted and Observed Torque

Torque VAF (%)		Subject		
		TG	CB	BE
TQ_I	mean ± std	27 ± 3	62 ± 3	36 ± 5
TQ_R	mean ± std	66 ± 2	29 ± 6	41 ± 4
TQ_{Total}	mean ± std	81 ± 1	75 ± 1	72 ± 2

4.5.5 TV versus TI System Identification

The TV system estimates were averaged to produce a mean intrinsic stiffness, compliance, reflex stiffness and static non-linearity. TI estimates were computed using the same data as the TV analysis, however, prior to segmenting into the input-output ensemble. The mean TV systems were compared with those produced by the TI analysis. The TI and mean TV system estimates for Subject TG are shown in Figure 30; the estimates are in close agreement, with nearly 100% VAF for each system. The VAF was equally high for Subjects CB and BE with values ranging from 87-99%. This indicates that the TV method is capable of identifying reflex and intrinsic mechanisms consistent with our established TI method.

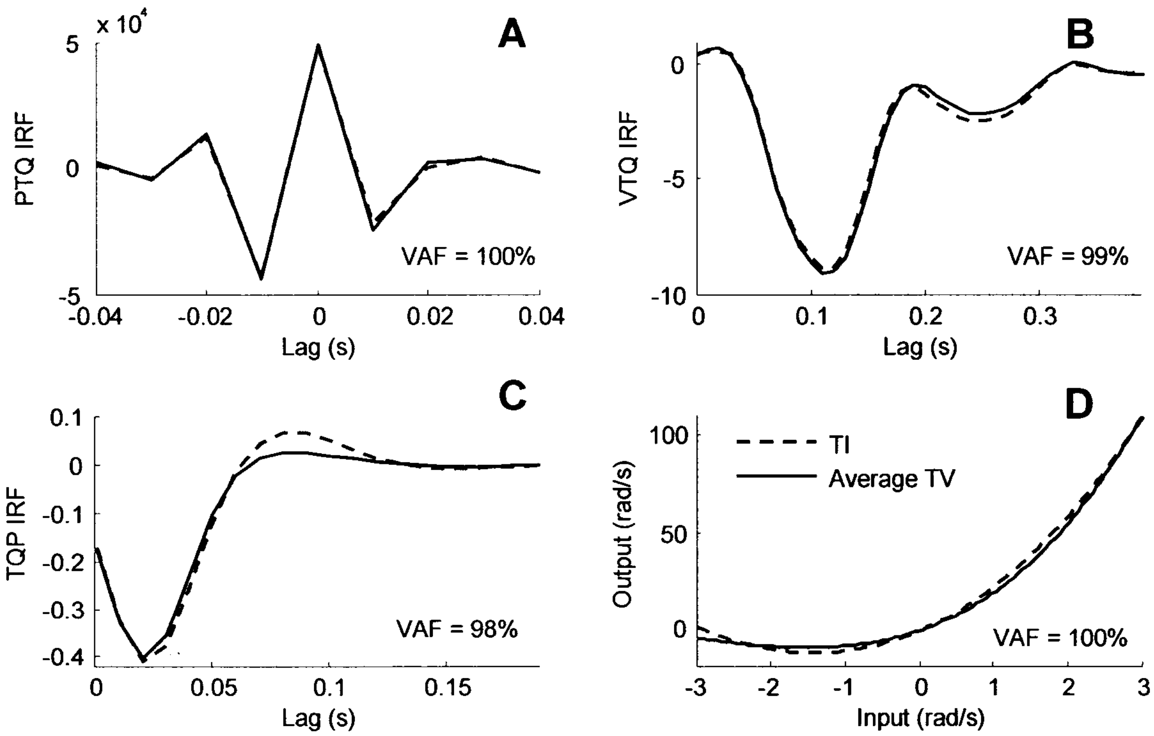

Figure 30: Estimated TI systems (dashed) and mean TV systems (solid). (A) Intrinsic stiffness, $\hat{PTQ}$; (B) Intrinsic compliance, $\hat{TQP}$; (C) Reflex stiffness, $\hat{VTQ}$; (D) Static non-linearity, $\hat{SNL}$.

4.5.6 Identification versus Ensemble Size

TV system identification was performed using various ensemble sizes to determine the amount of data required for future experiments. Data from Subject TG was used for this analysis. The VAF between predicted and observed total, intrinsic and reflex torque were examined as a function of ensemble size. Figure 31 illustrates the mean VAF and standard deviation (shown as error bars) for ensemble sizes ranging from 250 to 1011 realizations. A TI analysis was also conducted as a target for the TV results. It is clear from Figure 31 that the average TV estimates of torque variance converged to the TI results for ensemble sizes greater than 600 realizations. In true time-varying conditions, more than 1000 realizations should be used to ensure reliable results.

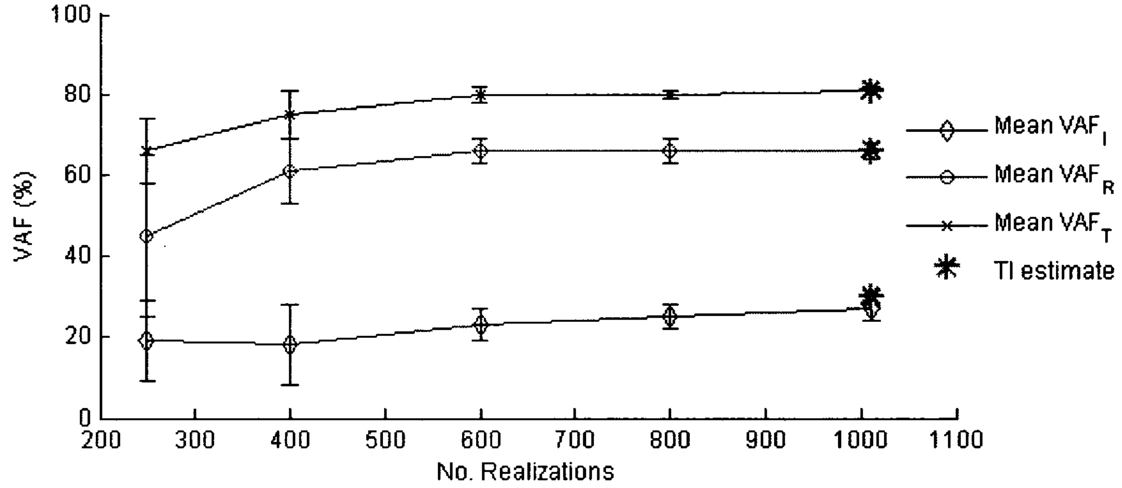

Figure 31: Mean VAF for predicted and observed torque versus ensemble size. Mean TV values converge to TI values at 600+ realizations. Error bars represent the standard deviation of the VAF for TV estimates.

4.6 DISCUSSION

Few methods exist to examine the time-varying behaviour of joint dynamics. Ensemble methods are one such approach that have been found to provide robust results for several biological systems [55, 58, 61]. The approach, pioneered by Soechting [61], initially imposed strict requirements on the synchronization between the input sequence and TV behaviour. Our lab successfully developed a least-squares method for identifying TV system dynamics that placed few conditions on the input signal [5]. The nonparametric approach was based on the singular value decomposition (SVD) of the input ensemble, estimating system dynamics as TV IRFs. The technique was later improved for noise resistance and coloured inputs by employing a pseudoinverse in the algorithm [6]. A similar ensemble method was developed for Hammerstein systems, intended to identify reflex dynamics during TV conditions [7]. These methods used in conjunction with a parallel-cascade model for dynamic joint stiffness [2], enable the simultaneous identification of intrinsic and stretch reflex dynamics during time-variant movements.

The present study demonstrates that the time-varying, parallel-cascade method is capable of tracking rapid changes in intrinsic and reflex stiffness and produces reliable nonparametric estimates of system dynamics. Simulation studies confirmed that the identification algorithm correctly tracked the TV properties of the simulated systems with no *a priori* information of the TV behaviour (Figure 27). Indeed, the VAF between simulated and identified systems exceeded 97%, while the VAF between simulated and predicted torque was 99%. Moreover, the algorithm produced reliable estimates in the presence of considerable output noise (Figure 28) resembling experimental conditions.

The experimental study, conducted under stationary conditions, enabled us to assess the quality of system identification with real data. Time-varying estimates of intrinsic and reflex dynamics were computed at each 10 ms time increment. Stationary behaviour was confirmed since the estimates were constant along the time axis (Figure 29). Considerable subject-to-subject variability was observed in the relative contribution from intrinsic and reflex mechanisms to total torque VAF, which spanned 35 and 37%, respectively. However, the total torque VAF was high for all three subjects, indicating that the algorithm produced good predictions of torque. Output noise sources, likely due to fluctuating levels of voluntary muscle activation, contributed 19-30% of the torque variance. Average TV estimates were consistent with those computed using an established TI method and results converged for ensemble sizes exceeding 600 realizations (Figure 30 and Figure 31).

The next stage in validating the time-varying, parallel-cascade algorithm will examine intrinsic and stretch reflex dynamics during a large imposed movement. Large amplitude inputs elicit time-varying properties within the ankle joint, which will be identified using the TVPC algorithm.

5 Identification of Time-varying Intrinsic and Reflex Joint Stiffness: Imposed gait movement

Chapter 5 applies the TVPC method to examine joint dynamics during an imposed gait movement. This study confirms the method's ability to track changes in joint dynamics with no *a priori* information of the time-varying behaviour. The modulation of intrinsic and reflex properties is examined throughout the movement and compared with similar studies. The results of this study motivate the need for additional time-varying experiments.

Identification of Time-varying Intrinsic and Reflex Joint Stiffness: Imposed gait movement

Heidi Giesbrecht, Robert E. Kearney

Target Journal:
IEEE Transactions on Neural Systems and Rehabilitation Engineering

5.1 ABSTRACT

We examined time-varying intrinsic and reflex dynamics of the human ankle joint while imposing a gait movement similar to 1.5 km/hr walking. The subject was relaxed during the course of the experiment. An ensemble of input-output data having the same time-varying behaviour was acquired and analyzed using the time-varying, parallel-cascade algorithm. Joint dynamics were estimated as time-varying IRFs, which tracked changes in intrinsic and reflex properties throughout the imposed movement. The algorithm successfully predicted intrinsic and reflex mechanisms with 92% mean VAF between predicted and observed torque. Intrinsic mechanisms dominated during the movement, but stretch reflexes periodically contributed small amounts toward torque generated at the ankle. The low reflex activity for this experiment may be attributed to the large mean absolute velocity and the passive experimental conditions. Time-varying results were compared with steady-state data, which suggested that stretch reflexes contributed less toward torque during movement than at matched operating positions. This pilot study confirmed the TVPC algorithm's ability to track rapid time-varying changes in joint dynamics during a large imposed movement.

5.2 INTRODUCTION

The role of stretch reflexes in maintaining posture and executing movement is an ongoing topic of debate despite the apparent simplicity of the monosynaptic pathway connecting spindle afferents to motoneurons [19, 20]. Many groups have attempted to evaluate the behaviour of the stretch reflex using various methods such as EMG recordings [15], surgical deafferentation [27, 28], nerve blocks [29, 30], or electrical stimulation [19, 31]. Studies have shown that the stretch reflex response in the human ankle nonlinearly depends on the amplitude and bandwidth of joint displacement [2, 34], mean ankle position [35, 36] and level of voluntary drive [15].

The Hoffman, or H-reflex is commonly used to examine the role of reflexes during movement. The H-reflex is evoked by direct electrical stimulation of the Ia afferent fibres, which excites the motor neuron pool giving rise to a monosynaptic reflex response [41]. The H-reflex was found to vary in amplitude throughout walking [41-43], beam balancing [44], running [39], and cycling [45-47]. H-reflexes are often reported smaller during movement compared to matched postures [43].

In general, the stretch reflex and H-reflex exhibit similar characteristics; however, the H-reflex reflects the excitability of the motor neuron pool, whereas the stretch reflex reflects a combination of motor neuron excitability with muscle receptor sensitivity. The sources of modulation may differ because the H-reflex does not depend on peripheral effects such as fusimotor excitation [41, 42]. Alternatively, many researchers have focused on EMG to measure stretch reflexes [51, 52, 65, 72] and found that reflexes were substantially modulated for a variety of tasks and movements. Kearney *et al.* examined the stretch reflex response during an imposed gait movement and found reflex EMG was significantly lower during movement than at matched stationary positions throughout the walking cycle [52]. Kirsch *et al.* imposed a rapid ramp movement at the ankle joint while subjects maintained various levels of tonic muscle activation. Results suggested that stretch reflex properties were modulated independently of motor neuron pool activation level and the behaviour was largely mediated by peripheral mechanisms [57].

One of the major difficulties in determining the functional role of stretch reflexes is distinguishing reflex activity from the intrinsic properties of the joint and muscle [2]. Reflex EMG alone does not provide insight into the mechanical effects of reflexes [52] and therefore, simultaneous analysis of intrinsic and reflex mechanics is required to fully describe the functional role of the stretch reflex. Our lab previously developed a parallel-cascade, nonlinear system identification method to separate intrinsic and reflex contributions to dynamic ankle stiffness [1]. The parallel-cascade model relates the position of the ankle to torque via two separate pathways, representing intrinsic and reflex mechanics. The technique was successfully used to predict joint dynamics for a variety of operating conditions for both normal and spastic spinal cord injured (SCI) subjects [1, 3, 4].

The method relied on stationary (time-invariant) methods to evaluate intrinsic and reflex properties at a specific operating condition, such as a particular posture or contraction level. However, this technique cannot be used to evaluate reflexes during movement, because movement can not be treated as an assembly of operating points—the motion itself tends to change the system dynamics. Recently, the parallel-cascade method has been extended to the time-varying case to allow for simultaneous identification of intrinsic and reflex mechanisms during movement [8]. Each pathway uses a separate ensemble method to identify system dynamics as time-varying impulse response functions relating ankle position to torque [6, 7]. Chapter 4 demonstrated the algorithm's ability to accurately predict joint dynamics during realistic simulated and experimental conditions.

In the present study, we examined the time-varying properties of intrinsic and reflex dynamics during an imposed gait sequence equivalent to 1.5 km/hr walking speed. Ensemble, time-varying techniques were used in conjunction with the parallel cascade method, to separately identify intrinsic and reflex dynamics as time-varying impulse response functions. One thousand cycles of recorded position and torque were used to generate the input-output data ensemble for system identification. The technique produced a nonparametric estimate of intrinsic and reflex dynamics at each point throughout the time-varying motion.

5.3 METHODS

5.3.1 Apparatus

Subjects lay supine with their left foot attached to a rotating foot pedal via a custom-made fibreglass boot. The foot pedal was controlled by an electrohydraulic actuator, which rotated the subject's ankle in the plantar and dorsiflexion direction. Motion at the knee joint was restricted by a strap placed over the lower thigh. The actuator was controlled by a proportional position servo using xPC Target, a real time digital signal processing system. Three safety mechanisms were implemented to prevent the actuator from moving beyond the subject's comfortable range of motion: (1) mechanical stops were placed at the plantar and dorsiflexion limits of the test subject, (2) a flow bypass valve cut hydraulic fluid to the actuator when rotations approached the subject's ROM, and (3) a panic button disabled the hydraulic actuator, leaving the pedal in a pliable state when activated.

Position, torque, gastrocnemius EMG and tibialis anterior EMG were sampled at 1 kHz by a dynamic signal acquisition card (National Instruments, 4472). Anti-aliasing was performed by the card, which over-sampled the data and then applied a digital brick wall filter with a cut-off frequency of 486.3 Hz. Position and torque were then decimated to 100 Hz for the purpose of system identification.

5.3.2 Experimental Procedure

One female subject, with no known history of neuromuscular disease, was studied in detail. The subject was 25 years old. The subject gave informed consent to the experimental procedure, which was approved by the McGill University Research Ethics Board (see Appendix A).

5.3.2.1 Position Inputs

Two types of inputs were applied to the subject's ankle: a small amplitude perturbation intended to stimulate the joint for system identification, and a large amplitude periodic sequence used during time-varying experiments:

i. PRBS PERTURBATION: The perturbation consisted of continuous pseudo-random binary sequence (PRBS) displacements with 0.0375 rad peak-to-peak amplitude and 200ms switching interval.

ii. TIME-VARYING GAIT: The time-varying trajectory was equivalent to walking at 1.5 km/hr, with 0.44 rad peak-to-peak amplitude and mean absolute velocity (MAV) equal to 0.5283 rad/s. The period for one cycle was 2340 ms. The input trajectory was obtained in a previous set of experiments in which ankle position was recorded while a subject walked on a treadmill [52]. Several cycles of data were collected and subsequently averaged to obtain the gait sequence used here. Figure 33-A illustrates two cycles of the time-varying sequence applied to the subject's ankle.

5.3.2.2 Trials

Both stationary and time-varying experiments were conducted. The results from the stationary trials were compared with the time-varying experiments at matched operating positions. The following data sets were acquired:

i. STATIC TRIALS: Time-invariant dynamics were assessed through a series of stationary trials conducted at various operating positions throughout the subject's range of motion. At each position, PRBS perturbations were applied to the subject's ankle for 60 seconds while the subject remained relaxed.

ii. TIME-VARYING GAIT: Time-varying intrinsic and reflex dynamics were analyzed during an imposed gait cycle while the subject remained relaxed. PRBS perturbations were superimposed on the larger, walking movement for the purpose of system identification. Cycles ran continuously and trials lasted five minutes. The subject was then given a short break before proceeding with the next trial for a total of ten sets of trials and approximately 1280 cycles.

5.3.3 Time-Varying Analysis

The continuous stream of time-varying data was segmented into an ensemble of input-output pairs—each realization composed of two time-varying cycles. To maximize the number of realizations in the ensemble, the second cycle of data was used as the first in the following realization. This form of bootstrapping was acceptable, since the time-varying analysis was conducted across the ensemble.

The subject was instructed to remain relaxed while the TV movement was applied to her ankle. If done correctly, each trial in the ensemble should have exhibited the same time-varying behaviour. However, due to the lengthy acquisition process, the subject inevitably adjusted her resting position or contraction, which resulted in several atypical trials. The quality of system identification relied on the assumption that each trial in the ensemble was consistent. Therefore, outlying trials within the ensemble were identified by a trial selection process, which proceeded as follows:

1. The ensemble average was computed by taking the mean torque at each time throughout the TV movement.
2. The ensemble average was removed from each realization to produce residual torque.
3. The standard deviation (SD) of residual torque was computed for each realization and sorted in ascending order, shown in Figure 32.
4. Trials corresponding to significant outliers were discarded, by selecting a threshold SD (shown as a dashed line in Figure 32). A cut-off value of 1.7 Nm was chosen to produce an ensemble with consistent time-varying behaviour. The resulting ensemble was composed of 1111 realizations.

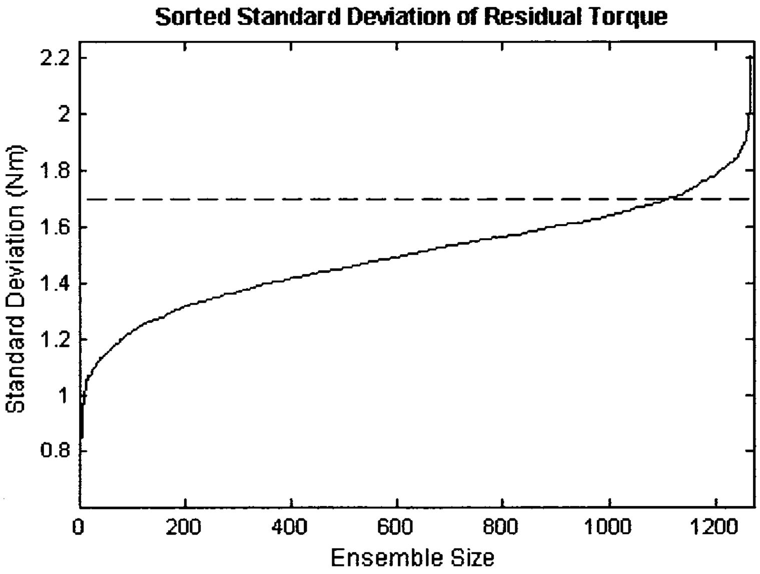

Figure 32: Standard deviation of residual torque sorted in ascending order. Realizations beyond the tolerance level (dashed line) were discarded.

Trials within the selected ensemble were processed by removing the ensemble average from both the position and torque traces. This step removed the larger time-varying process from the input-output traces, but preserved the perturbation excitation and response used for system identification. The time-varying, parallel-cascade algorithm was then applied to the input-output data to identify intrinsic and reflex dynamics. The algorithm was described in the preceding manuscript and briefly reviewed here. A parallel-cascade model was used to separate intrinsic and reflex mechanisms into two pathways. The intrinsic pathway related position of the joint to torque via a TV linear dynamic element. The reflex pathway related velocity of the joint to torque via a differentiator, delay and TV Hammerstein system. The contribution from each pathway was assumed to add linearly to give the total torque produced by the joint. An iterative algorithm was used to independently identify the systems using separate TV techniques based on ensemble methods. Input auto-correlation and input-output cross-correlation matrices were estimated at each sample time using data across the ensemble. Intrinsic stiffness and its inverse, compliance, were estimated as TV impulse response functions (IRFs). The reflex Hammerstein system was estimated as a TV static non-linearity in series with a TV IRF. The algorithm alternated between the two pathways until successive iterations failed to improve the %VAF between observed and predicted torque.

5.3.4 Parametric Fits

Physically meaningful parameters representing intrinsic and reflex mechanics were generated by fitting a parametric model to the estimated IRFs. Intrinsic dynamics were parameterized by first inverting intrinsic stiffness to obtain compliance, then applying a Levenberg-Marquardt non-linear, least-square fit algorithm to find the second-order, low-pass system relating torque to position. Intrinsic compliance was used rather than stiffness, because the time-varying properties of interest (viscosity and elasticity) were more evident in the low-pass representation of intrinsic mechanics. Furthermore, intrinsic stiffness was anti-causal, making it difficult to interpret the physical significance. The low-pass model used to generate the intrinsic fits was of the form [2]:

$$TQP(s) = \frac{\theta(s)}{TQ_I(s)} = \frac{1}{Is^2 + Bs + K}$$

where $\theta(t)$ is the joint angular position, $TQ_I(t)$ is the joint torque related to intrinsic mechanisms, and I, B and K are inertial, viscosity, and elasticity parameters, respectively. The fitting procedure was applied to each IRF throughout the TV movement. The time-varying, intrinsic properties were then extracted from the parametric fits. Estimates of inertial, viscous, and elastic terms were retrieved and compared with matched stationary values. Stationary parametric estimates were obtained using the same parametric model fit to the intrinsic estimates from the static trials.

The following second-order model was used to generate parametric fits for reflex stiffness [2]:

$$VTQ(s) = \frac{TQ_R(s)}{V^+(s)} = \frac{G\omega_2^2}{\left(s^2 + 2\zeta\omega_2 s + \omega_2^2\right)\left(s + \omega_1\right)}$$

where $V^+(t)$ is the rectified joint angular velocity, $TQ_R(t)$ is the joint torque related to reflex mechanisms, and G, ζ, ω_1 and ω_2 are the gain, damping, and frequency parameters, respectively. The fitting procedure was applied to the reflex stiffness IRFs in the same manner as for intrinsic fits—at each sample time throughout the time-varying movement. Stationary reflex estimates were not available for comparison with time-varying results at the time.

5.4 RESULTS

5.4.1 Time-Varying Gait

Figure 33 shows two cycles of position and torque data. Figures A-B display the ensemble averages, while Figures C-D show four realizations extracted from the ensemble. The PRBS perturbations and corresponding torque responses are visible as pronounced inflections superimposed on the larger time-varying process. The ensemble averages reflect only the repeated time-varying behaviour since the PRBS was a random process. Therefore, when computing the mean across the ensemble, the perturbations averaged to zero leaving behind the time-varying process. Note that this procedure only applies when each realization in the ensemble reflects the same time-varying behaviour.

The repeating motion was composed of the primary phases of natural gait—stance and swing, delimited by heel-strike (HS) and toe-off (TO). The cycle was imposed at the subject's ankle to emulate gait while the subject was supine and relaxed. The trace began during a period of steady dorsiflexion lasting ~1000 ms, corresponding to the stance phase of walking. Maximum deflection marked the transition from stance to swing (TO), at which point the ankle underwent a rapid, 400 ms plantar flexion (downward deflection) to return to the original plantar flexed position. The ankle then dorsiflexed slightly and remained at a nearly constant position until heel-strike (HS), at which point the ankle briefly plantar flexed until a large dorsiflexion stretch was initiated during stance.

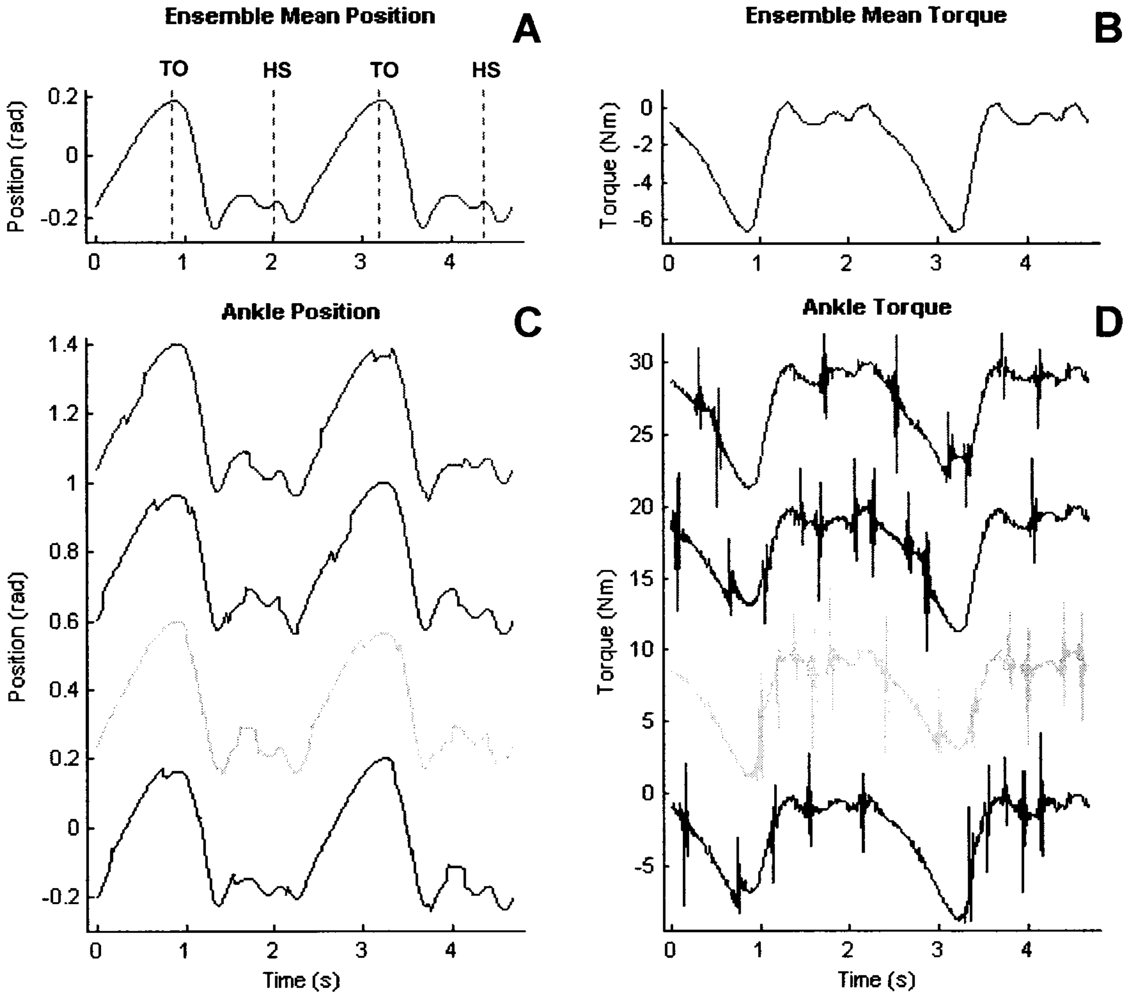

Figure 33: Position and torque. (A) Ensemble mean position; (B) Ensemble mean torque; (C-D) Four position traces and corresponding torque responses extracted from the input-output ensemble.

5.4.1.1 Identified Systems

Figure 34 illustrates the time-varying intrinsic and reflex system estimates obtained from the TV data. Intrinsic stiffness was estimated as a two-sided, 40 ms IRF. Intrinsic compliance and reflex stiffness were estimated as single-sided IRFs of length 200 ms and 400 ms, respectively. The reflex static non-linearity defined the relationship between input and output velocity. Horizontal axes for IRFs are marked '*Lag*' and '*Time*', since the time-varying method produced system estimates that tracked dynamics at each point in time throughout the imposed movement. Due to start-up transients, the first set of estimates corresponding to the IRF lag length was null.

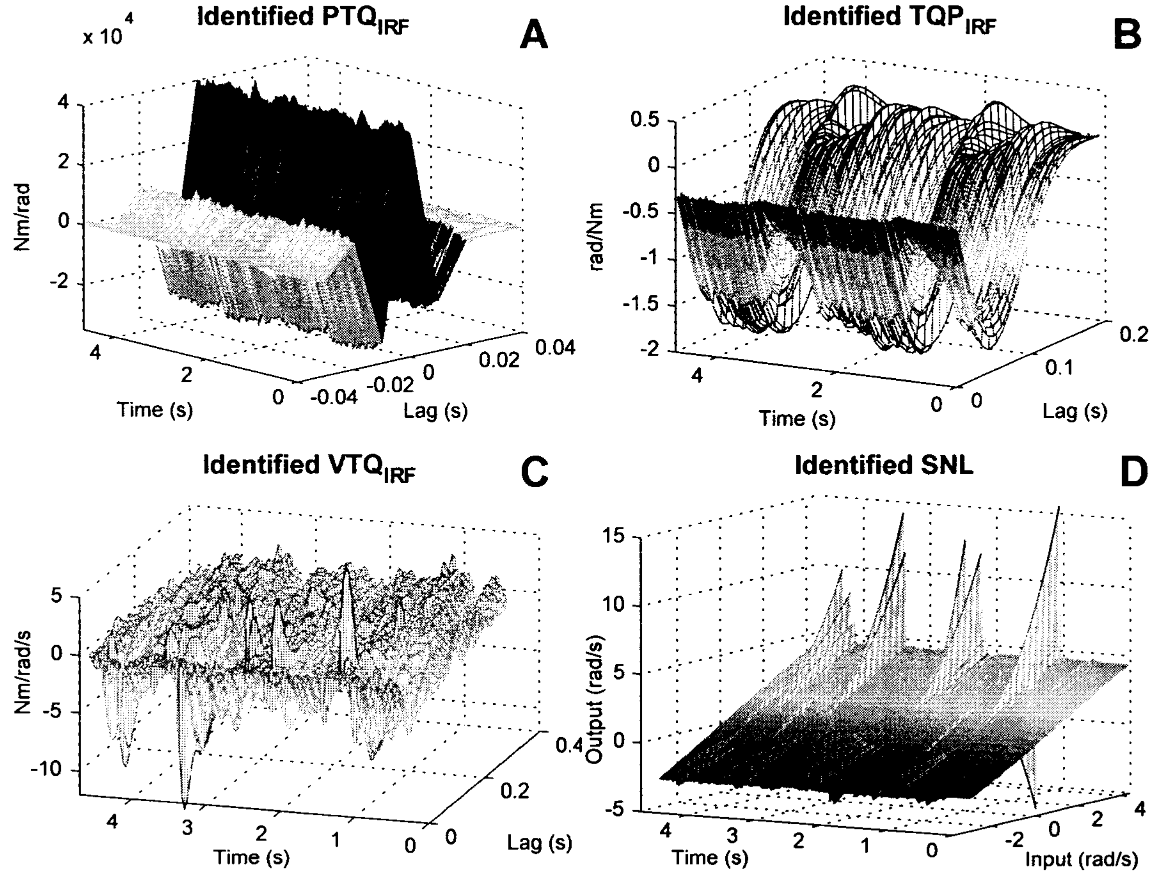

Figure 34: Identified time-varying systems. (A) Intrinsic stiffness; (B) Intrinsic compliance; (C) Reflex stiffness; (D) Reflex static non-linearity.

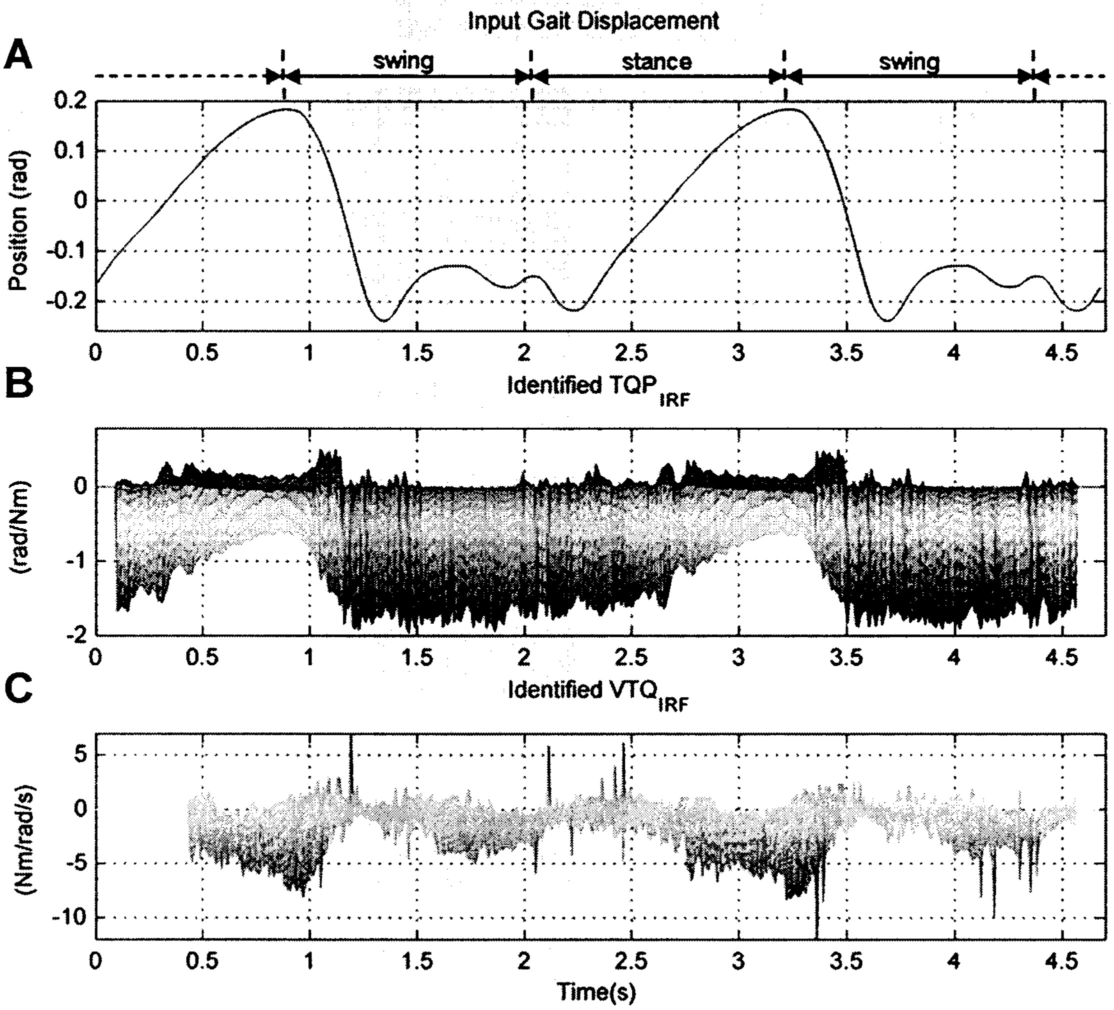

Figure 35: Time-varying position and estimated, nonparametric IRFs. (A) Imposed gait sequence; (B) 2-dimensional view of intrinsic compliance and (C) reflex stiffness illustrating the time-varying changes in ankle dynamics with respect to the movement trajectory.

Time-varying modulations are most evident in the 2-dimensional view of intrinsic compliance and reflex stiffness (Figure 35). These figures chart the time-varying changes in ankle dynamics with respect to the movement trajectory. Here we see significant variation in the compliance estimates correlated with the gait trajectory. Compliance was reduced markedly during periods of increased dorsiflexion, corresponding to the late stance and early swing phase of gait. There are no observable changes in intrinsic compliance during the late swing phase, when the ankle was plantar flexed.

Figure 35 also shows modulation of reflex stiffness, which often complemented intrinsic compliance: during dorsiflexion, reflex stiffness increased while intrinsic compliance decreased. The largest contribution from reflexes occurred at the point of maximum dorsiflexion. This position corresponded to the transition from stance to swing in the emulated trajectory. Elevated levels of reflex stiffness are also seen during the late swing phase of the movement (1600-2000 ms), when the ankle maintained a slightly plantar flexed position prior to heel-strike. At corresponding positions during swing (1250 ms) and stance (2400 ms) reflex stiffness was minimal, which suggests that it was phase-modulated. There was no corresponding change in intrinsic compliance during this period. The SNL emerged during periods of increased reflex stiffness. The polynomial function somewhat resembled a half-wave rectifier often used to represent the unidirectional sensitivity of stretch receptors. At all other times, the SNL defined a linear relationship between input and output velocity.

5.4.1.2 Predicted Torque VAF

Predicted torques were produced by applying time-varying convolution to the input position ensemble and time-varying system estimates. Figure 36 shows four realizations of recorded input position, output torque and predicted torque. Ensemble means have been removed from the torque traces for clarity. Predicted torques were in excellent agreement as shown by the superimposed recorded torque (displayed in red). Clearly, intrinsic and reflex mechanisms were predicted well in the estimated responses.

Figure 37 shows the percent VAF between observed and predicted total, intrinsic and reflex torque as a function of time. Results are plotted for one gait cycle between 2000 and 4340 ms. The mean VAF for total torque was 92%, which quantitatively indicates that the algorithm predicted total torque well. The total VAF dropped during a period between 2500 and 3500 ms, which mirrored an increase in reflex VAF (Figure 37-D). This period corresponded to the late stance and early swing phase of the input trajectory in which we saw increased reflex stiffness. This suggests that as reflexes contributed toward torque at the ankle, the algorithm's ability to predict torque diminished. The maximum VAF attributed to reflex torque was 10.6%, which occurred at 3270 ms. The proportion of intrinsic torque to total torque is reflected in Figure 37-C, where it shows clearly that intrinsic mechanisms dominated during this movement for relaxed conditions.

Data from static trials were used to determine the intrinsic and reflex dynamics at matched, stationary operating positions throughout the gait movement. Parallel cascade identification was applied to the stationary data in a manner equivalent to the time-varying method. Overlaid on the VAF plots are the corresponding stationary results at matched operating positions (displayed as stars). The tendency for VAF to decrease during elevated reflex activity is also evident in the static results (Figures B-C). Reflexes contributed less to torque generated at the ankle during movement compared to matched postures (Figure D). Furthermore, we see that at matched positions throughout the movement the time-varying, VAF was irregular, whereas the steady-state results were fixed. For example at 3000 ms the VAF equalled 4.3%, whereas at 3356 ms the VAF equalled 8.4%, despite being at the same absolute position of 0.144 rad. This inconsistency between matched positions suggests that reflexes were phase-modulated.

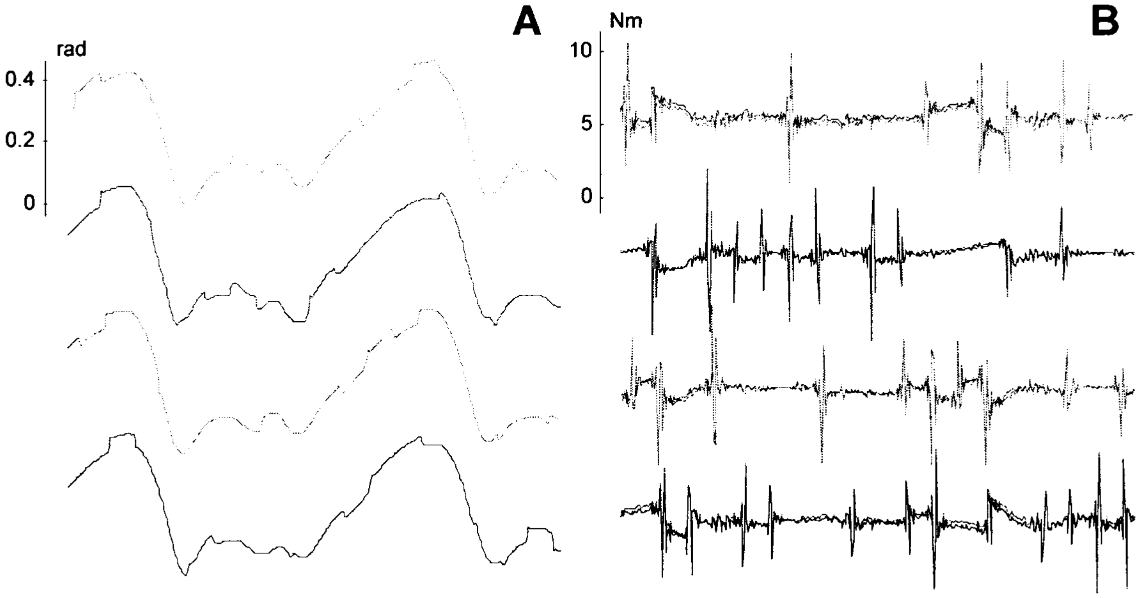

Figure 36: (A) Four realizations of recorded input position; (B) Corresponding realizations of predicted torque overlaid on observed torque in red.

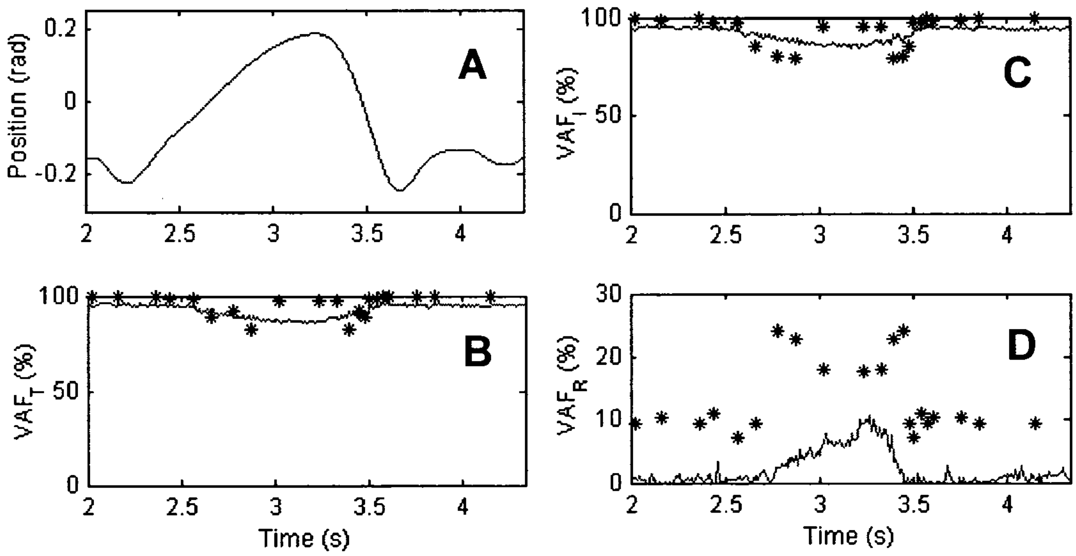

Figure 37: %VAF for observed and predicted torque. (A) Imposed gait input; (B) Total torque; (C) Intrinsic torque; (D) Reflex torque. Stationary values at matched operating points are shown as red stars.

5.4.1.3 Parametric Fits

Figure 38 shows intrinsic IRF estimates at specific times during the gait movement. Intrinsic stiffness and compliance are shown at heel-strike, late-stance, tow-off, and mid-swing. The parametric fits to intrinsic compliance, shown in red, were largely similar to the estimated IRFs at each time point. The magnitude of intrinsic compliance was clearly modulated between each location being lowest during the stance phase of the cycle.

Figure 39 shows the time-varying behaviour of the intrinsic parameters retrieved from the parametric fits to intrinsic compliance. The percent VAF for the parametric fits remained high throughout the movement, only dipping slightly during periods of elevated reflex activity. As expected, the inertial term remained relatively constant throughout the movement. Viscosity and elasticity showed elevated levels between 2800 and 3400 ms corresponding to the period of maximum dorsiflexion and decreased intrinsic compliance. Stationary values were consistent with the time-varying inertial and viscous estimates at matched operating positions; however stationary estimates for elasticity displayed an elevated baseline relative to the time-varying parameters.

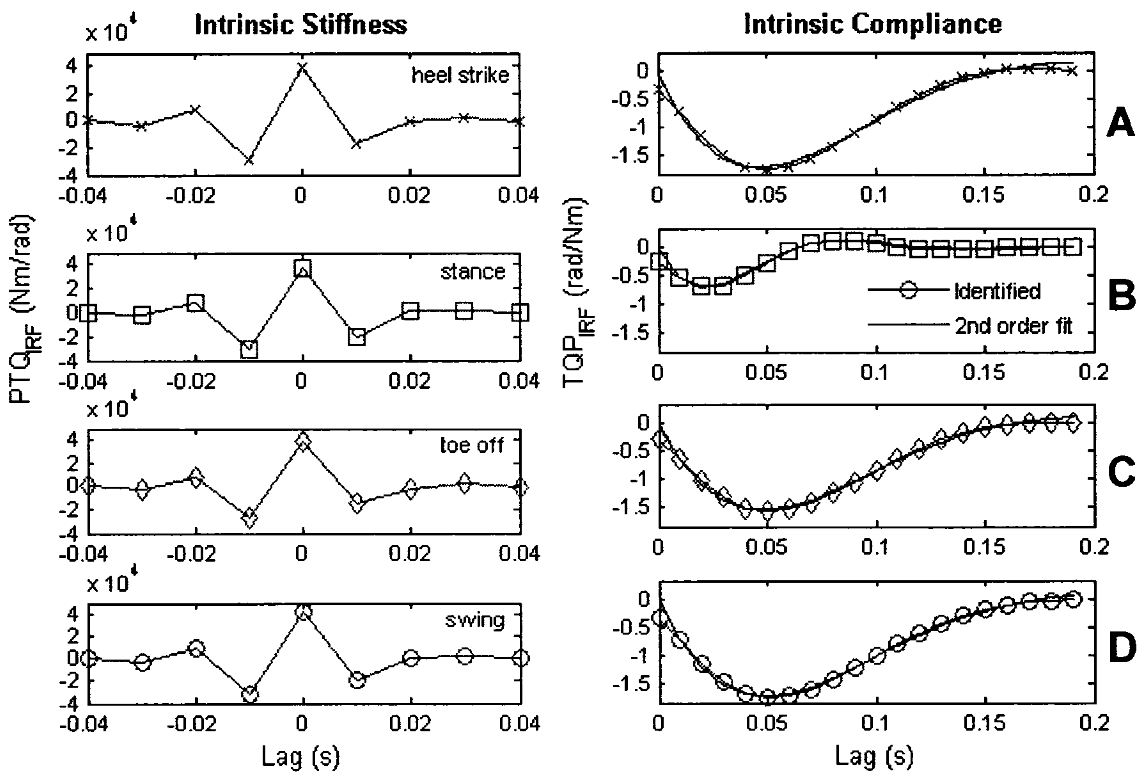

Figure 38: Intrinsic stiffness (left), compliance (right) and 2^{nd} order parametric fits at four locations during the gait cycle. (A) Heel strike; (B) Stance; (C) Toe off; (D) Swing.

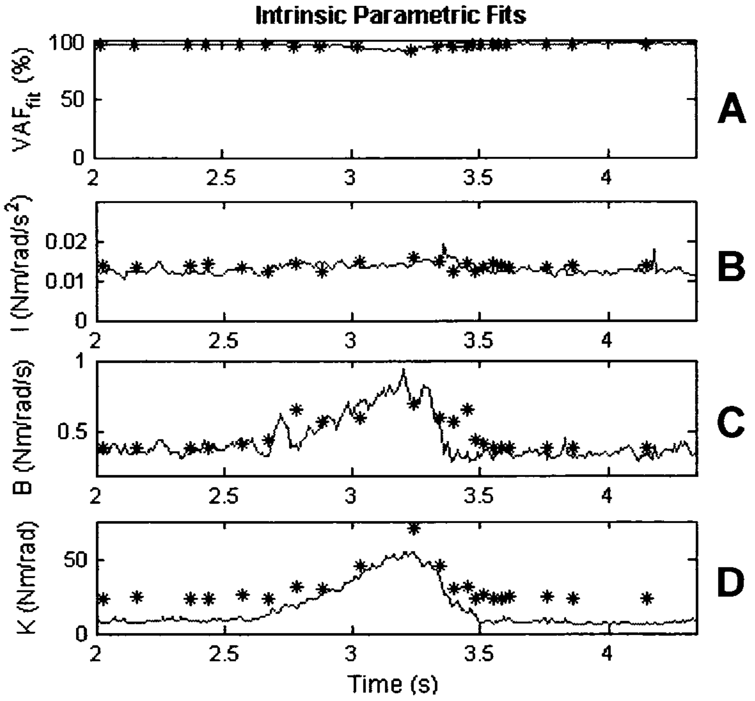

Figure 39: Time-varying intrinsic parameter estimates. (A) %VAF for parametric fits; (B) Inertial parameters; (C) Viscosity parameters; (D) Elasticity parameters. Stationary values at matched operating points are shown as red stars.

Figure 40 shows estimates of reflex stiffness and static non-linearities for two time points at which the parametric fitting was successful (3350 and 4300 ms). The magnitude of reflex stiffness was similar for the two locations, but the characteristics of the SNL were quite different. At 3350 ms the relationship was linear, whereas at 4300 there was a distinct non-linear trend between input and output velocity. The curvilinear shape of the SNL reflects the unidirectional sensitivity of spindle afferents to a stretch.

Figure 41 shows the time-varying behaviour of the reflex parameters retrieved from the parametric fits to reflex stiffness. Results are presented only for those values in which the parametric fit accounted for at least 50% of the variance. Fits accounting for less than 50% were unreliable, since the parameters modelled noise rather than an estimate of reflex stiffness. The fitting procedure was only successful at a handful of locations throughout the time-varying movement as seen by examining the percent VAF for the parametric estimates (Figure 41-A). The sporadic and low VAF may be attributed to a number of possibilities, two of which are discussed here. Firstly, reflexes only contributed to total torque at select phases of the movement, so any changes in reflex dynamics that were undetectable because the gain decreased below the noise level was unlikely to have much functional significance and therefore no need for a parametric fit. Secondly, during periods of reflex activity the total torque VAF was already shown to decrease (Figure 37). This suggests that the algorithm inadequately predicted joint stiffness when reflexes were significant—whether this is a limitation of the algorithm and specifically the reflex pathway, or a deficiency in the input-output ensemble remains unknown. Alternatively, the parametric model for reflex stiffness may be inadequate.

However, it is clear from Figure 41-B that there were small levels of time-varying modulation correlated with the gait movement. We see that the quality of the parametric fitting was best between 2800 and 3400 ms, which was expected since this was the phase of increased reflex activity. Overall, reflex gain fluctuated between 0 and 2 Nm/rad, following a pattern somewhat similar to the input trajectory. There was a marked decrease in reflex gain following the transition stage from dorsi- to plantar flexion, which indicates that reflexes were abruptly reduced immediately after the directional change. Little information can be inferred from the parametric estimates of frequency and damping, although there does appear to be fluctuating trends in the average values.

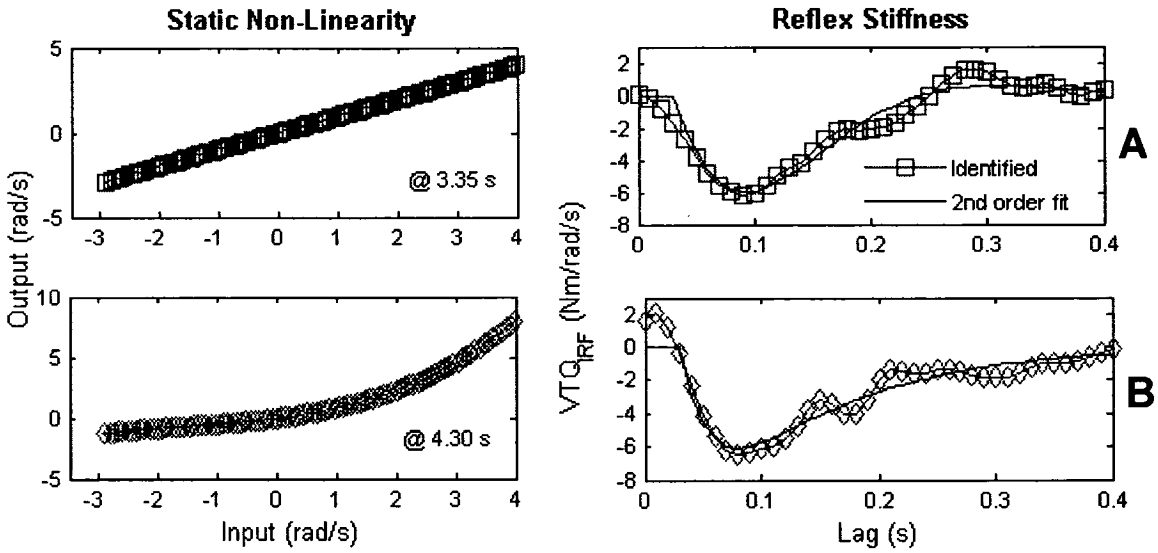

Figure 40: Reflex static non-linearity (left), stiffness (right) and 2nd order parametric fits at two locations during the gait cycle. (A) 3350 ms; (B) 4300 ms.

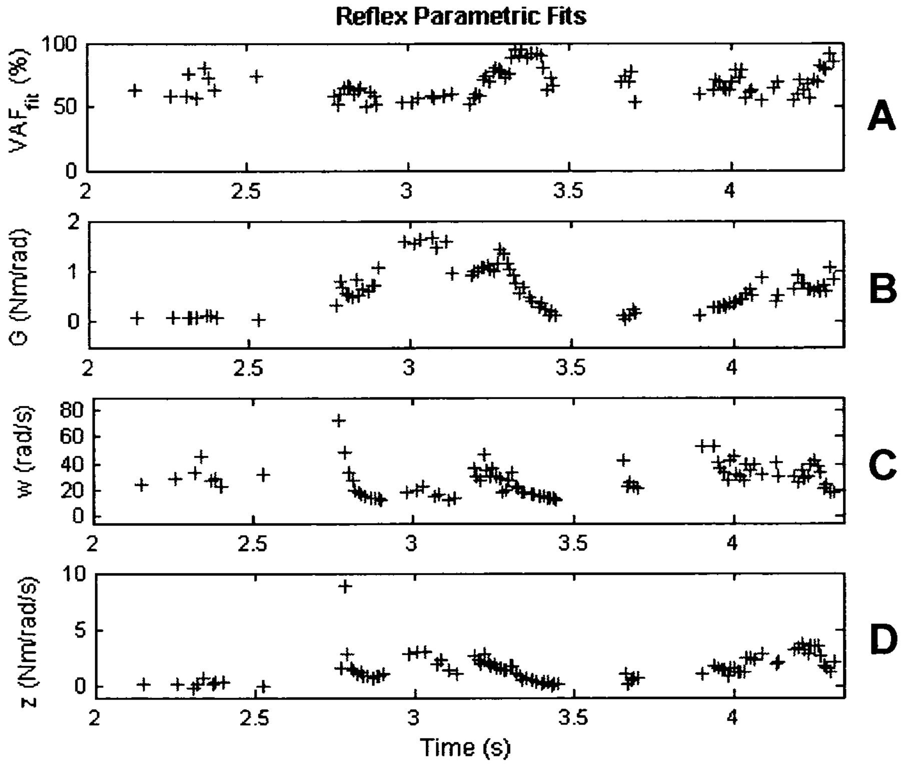

Figure 41: Time-varying reflex parameter estimates. (A) %VAF for parametric fits; (B) Reflex gain parameters; (C) Frequency parameters; (D) Damping parameters. Results are presented only for those values in which the parametric fit accounted for at least 50% of the variance

5.5 DISCUSSION

5.5.1 Methodological Considerations

5.5.1.1 Model adequacy

Model efficacy was evaluated by computing the percent VAF between the observed and predicted total torque. Total predicted torque was calculated as the linear sum of intrinsic and reflex torque, which were generated by applying time-varying convolution to the input position ensemble and time-varying system estimates. The mean total VAF was 92%, which clearly demonstrates that the time-varying, parallel-cascade algorithm is capable of predicting joint stiffness during a large amplitude, imposed movement.

The subject was relaxed while the gait trajectory was applied to the ankle and intrinsic mechanisms undoubtedly dominated for these conditions. This is seen by the high VAF attributed to intrinsic torque in Figure 37. These findings are consistent with previous studies that also identified intrinsic mechanisms as the primary source for joint torque during relaxed conditions [1, 34]. This type of movement yielded some reflex activity, albeit very small and only at specific phases during the movement. Reflexes contributed most toward total torque during the phase corresponding to late stance and early swing. It was also during this time that the overall VAF decreased. This suggests that the quality of system identification diminished as reflexes became more significant. One likely explanation for this is increased system noise as a result of reflex activation, which made system identification more complex and difficult. We investigated the possibility that the problem was directly associated with the time-varying algorithm by conducting static trails at operating positions throughout the movement. It is interesting to note that the overall VAF was also more volatile in the stationary results at positions corresponding to increased reflex activity (Figure 37).

5.5.1.2 Effect of displacement properties on reflexes

Small amplitude perturbations were applied to the subject's ankle to stimulate joint dynamics for system identification. To characterize the dynamic response of the reflex, the input signal required a broad range of amplitudes and frequencies. In these experiments, pseudo random binary sequence perturbations were selected as the input and superimposed on the larger time-varying sequence. The time-varying trajectory imposed time-dependent characteristics on the system properties, while the perturbations permitted system identification. PRBS perturbations were ideal for this application due to the wide-bandwidth and low-mean absolute velocity properties of the signal.

The reflex response is known to depend nonlinearly on the amplitude, direction, and duration at which a stimulus is applied [34]. Muscle spindle afferents are highly sensitive to small perturbations [73] and studies have found that stochastic perturbations typically used for system identification procedures, profoundly modify the properties of stretch reflexes they are meant to measure. It was found that the reflex response is in fact suppressed in proportion to the mean absolute velocity of the random perturbation and velocity was an important variable in depressing the reflex [34]. Researchers suggested that presynaptic inhibition resulting from activity in spindle afferents was the likely mechanism behind the suppression of reflexes.

According to results found by Stein and Kearney, a signal with MAV above 0.25-0.3 rad/s potentially exposes the subject to reflex suppression. The MAV of the combined gait and perturbation input used for this study was 0.5283 rad/s. This value is nearly double that of the suggested range for preserving reflexes. Therefore, the large MAV for this type of movement is one likely reason for the low level of reflex activity found here.

5.5.1.3 Central drive

In addition to input characteristics, reflexes are well known to depend on the level of voluntary activation produced by the subject [34]. Increasing the level of muscle activation increases the fraction of motoneurons that are close enough to threshold to be activated by the stretch; such phenomenon is known as "automatic gain control". The experiments performed during this investigation were conducted while the subject was relaxed (no voluntary activation). These conditions resulted in a further reduction in reflex activity generated for this type of movement. A supplementary set of experiments were conducted while the subject maintained a low-level, active voluntary contraction. However, reflex activity remained small and too difficult to identify relative to the increased noise produced by fluctuations in the subject's central drive. Essentially, the subject found it difficult to maintain a constant level of voluntary activation, resulting in an additional noise source. It was at this point that a smooth ramp, of similar period, but lower amplitude and MAV was selected for the active, time-varying experiments (Chapter 6).

5.5.2 Mechanisms

5.5.2.1 Time-varying modulation

Intrinsic stiffness arose from the mechanical properties of the joint, active muscle and passive tissues. As the subject's ankle underwent the imposed movement, intrinsic properties varied in a manner correlated with the displacement trajectory. During periods of large dorsiflexion, intrinsic stiffness of the joint increased (compliance decreased). This corresponded to the late stance and early swing phases of the gait trajectory. The modulation of intrinsic properties is readily seen in the time-varying, parametric estimates of viscosity and elasticity. Both parameters showed a marked increase during the dorsiflexion stage between 2800 and 3400 ms. The joint inertia (Figure 39-B) remained relatively constant for the duration of the movement. This was expected, since the mass properties of the joint were constant. Movement in plantar flexion had no observable effect on the intrinsic properties of the joint.

Reflex stiffness resulted from muscle activation in response to small amplitude perturbations superimposed on the larger, time-varying movement. Reflexes were absent during most of the movement; however, small increases in reflex gain and torque VAF were observed throughout the dorsiflexion phase (Figure 37 and Figure 41). At identical positions, reflex torque accounted for differing amounts of total torque, which suggests that reflexes were adapted to the phasic requirements of the movement.

Comparison between stationary and time-varying results indicates that the movement acted to suppress the tonic level of reflex activity; reflexes contributed less to ankle torque during movement than at matched steady-state positions (Figure 37). These results are consistent with previous findings from our lab, which reported a significant drop in the stretch reflex EMG and torque compared to that observed during steady-state conditions, while subjects underwent an imposed gait [52]. Furthermore, they found that the reflex response was modulated throughout the step cycle in a manner qualitatively similar to that observed during active walking. Pulse disturbances evoked large reflex torques in early to mid-stance, whereas pulses applied late stance and swing generated little reflex torque. Sinkjaer *et al.* similarly reported large stretch reflexes in the stance phase, complete suppression from stance to swing, and small values in the early swing phase [72]. Our findings agree that reflexes increase throughout the stance phase, but conversely we found strongest reflexes during the late stance and early swing phase of gait, with maximum contribution to reflex torque occurring at the transition from stance to swing. However, differences in experimental methods may account for the discrepancy as the present study was conducted passively and for slower walking.

6 Identification of Time-varying Intrinsic and Reflex Joint Stiffness: Imposed smooth-ramp

Chapter 6 applies the TVPC method to examine joint dynamics during a cyclic ramp stretch. Intrinsic and reflex properties are examined throughout the movement and compared with results from the previous study. The chapter identifies limitations of the current TVPC method and examines the functional significance of our findings.

Identification of Time-varying Intrinsic and Reflex Joint Stiffness: Imposed smooth-ramp

Heidi Giesbrecht, Robert E. Kearney

Target Journal:
IEEE Transactions on Neural Systems and Rehabilitation Engineering

6.1 ABSTRACT

We examined time-varying intrinsic and reflex dynamics of the human ankle joint during an imposed, periodic, smooth-ramp trajectory in which the subject's ankle underwent a rapid, 400 ms stretch followed by a 600 ms pause. The experiment was conducted while the subject maintained an active voluntary contraction of the GS muscle group aided by visual feedback of EMG. Ensemble position and torque data were acquired and analyzed with the TVPC algorithm. Intrinsic and reflex dynamics were estimated as time-varying IRFs, which characterized system properties at each point in time throughout the movement. Intrinsic and reflex properties were modulated strongly during the time-varying motion. Stretch reflexes contributed four times more toward torque and reflex gain was ten times greater than during the previous gait movement. The mean %VAF between predicted and observed torque was low for this study. Subject fatigue was established as a likely cause by examining the mean torque and EMG over the course of the experiment. Current methods should be improved to correctly identify trials in which the subject does not maintain a constant voluntary contraction.

6.2 INTRODUCTION

The mechanical behaviour of the ankle joint may be characterized by a quantity known as dynamic stiffness [1]. Dynamic joint stiffness defines the relationship between the position of a joint and the torques acting about it. Joint stiffness may be separated into two primary components: intrinsic and reflex. Each component is influenced by a number of interrelated factors. For steady-state conditions, the level of voluntary muscle activation [15, 34] and the angular position [34, 36] of the joint are two factors that have been shown to affect both intrinsic and reflex properties of a joint. During movement, additional complexities arise from the influence of the motion itself. The phase, amplitude and speed of a given motion all affect the properties of joint dynamics [52, 72]. Reflexes are considered particularly elusive during movement and their functional role remains an open topic of debate.

In the previous study, we examined the time-varying properties of intrinsic and reflex dynamics during an imposed gait cycle. Intrinsic mechanisms clearly dominated for the movement conditions, however, reflexes made small contributions to torque during periods of dorsiflexion. The low levels of reflex activity may be attributed to two factors: (1) the study was conducted during relaxed conditions, and (2) the mean absolute velocity (MAV) for the movement was far greater than the recommended range to elicit reflexes [34]. Kirsch *et al.* imposed a rapid ramp movement to the ankle joint while subjects maintained various levels of tonic muscle activation. The imposed ramp successfully evoked stretch reflexes at various stages throughout the motion. Time-varying analysis was conducted using ensemble methods, which treated half-wave rectified velocity as the input and rectified TS EMG as the output. Time-varying modulations were apparent in the estimates of reflex dynamics and results suggested that stretch reflex properties were modulated independently of motor neuron pool activation level. The changes in reflex dynamics were largely mediated by peripheral mechanisms [57].

In the present study, we used a similar experimental paradigm to examine the dynamic properties of the ankle while imposing a cyclic, smooth-ramp movement upon a moderate contraction level. The imposed movement emphasized the role of peripheral mechanisms by stimulating the muscle spindles while the subject maintained a constant level of voluntary drive. The cyclic motion consisted of a dorsiflexion stretch, followed by a pause, then a plantar flexion return stretch, followed by a pause. The peak dorsiflexion position corresponded to the optimal operating point for reflex activity. The MAV for this input was 0.3675 rad/s—much lower than the previous study. In brief, the experimental conditions were catered to maximize reflex activity. Time-varying techniques described in the preceding chapters were used to separately identify intrinsic and reflex dynamics. One thousand cycles of recorded position and torque comprised the input-output data ensemble for system identification. The time-varying technique produced a nonparametric estimate of intrinsic and reflex dynamics at each point throughout the time-varying motion. System properties were effectively frozen at each point throughout the time-varying behaviour, which allowed us to track changes in intrinsic and reflex dynamics due to the imposed movement.

6.3 METHODS

6.3.1 Apparatus

Subjects were tested using the same apparatus described in Chapter 5. In addition, an LCD monitor was mounted above the subject to provide visual feedback during experiments in which the subject was required to maintain a constant level of voluntary muscle activation. Subjects were asked to hold steady a visual cue displayed on the LCD monitor. The cue represented their tonic level of muscle activity as determined by computing the error signal between GS EMG and a target level of EMG. The target level corresponded to five percent of the subject's maximum voluntary contraction. The GS EMG signal was rectified and low-pass filtered (Bessel filter, 0.4 Hz cut-off frequency) to eliminate the cyclic oscillations generated in response to the time-varying motion. Then the signal underwent a sample-and-hold triggered by stretch onset to eliminate the transient effects due to stretch reflexes. This procedure effectively took a snapshot of the sensor signal, holding the value constant during the burst of EMG during the muscle reflex. As a result, the net feedback signal represented the baseline level of EMG.

Ankle position, torque, and surface EMGs from gastrocnemius (GS) and tibialis anterior (TA) were sampled at 1 kHz by a dynamic signal acquisition card (National Instruments, 4472). Anti-aliasing was performed by the card, which over-sampled the data and then applied a digital brick wall filter with a cut-off frequency of 486.3 Hz. Position and torque were then decimated to 100 Hz for the purpose of system identification.

6.3.2 Experimental Procedure

One female subject aged 25 years was tested. The subject had no known history of neuromuscular disease and gave informed consent to the experimental procedure, which was approved by the McGill University Research Ethics Board (see Appendix A).

6.3.2.1 Position Inputs

Several types of input displacements were applied to the subject's ankle. Pulses and perturbations functioned to stimulate the joint for reflex analysis or system identification. Time-varying changes were induced within the joint by a large amplitude periodic sequence imposed upon the ankle joint. The following describes the detailed characteristics of each type of displacement:

i. PULSE PERTURBATION: Small amplitude (0.03-0.04 rad), short (40-60 ms) pulse displacements in the dorsiflexion direction. Figure 43-A illustrates one recorded pulse generated by the position servo.

ii. PRBS PERTURBATION: Continuous pseudo-random binary sequence (PRBS) displacements with 0.0375 rad peak-to-peak amplitude and 200 ms switching interval.

iii. TIME-VARYING RAMP: A periodic, smooth ramp with a two second period and 0.3 rad peak-to-peak amplitude. Each cycle was composed of a 400 ms dorsiflexion stretch of the GS, followed by a 600 ms pause, then a 400 ms plantar flexion return stretch of the TA, followed by a 600 ms pause. The position of maximum dorsiflexion corresponded to the optimal operating point (OOP) for reflex activity as determined by an initial series of pulse trials. The MAV for this sequence was 0.3675 rad/s. Figure 44-A illustrates two cycles of the time-varying ramp trajectory applied to the subject's ankle.

6.3.2.2 Trials

A series of preliminary experiments were conducted prior to the time-varying trials. The results were used to define the parameters for the time-varying experiment. The following explains each experiment in detail:

i. MAXIMUM VOLUNTARY CONTRACTION: With the ankle in the zero position, the subject was instructed to perform a maximum contraction of the GS muscle (plantar flexes) for several seconds. The subject was then asked to relax, before performing a maximum contraction of the TA muscle (dorsiflexes). Torque and EMGs were recorded throughout the contraction and inspected afterwards to ensure a sustained contraction. The maximum contraction achieved during plantar flexion was used to establish the 5% MVC level. This value was then used as the target in subsequent experiments requiring the subject to maintain an active voluntary contraction. The position servo maintained ankle position constant during the MVC tests.

ii. OPTIMAL OPERATING POINT: The static position dependence of the stretch reflex was assessed through a series of pulse trials conducted at different positions throughout the subject's range of motion during isometric conditions. The positions ranged from maximum plantar flexion to maximum dorsiflexion. At each operating point, ten flexion pulses were applied to the subject's ankle, while maintaining a tonic 5% MVC contraction of the GS. The reflex response was then averaged and the static position corresponding to the largest reflex torque concluded as the optimal operating point.

iii. TIME-VARYING RAMP: Time-varying intrinsic and reflex dynamics were analyzed during an imposed, smooth ramp cycle while the subject maintained an active contraction at 5% MVC. PRBS perturbations were superimposed on the continuous sequence to stimulate system dynamics. Cycles ran continuously and trials lasted five minutes. The subject was then given a short break before proceeding with the next trial for a total of ten sets of trials and approximately 1500 cycles.

6.3.3 Time-Varying Analysis

Time-varying data acquired during ramp experiments were processed in the same fashion as described in Chapter 5. Briefly, the data were pre-processed by segmenting the continuous position and torque records into an ensemble of input-output realizations. Each realization in the ensemble comprised two cycles of the smooth ramp trajectory. Significant outliers were discarded, leaving behind 1044 realizations in the ensemble. The time-varying, parallel-cascade algorithm was applied to the input-output ensemble. Intrinsic and reflex dynamics were estimated as nonparametric IRFs at each point throughout the time-varying motion. Parametric estimates of intrinsic and reflex dynamics were generated by fitting second-order, low-pass systems to intrinsic compliance and reflex stiffness. Physically meaningful parameters representing intrinsic and reflex mechanics were retrieved from the parametric fits.

6.4 RESULTS

6.4.1 Maximum Voluntary Contraction

Figure 42 shows the torque and corresponding EMG generated by one subject during a maximum voluntary contraction (MVC) experiment.

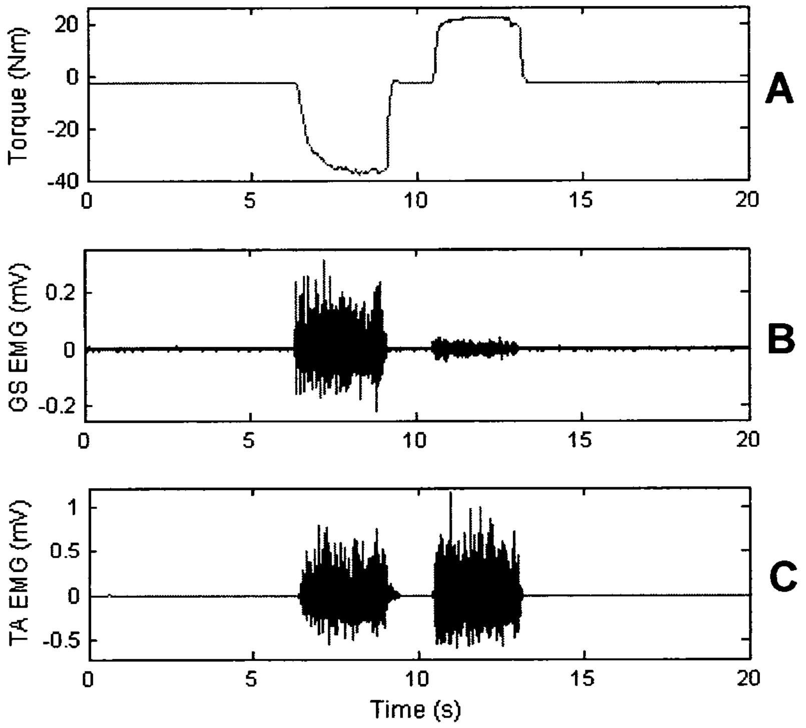

Figure 42: Maximum voluntary contraction. (A) Maximum voluntary torque generated during plantar and dorsiflexion; (B-C) GS and TA EMG generated during maximum voluntary contraction test.

By convention, negative position and torque represent plantar flexion, while positive position and torque represent dorsiflexion. The elevated level of GS activity between 5 and 10 seconds in Figure 42-B corresponds to the plantar flexion stage of the test. The TA also shows activity during this period, however, this was likely due to cross-talk during EMG recording. The second burst of activity between 10 and 15 seconds represents the contraction of the TA muscle during dorsiflexion. In subsequent experiments, subjects were required to maintain a tonic level of voluntary contraction equal to five percent of the maximum voluntary level produced during plantar flexion.

6.4.2 Optimal Operating Point

Figure 43 illustrates the ensemble average of position, torque and EMG of 10 pulses applied at the same operating position. The torque response shown in Figure 43-B is comprised of two components: the earliest component is referred to as the intrinsic response and the second, longer latency component is referred to as the reflex response. The intrinsic response results from the inertia of the ankle and passive, visco-elastic properties of the joint. The reflex response results from reflex activation and occurs well after the position has returned to baseline—typically at a latency of 40 ms. This type of pulse response has been well documented in the literature [34]. The reflex response is also visible in the GS EMG traces (Figure 43-D) as a burst of activity relative to the baseline measurement. The stretch was applied in the dorsiflexion direction and therefore activated the GS muscle group during the stretch reflex. The TA EMG also shows some activity, but this was most likely due to cross-talk in EMG recording.

Reflex torque was computed by locating the minimum of the long latency component of the torque response. This is marked by the crosshair in Figure 43-B. The minimum value was measured relative to the baseline torque taken before stretch onset. The reflex EMG was similarly computed by measuring the burst amplitude relative to the baseline signal. Table 2 outlines the ensemble average reflex EMG and reflex torque computed for several positions throughout the subject's range of motion. The optimal operating point (OOP) was chosen by the position corresponding to the maximum reflex torque. For this subject, the OOP was 0.05 rad, which generated a reflex torque of 7.79 Nm.

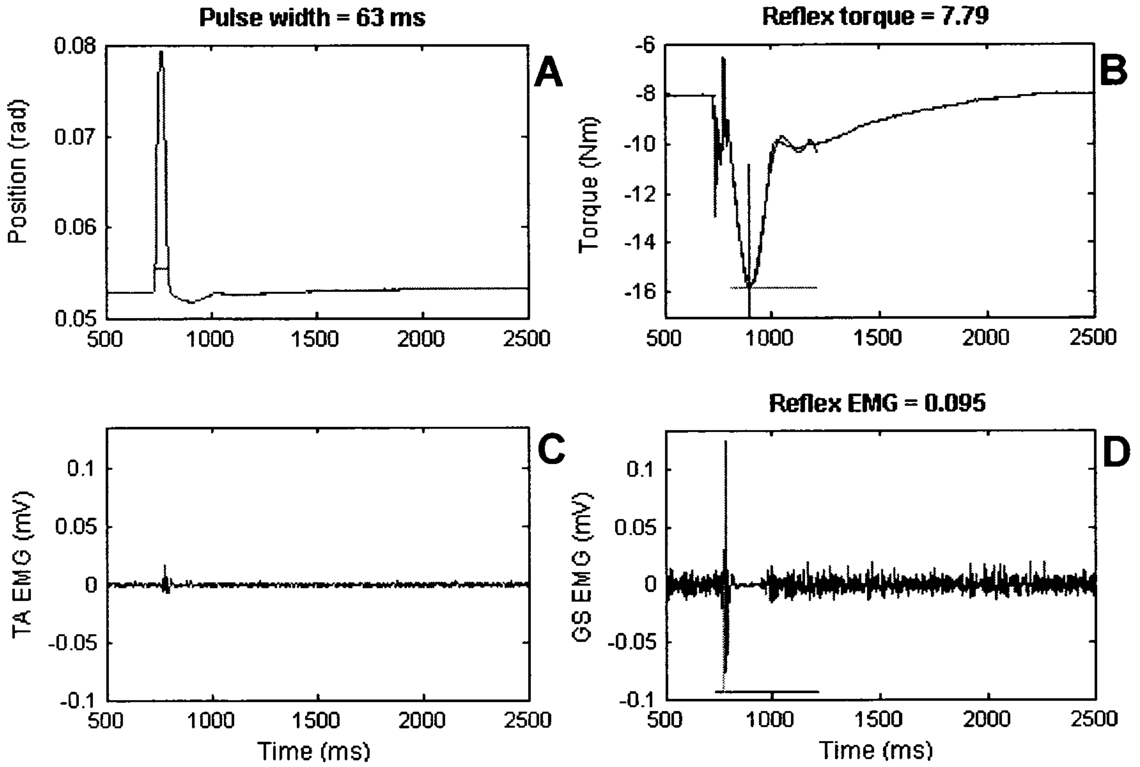

Figure 43: Optimal operating point. (A) Pulse perturbation applied to subject's ankle; (B) Reflex torque generated in response to pulse; (C-D) TA and GS EMG generated in response to pulse.

Table 2: Reflex torque and reflex GS EMG at various static positions

Ankle Position (rad)	Reflex EMG (mV)	Reflex Torque (Nm)
-0.15	0.066	4.42
-0.10	0.049	5.06
-0.05	0.078	5.69
0.00	0.048	7.56
0.05	**0.095**	**7.79**
0.10	0.062	7.42

6.4.3 Time-Varying Ramp

Figure 44 shows ensemble averages and four extracted realizations. Each realization was composed of two ramp cycles. The ensemble mean position (Figure 44-A) displays the repeated, time-varying motion imposed on the subject's ankle. The periodic ramp oscillated between a position of plantar flexion and the optimal operating point. Ensemble mean torque (Figure 44-B) roughly mirrors the ensemble position, with a slight drift during the pause between ramps. PRBS perturbations, superimposed on the time-varying motion, are visible in the position traces (Figure 44-C) as projections on the underlying motion. The corresponding torque responses are distinguished by fast transients in Figure 44-D.

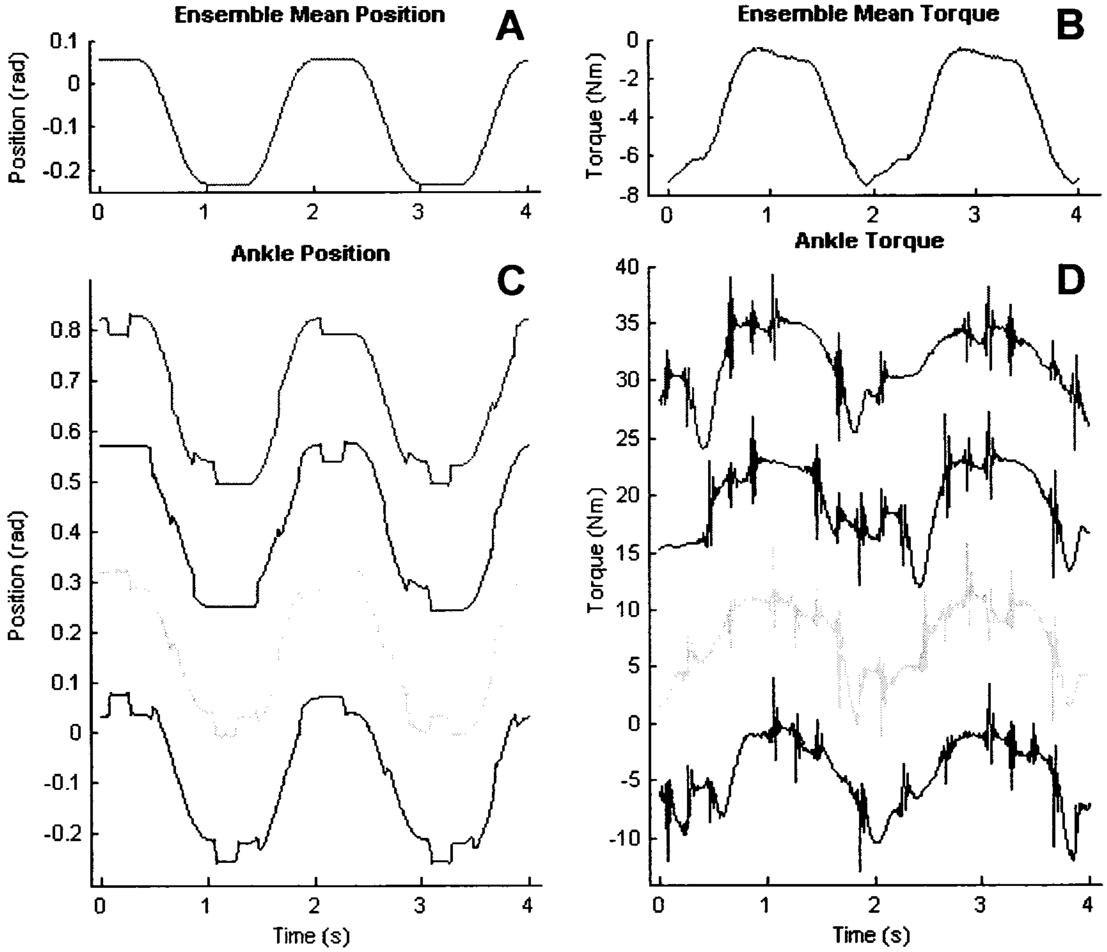

Figure 44: Position and torque. (A) Ensemble mean position; (B) Ensemble mean torque; (C-D) Four position traces and corresponding torque responses extracted from the input-output ensemble.

6.4.3.1 Identified Systems

The time-varying system identification procedure computed an estimate of intrinsic and reflex dynamics at each 10 ms interval throughout the periodic motion. Figure 45 illustrates the time-varying estimates of intrinsic stiffness, compliance, reflex stiffness and static non-linearity. The axes denoted '*Time*' indicate the progression through the imposed movement, while the axes '*Lag*' represent the memory of the IRFs. The static non-linearity defined the relationship between the input and output velocity at each time point throughout the movement.

Figure 46-B and C reveal the time-variant profile of intrinsic compliance and reflex stiffness. These figures chart the time-varying changes of intrinsic and reflex dynamics with respect to the movement trajectory (Figure 46-A). Intrinsic compliance and reflex stiffness were modulated throughout the time-varying movement and display complementary changes in magnitude. The ankle joint was most compliant during the plantar flexion stages of the motion, demonstrated by increased levels of intrinsic compliance. Reflex mechanisms prevailed most during the dorsiflexion stages of the motion and especially during the smooth transition from stretch to pause. Furthermore, reflex stiffness was not constant during the pause at optimal operating point, but rather declined during this phase. The reflex SNL, which reflects the unidirectional sensitivity of stretch receptors, also exhibited time-dependent changes characterized by the pronounced, nonlinear segments in Figure 45-D.

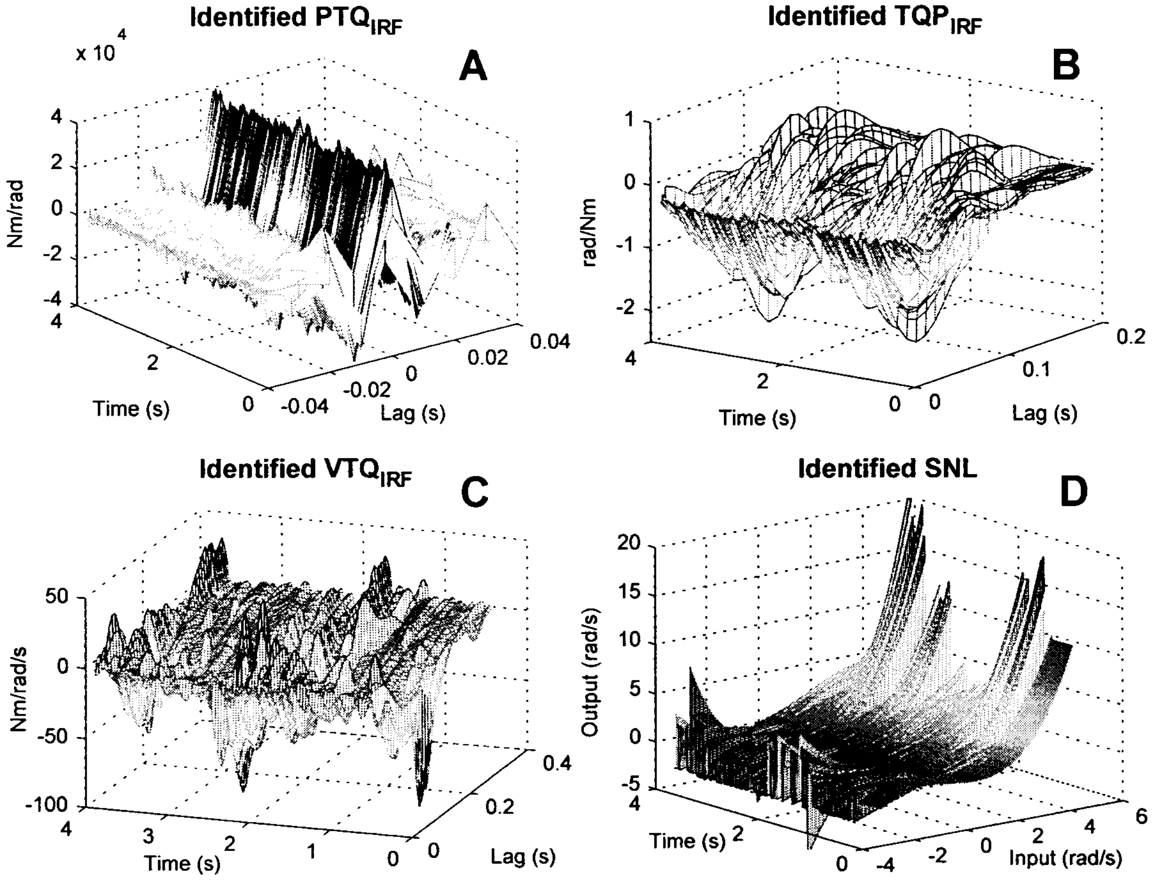

Figure 45: Identified time-varying systems. (A) Intrinsic stiffness; (B) Intrinsic compliance; (C) Reflex stiffness; (D) Reflex static non-linearity.

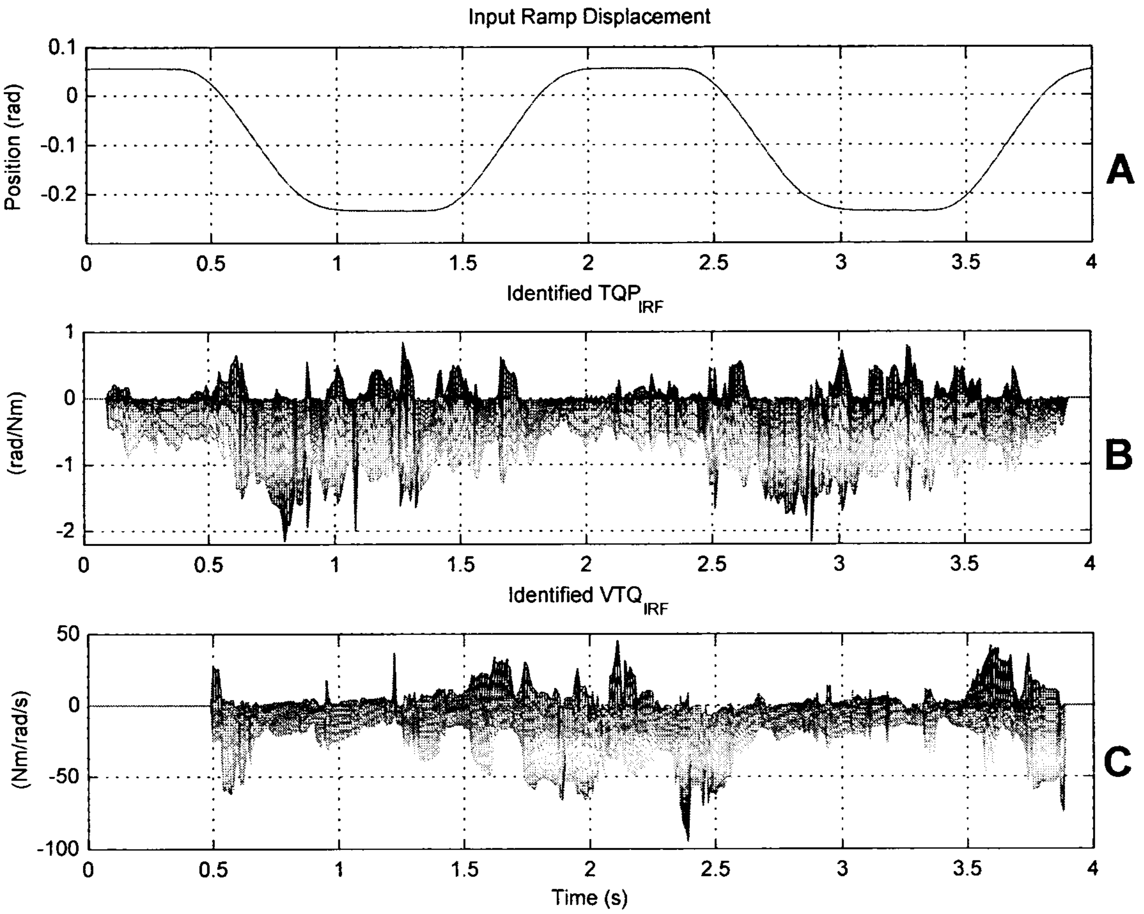

Figure 46: Time-varying position and estimated, nonparametric IRFs. (A) Imposed ramp sequence; (B) 2-dimensional view of intrinsic compliance and (C) reflex stiffness illustrating the time-varying changes in ankle dynamics with respect to the movement trajectory.

6.4.3.2 Predicted Torque VAF

Figure 47 shows the percent VAF between observed and predicted total, intrinsic and reflex torque as a function of time. These plots illustrate the relative contribution from intrinsic and reflex torque to the total torque generated at the ankle. For clarity, results are plotted for one ramp cycle between 1400 and 3400 ms. The total VAF reached a peak value of 84.3% and an overall mean of 55.0%. The low mean VAF may be attributed to a number of possibilities, including variability in the level of tonic contraction or fatigue. Consequently, this would generate variable levels of mean ankle torque, which would produce an additional noise source in the output data. Our algorithm is not currently capable of accounting for such signals. This topic is further addressed in the section titled 'Fatigue' during the discussion of methodological issues, where we examine the subject's ability to maintain a constant level of muscle activation.

The majority of the torque variance for this movement was attributed to intrinsic mechanics; however, between 1800 and 2500 ms there was a significant increase in the variance attributed to reflexes. In the time-varying movement, this segment corresponded to the dorsiflexion ramp and pause at the optimal operating point. The maximum VAF associated with reflex mechanisms was 40.4%, which occurred after the pause near maximum dorsiflexion on the down-ramp phase of the cycle (2480 ms). A corresponding decrease in the variance attributed to intrinsic mechanics occurred during this time. This suggests that as reflexes contributed more toward torque, intrinsic mechanics participated less in torque generation.

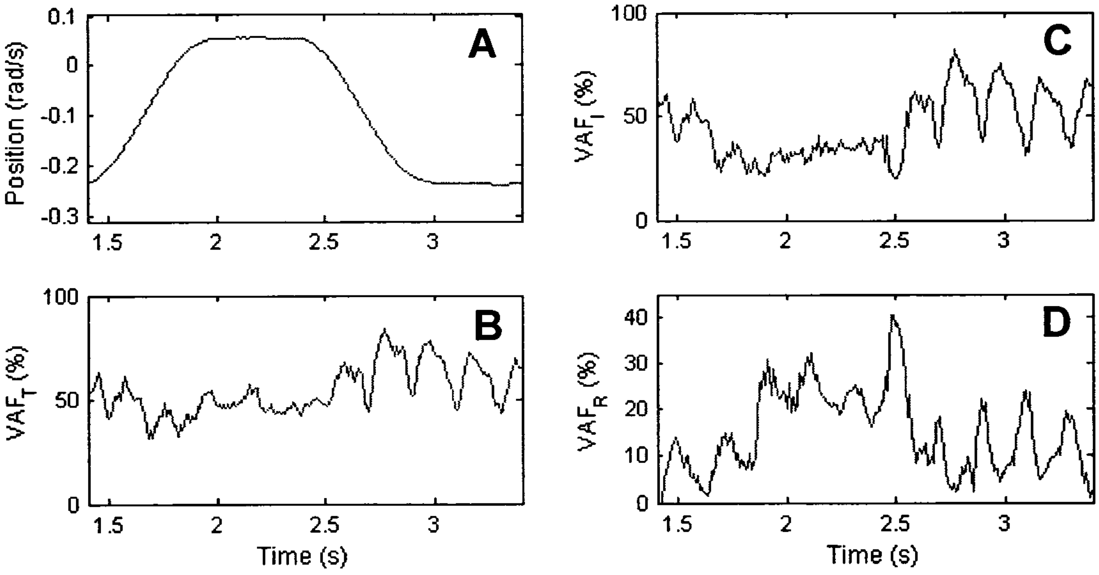

Figure 47: %VAF for observed and predicted torque. (A) Imposed ramp input; (B) Total torque; (C) Intrinsic torque; (D) Reflex torque.

6.4.3.3 Parametric Fits

Parametric models were fit to the estimated intrinsic compliance and reflex stiffness IRFs. Figure 48 and Figure 49 show system estimates at three points throughout the movement: 1840, 2090 and 2540 ms. These positions correspond to three locations just before, during and after the dorsiflexion ramp, selected because the reflexes were found to contribute significantly at these points. In addition, the intrinsic stiffness estimates and static non-linearity are also shown for these sample times. The general dynamics at the three locations were unchanged, but the magnitude was time-dependent. The static non-linearity matched a half-wave rectifier at 2540 ms, but clearly resembled a polynomial at 1840 and 2090 ms.

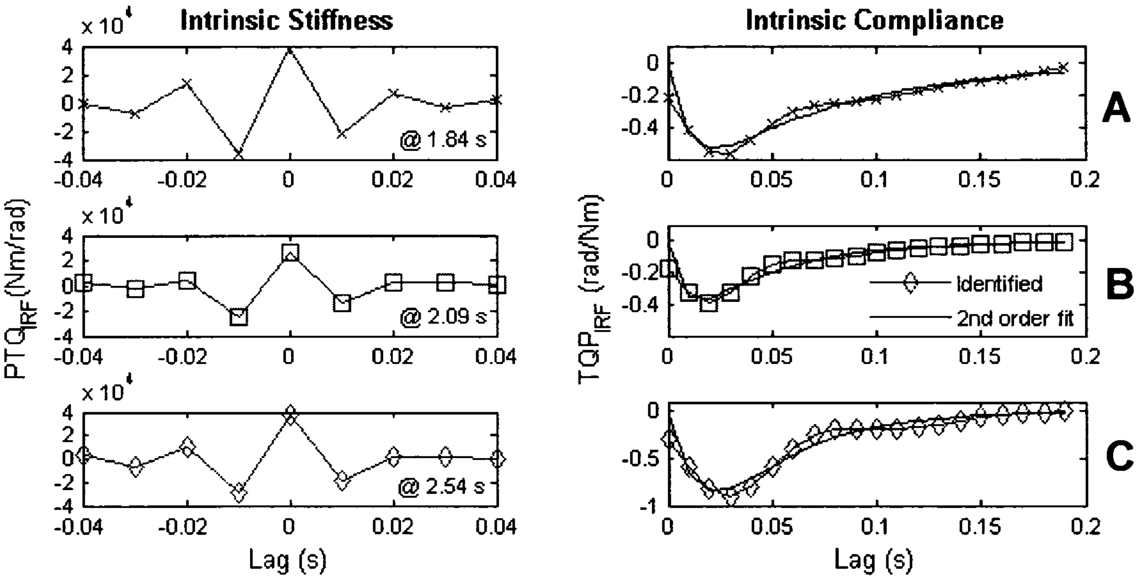

Figure 48: Intrinsic stiffness and intrinsic compliance at three locations throughout the time-varying movement: 1.84 seconds (crosses), 2.09 seconds (squares), 2.54 seconds (diamonds). Parametric fits are shown in red.

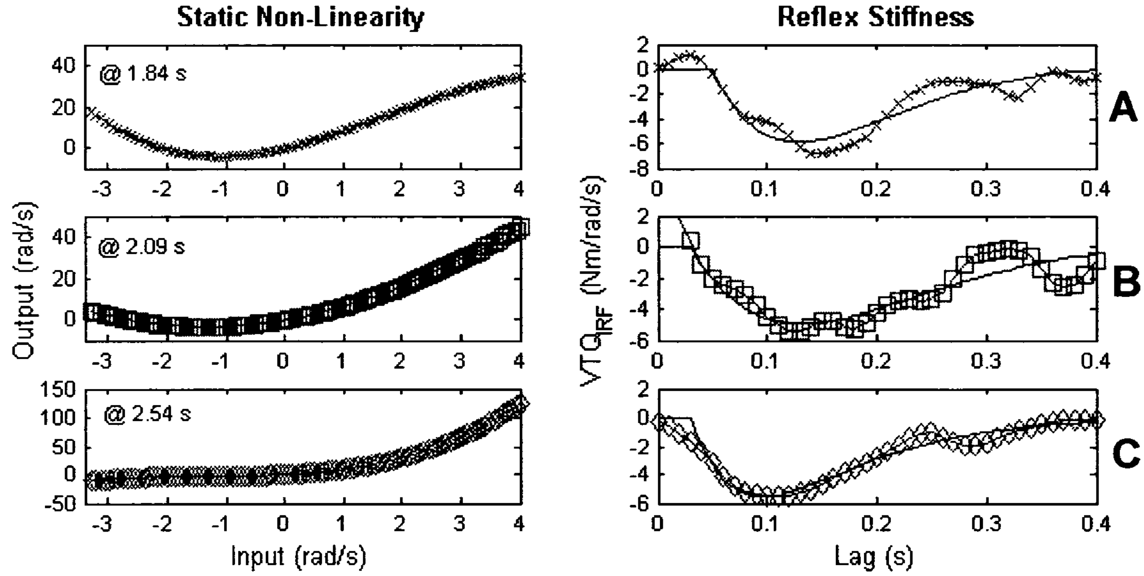

Figure 49: Reflex static non-linearity and reflex stiffness at three locations throughout the time-varying movement: 1.84 seconds (crosses), 2.09 seconds (squares), 2.54 seconds (diamonds). Parametric fits are shown in red.

Figure 50 and Figure 51 show the time-varying behaviour of the intrinsic and reflex parameters retrieved from the fitting procedure. The parameters are plotted for one ramp cycle between 1400 ms and 3400 ms. Results are presented only for those values in which the parametric fit accounted for at least 50% of the IRF variance. Fits accounting for less than 50% were unreliable, since the parameters modelled noise rather than an estimate of joint dynamics. The percent VAF for the intrinsic fits remained high throughout the movement, but dropped between 1800 and 2400 ms when reflexes had increased activity. Viscosity and elasticity were elevated during this period, indicating increased stiffness (decreased compliance) of the joint and surrounding tissues. The VAF for reflex fits displays sporadic high and low levels. More importantly, the IRF fits were reasonably successful during periods of increased reflex stiffness (1800-2500 ms), which is confirmed by large reflex gains. A notable observation is that the reflex gain was variable during the steady-state pause at the OOP (2000-2500 ms). Little can be deduced from the frequency and damping terms, however they appear relatively constant for the duration of the movement.

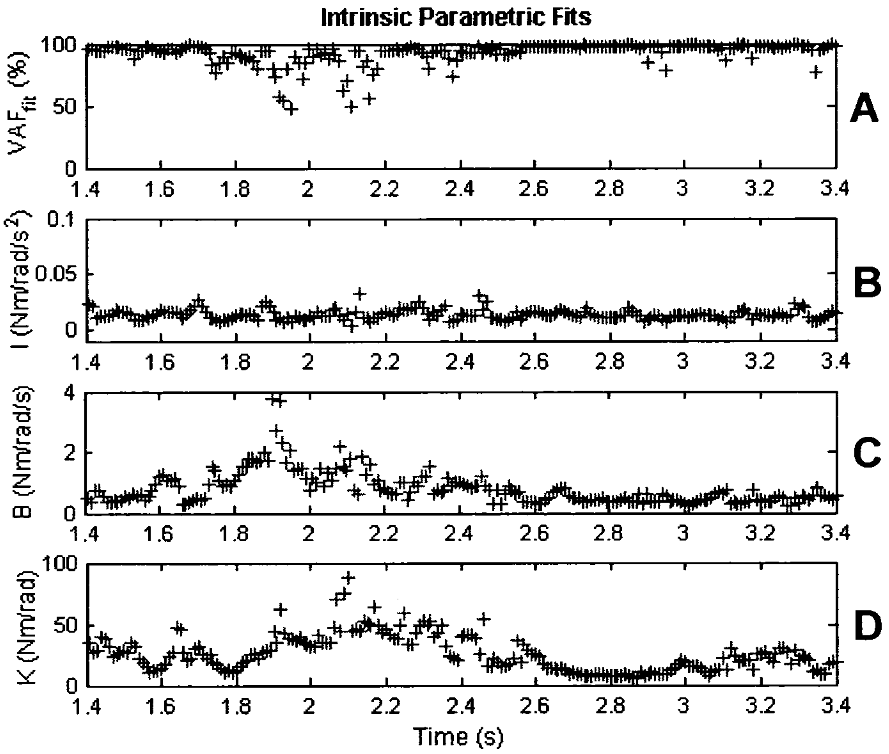

Figure 50: Time-varying intrinsic parametric estimates. (A) %VAF for parametric fits; (B) Inertial parameters; (C) Viscosity parameters; (D) Elasticity parameters.

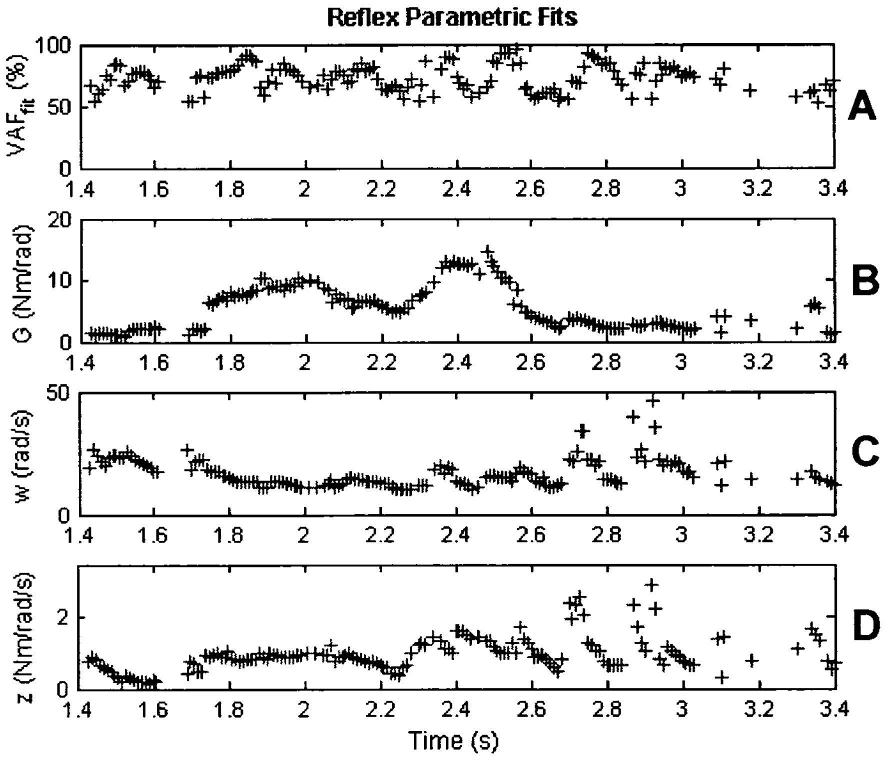

Figure 51: Time-varying reflex parameter estimates. (A) %VAF for parametric fits; (B) Reflex gain; (C) Frequency parameters; (D) Damping parameters.

6.5 DISCUSSION

6.5.1 Methodological Considerations

6.5.1.1 Fatigue

The experimental method used to gather time-varying data required the subject to maintain a constant level of muscle contraction for a period of five minutes. The subject was then given a short one to two minute break before proceeding with the next five minute segment. It was necessary to collect all time-varying data during the same experimental session, because the analysis method relied on the assumption that each trial in the ensemble originate from the same time-varying behaviour. However, requiring the subject to sustain an active contraction for a long duration led to the possibility of fatigue and consequently changes in the dynamic properties of the joint. To limit the effects of fatigue, a background contraction level equal to five percent of the subject's MVC was used; it has been shown that such a level can be maintained indefinitely without fatigue

[74]. Indeed previous experiments conducted over a period of several hours did not find significant fatiguing at a background contraction level equal to 15% MVC [57].

Nonetheless, the low mean VAF for predicted torque led us to question how well the subject maintained the active contraction of the GS muscle group and whether fatiguing occurred. To investigate this, we examined the change in mean torque and mean GS EMG over the course of the experiment. GS EMG was first rectified and then filtered to eliminate the transient effects of the stretch reflex. The procedure applied a threshold of 0.01 mV to the EMG signal; activity above the threshold was discarded. In doing this, only the baseline level of muscle activity was measured.

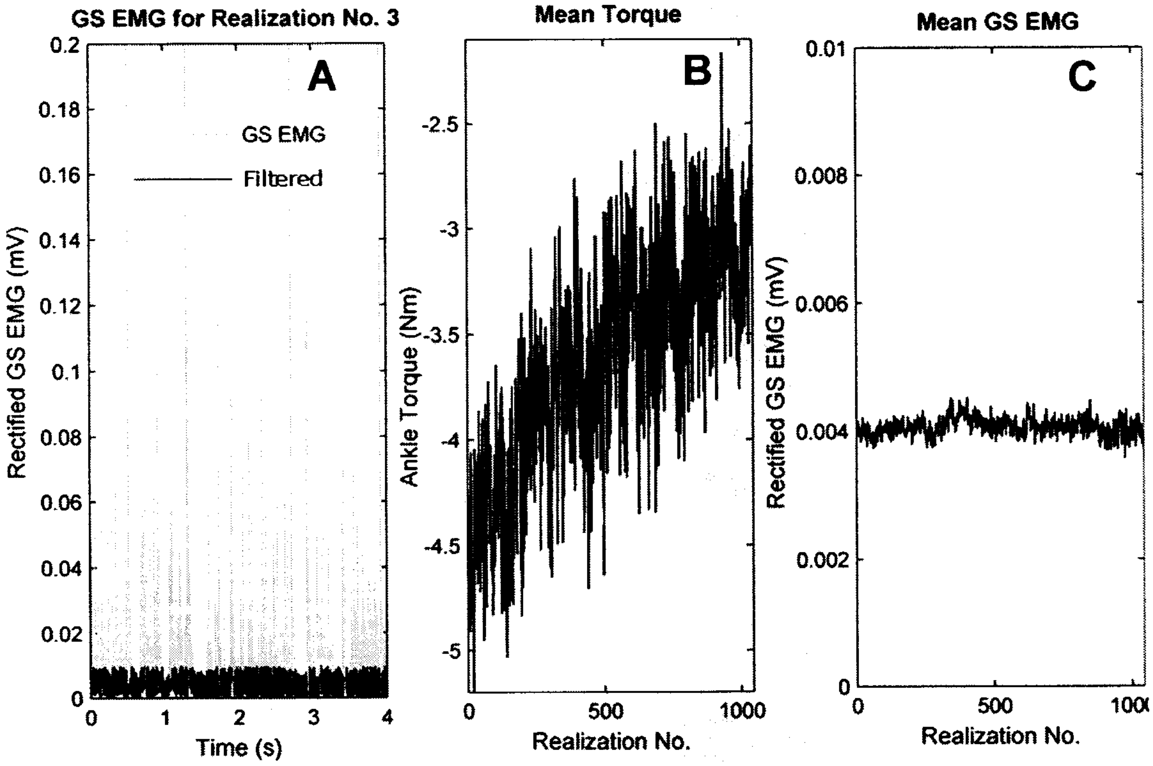

Figure 52: Analysis of subject fatigue. (A) GS EMG before and after truncation; (B) Mean torque and (C) mean GS EMG over the duration of the time-varying experiment.

Figure 52-A illustrates the EMG signal for one realization before and after removing the bursts of activity corresponding to stretch reflexes. Figure 52-B and C display the mean torque and EMG for each realization in the ensemble. Over the course of the experiment, the mean torque varied by nearly 40 percent, whereas the mean EMG

remained relatively constant. The TVPC algorithm relied on the consistent performance of a voluntary contraction to accurately remove the ensemble mean from each trial. Certainly, a change in torque of this magnitude would produce a trend in the output ensemble not removed by the ensemble average. This discrepancy is a likely explanation for the low VAF achieved for this experiment.

The mean EMG across the ensemble does not reflect the same variation as the mean torque. In fact, the mean EMG remained relatively constant over the course of the experiment. The inconsistent trends in torque and EMG suggest that the subject was not able to maintain the active contraction as a result of muscle fatigue. As the experiment progressed, the same level of EMG (electrical activity in the muscle) produced successively less force. This is a likely explanation for the steady decrease in mean torque across the ensemble and resulting low VAF in predicted torque.

6.5.1.2 Effect of displacement properties on reflexes

The imposed smooth-ramp experiment conducted during active conditions resulted in significantly more reflex contribution throughout the movement than the previous gait input. Intrinsic mechanisms still dominated the overall dynamics; however, reflex VAF was significant throughout the dorsiflexion stages of the cycle and reached a maximum value of 40.4%—a four-fold increase compared to the previous gait experiment. The smooth ramp input also resulted in a ten-fold increase in reflex gain, which clearly demonstrates the profound relationship between input properties and stretch reflexes. The MAV for the ramp and perturbation sequence was 0.3675 rad/s, whereas the MAV for the gait and perturbation sequence was 0.5283 rad/s. Stretch reflexes are a function of many interconnected properties, many of which are out of the hands of the experimenter. However, it is evident that displacement MAV is one property that can significantly alter the reflex response.

6.5.2 Mechanisms

6.5.2.1 Passive versus active conditions

The mean contribution from reflexes during the passive-gait experiment was substantially less than during the active-ramp experiment as seen by comparing Figure 37 and Figure 47. Reflexes are known to nonlinearly depend on the level of voluntary torque at which the stimulus is applied [34]. Increasing the level of muscle activation increases the fraction of motoneurons that are close enough to threshold to be activated by the stretch; such phenomenon is known as “automatic gain control”. Kirsch and Kearney found that stretch reflex gain covaried with fluctuations in background activation level during steady-state periods before and after an imposed stretch [57]. These findings agreed with results obtained during a time-varying experiment in which subjects changed contraction levels under isometric conditions [63] and with other studies conducted under quasi-static conditions [1]. Our results are consistent with these findings: reflexes strongly depend on the level of excitability of the motoneuron pool during large imposed movements.

6.5.2.2 Time-varying modulation

Intrinsic and reflex properties were modulated throughout the periodic cycle for both imposed gait and smooth ramp experiments. Intrinsic mechanisms were strongly correlated with the movement and compliance was noticeably reduced during periods of increased dorsiflexion; this was consistent for both types of movement. As the stiffness of the muscle and connective tissue increased, so did the viscosity (Figure 39 and Figure 50), but the inertial component remained relatively constant, as expected.

Clearly, reflexes were stronger during active conditions; however, both passive and active experiments exhibited time-varying modulation. The strongest reflex response was elicited near the dorsiflexion limit of both time-varying movements, albeit the absolute position of the maximum response was different. During the pause at OOP between ramps the contribution from reflexes was not constant, but rather declined during this period (Figure 46 and Figure 51). It is unclear whether reflexes would have rematerialized had the pause between ramp stretches been longer.

In a similar experiment conducted by Kirsch and Kearney, smooth ramps of similar characteristics to those used in this study, were applied discontinuously [57]. Time-varying IRFs relating input position to reflex EMG were computed using the ensemble technique and found to capture the general character of stretch reflex dynamics during steady state periods (before and after the ramp). They also found that the percent

VAF declined significantly during a silent period immediately following the ramp and attributed this to one of several sources: presynaptic inhibition, effects of preceding reflex activity, changes in fusimotor drive, or variability in the level of voluntary contraction. It is likely that the silent period evident in the present study, was a result of similar mechanisms.

6.5.3 Functional Implications

The role of reflexes during functional motor tasks remains an open topic of debate. Logically, the efficacy of reflexes would vary depending on the dynamic requirements coupled to a certain posture or movement. The nervous system would take advantage of the nonlinear properties of the joint and peripheral system to initiate actions, and then continually modify those properties according to ongoing requirements. For example, throughout the walking cycle, reflexes would be suppressed when counterproductive to the motion (i.e. swing), but enhanced during stages when they would assist in force production and stabilize limb trajectory (i.e. stance) [20, 40, 75]. Essentially, reflex modulation would prevent inappropriate torques from being generated during certain phases of locomotion [39, 42], or in response to stimuli such as unexpected perturbations [52].

Even during a passively imposed gait movement, elevated levels of reflex stiffness were seen throughout stance and at the peak transition from stance to swing (Figure 35 and Figure 37), when reflexes would be useful in propelling the body up and forward. Increased stretch reflex activity was also observed during the late swing phase of the movement, prior to heel-strike, when reflexes would contribute to the activation of ankle extensor muscles in the early stance phase. Ramp experiments, conducted while the subject maintained an active contraction, also displayed considerable phasic modulation of stretch reflex gain. Reflex gain adjusted differently during dorsi- and plantar flexion stretches, even exhibiting variable levels during a constant pause between ramps (Figure 46 and Figure 51).

In general, stretch reflex gain was substantially modulated, both in a tonic and phasic manner, during movement (Figure 51). The source of reflex modulation during movement remains unknown, but researchers have suggested numerous mechanisms related to the excitation level of motoneurons [63], presynaptic effects of descending systems [61, 76], or level of fusimotor drive on muscle spindles [44]. Another possibility is that reflex modulation results from a cyclic variation in voluntary drive locked to the ankle motion, though we have attempted to correct for this by providing subjects with a heavily low-pass filtered feedback signal during experiments requiring a voluntary contraction. More than likely, the stretch reflex is subject to multiple sources of modulation during movement including peripheral mechanisms, which we have attempted to verify here using large, imposed movements.

Finally, it is important to note a few important differences between imposed movement studies and normal locomotion: Firstly, the range of muscle activation is much larger during natural movement as the subject supports body weight and sustains the body's inertia; secondly, the subject was required to maintain a constant voluntary drive to the GS muscles in an attempt to isolate peripheral mechanisms—not the case for natural conditions; and finally, normal locomotion involves the simultaneous movement of many joints, whereas we have isolated motion to the ankle joint. Nonetheless, we feel that the results presented here contributed toward the knowledge of how peripheral mechanisms affect the functional role of the stretch reflex response during movement.

7 Conclusion

The time-varying, parallel-cascade (TVPC) algorithm was used to examine the functional role of joint stiffness and specifically, stretch reflexes during movement. The previous implementation of the algorithm was enhanced to identify intrinsic and reflex dynamics during realistic simulated conditions as well as with real experimental data. This thesis demonstrates that the TVPC method is capable of tracking rapid changes in intrinsic and reflex stiffness with no *a priori* information about the time-varying behaviour provided it is consistent. The algorithm, experimental results and significant findings are summarized in the following sections, along with the clinical relevance of this work. Finally, suggestions for future work are discussed.

7.1 SUMMARY

7.1.1 Time-Varying, Parallel-Cascade System Identification

A parallel-cascade model was used to separate joint dynamics into two pathways. The intrinsic pathway represented the mechanical properties of the joint, active muscle and visco-elastic tissue surrounding the joint. This was modelled by intrinsic stiffness, a TV linear dynamic element, relating position of the joint to torque. The reflex pathway represented muscle activation in response to the stretch reflex, modelled by a TV Hammerstein system. An iterative algorithm was used to identify intrinsic and reflex mechanisms using separate TV techniques based on ensemble methods. The ensemble matrix was composed of trials of position and torque data corresponding to the same time-varying behaviour. Input auto-correlation and input-output cross-correlation matrices were estimated at each sample time to produce an instantaneous estimate of joint dynamics.

Simulated systems were generated using parametric approximations for intrinsic and reflex dynamics. TV modulations were introduced by adjusting the reflex gain, intrinsic elasticity and viscosity parameters. Pseudo-random binary sequences (PRBS) were used as the input position ensemble and convolved with the simulated systems to generate an ensemble of output torque. TVPC identification was performed on the input-output data to produce estimates of intrinsic and reflex dynamics. Simulated and identified systems matched with near perfect agreement. Even in the presence of significant output noise, torque was predicted with excellent accuracy. This study verified the algorithm's ability to track TV properties with no *a priori* information of the TV behaviour during realistic simulated conditions.

Real experimental data was collected from three subjects while perturbing their ankle with a PRBS about a fixed operating position. The stationary data was analyzed in two ways: first using an established, time-invariant (TI) algorithm and second using the time-varying (TV) algorithm, treating the data as an ensemble of responses to a time-varying condition. Average TV estimates of torque variance converged to the TI results for ensemble sizes greater than 600 realizations. This study verified the quality of system identification with real data, by providing a benchmark for the experimental results.

7.1.2 Joint Dynamics during Movement

Time-varying analysis of joint dynamics was assessed during two types of imposed movements. The first movement, a time-varying gait trajectory similar to 1.5 km/hr walking speed, was applied to the subject's ankle during relaxed conditions. Intrinsic and reflex mechanisms were well predicted, where intrinsic mechanisms clearly dominated for this type of movement. Reflex activity was phase modulated throughout the time-varying motion, contributing anywhere from zero to ten percent of the total variance accounted for (VAF). Reflexes increased throughout the replicated stance phase, with maximum contribution to torque occurring at the transition from stance to swing, when reflexes would be useful in propelling the body up and forward. The low, average reflex activity may be explained by the passive experimental conditions and/or the large mean absolute velocity (MAV) for this type of movement. Theories of automatic gain control and presynaptic inhibition were suggested as likely mechanisms behind reflex suppression. Stationary data, collected at matched operating conditions, was compared with the time-varying results and indicated that the imposed movement had the effect of decreasing the overall contribution from reflexes to total torque. In other words, the movement acted to suppress the tonic level of reflex activity.

The second movement was a cyclic smooth-ramp trajectory in which the subject's ankle underwent a rapid dorsiflexion stretch, followed by a pause, then a plantar flexion stretch, followed by a pause. This experiment was formulated to enhance reflex activity in two ways: (1) the MAV for this input was significantly smaller than the previous input, and (2) the experiment was conducted while the subject maintained an active contraction of the triceps surae. Intrinsic mechanisms still dominated the overall dynamics; however, reflexes contributed significantly more to total torque for this movement, with a four-fold increase in reflex VAF and ten-fold increase in peak reflex gain. Reflex gain underwent considerable phasic modulation, adjusting differently to dorsi- and plantar flexion stretches. Variable levels of reflex gain were also observed during the pause at the optimal operating position between ramps. Overall VAF between predicted and observed torque was low for this study. Subject fatigue was identified as a likely cause, which created variability in the output ensemble not accounted for by the TVPC method.

Although the functional role of reflexes during movement is not certain, based on the experiments conducted in this thesis, we can conclude that reflexes adapt to the different phases of a movement and modulation originates in part from peripheral mechanisms.

7.1.3 Clinical Relevance

The findings from this thesis are intended to contribute toward the global understanding of stretch reflexes and their functional significance during movement. In addition to fundamental research in motor control, the techniques presented here may be used to examine impaired movement. Patients suffering from stroke, spinal cord or brain injury often exhibit increased muscle tone or joint stiffness, commonly referred to as spasticity. An imbalance in muscle tone can impair motor control, requiring therapeutic intervention. Current methods of rehabilitation rely on qualitative measures to assess disease progression or improvement, such as the tendon tap or Ashworth scale [65]. Recently, intrinsic stiffness index (ISI), total stiffness index (TSI) and stretch reflex threshold speed (SRTS) have been shown as reliable indices for the quantitative assessment of muscle tone [77]. Tools such as the TVPC algorithm may be used as an advanced measure of movement control and stiffness irregularities. Furthermore, this research may be used to optimize the current design of medical devices such as limb prostheses.

7.2 FUTURE WORK

The time-varying gait and ramp experiments presented in this thesis were conducted on one subject. Several more healthy persons should be tested with both experimental paradigms. The results may then be used to inspect the subject-to-subject variability in the time-varying estimates of reflex and intrinsic dynamics.

Subject fatigue was identified as a significant source of error during the imposed ramp experiment. The subject was unable to maintain a constant level of voluntary activation, which resulted in a gradual decline in the mean torque generated at the ankle. This variability in the output ensemble was not accounted for by the TVPC algorithm. The current trial selection process identifies significant outliers based on the standard deviation of torque; however, a more stringent selection protocol should be implemented to account for the presence of fatigue and variable levels of mean EMG.

The ensemble methods used by the TVPC algorithm for system identification require upward of 600 trials reflecting consistent time-varying behaviour. Depending on the duration of the time-varying input and rest period permitted between trials, subject fatigue is a potential side-effect of a lengthy acquisition process. A method for monitoring the ongoing state of the subject by means of torque or EMG could offer insight into fatigue rates and consequently the preferred duty cycle for such experiments.

The present findings suggest that as the contribution from reflexes increased during a movement, the overall VAF between predicted and observed torque decreased. This indicates that as reflexes played a more significant role in the overall joint dynamics, the algorithm performed more weakly. Increased system noise, as a result of reflex activation, likely made system identification more difficult. One possibility is that reflex dynamics during movement are more complex than our current model is capable of predicting. For example, additional terms may need to be incorporated in the model to account for the non-linear behaviour of reflexes correlated with a movement. Currently, the torque produced by each pathway is assumed to add linearly to the total torque generated at the ankle; this also may be erroneous for certain types of movement conditions.

The TVPC algorithm produced nonparametric descriptions of joint dynamics in the form of impulse response functions. Physically meaningful parameters representing intrinsic and reflex mechanics were then retrieved from the IRFs by fitting second-order, low-pass systems to intrinsic compliance and reflex stiffness. Reflex gain, damping and frequency along with inertial, viscous and elastic properties of the joint were estimated; however, the confidence interval for these parameters was not provided. In future, the standard deviation should be supplied as bounds on the parametric estimates; this may be done by simply computing the covariance matrix produced by the Levenberg-Marquardt fit. Furthermore, many of the parametric fits for reflex stiffness were unsuccessful with variance accounting for less than 50% despite the apparent increase in reflex torque. Alternative forms of parameterization, such as third-order systems, should be explored as well as the possibility of deriving the parametric estimate directly from the data rather than using the intermediate IRF.

Finally, to more accurately match natural locomotion it would be ideal to conduct a preliminary experiment in which EMG or torque are measured while the subject performs a voluntary movement. This information may then be used as feedback in an imposed movement experiment, where the subject would track the same level of voluntary activity, while undergoing a position trace identical to the voluntary movement.

References

[1] M. M. Mirbagheri, H. Barbeau, and R. E. Kearney, "Intrinsic and reflex contributions to human ankle stiffness: variation with activation level and position," *Exp Brain Res,* vol. 135, pp. 423-36, Dec 2000.

[2] R. E. Kearney, R. B. Stein, and L. Parameswaran, "Identification of intrinsic and reflex contributions to human ankle stiffness dynamics," *IEEE Trans Biomed Eng,* vol. 44, pp. 493-504, Jun 1997.

[3] L. Galiana, J. Fung, and R. Kearney, "Identification of intrinsic and reflex ankle stiffness components in stroke patients," *Exp Brain Res,* vol. 165, pp. 422-34, Sep 2005.

[4] M. M. Mirbagheri, H. Barbeau, M. Ladouceur, and R. E. Kearney, "Intrinsic and reflex stiffness in normal and spastic, spinal cord injured subjects," *Exp Brain Res,* vol. 141, pp. 446-59, Dec 2001.

[5] J. B. MacNeil, R. E. Kearney, and I. W. Hunter, "Identification of time-varying biological systems from ensemble data," *IEEE Trans Biomed Eng,* vol. 39, pp. 1213-25, Dec 1992.

[6] M. Lortie and R. E. Kearney, "Identification of physiological systems: estimation of linear time-varying dynamics with non-white inputs and noisy outputs," *Med Biol Eng Comput,* vol. 39, pp. 381-90, May 2001.

[7] M. Lortie and R. E. Kearney, "Identification of time-varying Hammerstein systems from ensemble data," *Ann Biomed Eng,* vol. 29, pp. 619-35, 2001.

[8] M. Baker, "Identification of Time-Varying Ankle Stiffness," Master's Thesis, McGill University, Department of Biomedical Engineering, 2005.

[9] H. Gray, "Anatomy of the Human Body." vol. 2006, Bartleby, Ed. New York: BARTLEBY.COM, 2000.

[10] S. Rao, C. Saltzman, and H. J. Yack, "Ankle ROM and stiffness measured at rest and during gait in individuals with and without diabetic sensory neuropathy," *Gait & Posture,* vol. 24, pp. 295-301, 2006.

[11] E. P. Widmaier, H. Raff, and K. T. Strang, *Vander, Sherman, & Luciano's Human Physiology the Mechanisms of Body Function*, 9th ed. Boston: McGraw Hill, 2004.

[12] E. R. Kandel, J. H. Schwartz, and T. M. Jessel, *Principles of Neural Science*, 3rd ed. New York: Elsevier, 1991.

[13] http://www.infovisual.info, "Neuron," in *Volume 3: Human body*, 2005. Reproduction rights are reserved and strictly limited.

[14] R. B. Stein, *Nerve and Muscle: Membranes, Cells and Systems* New York: Plenum Press, 1980.

[15] R. E. Kearney and I. W. Hunter, "System identification of human triceps surae stretch reflex dynamics," *Exp Brain Res,* vol. 51, pp. 117-27, 1983.

[16] J. V. Basmajian and C. J. De Luca, *Muscles Alive*, 5th ed. Baltimore: Williams & Wilkins, 1985.

[17] W. F. Genadry, R. E. Kearney, and I. W. Hunter, "Dynamic relationship between EMG and torque at the human ankle: variation with contraction level and modulation," *Med Biol Eng Comput,* vol. 26, pp. 489-96, Sep 1988.

[18] I. W. Hunter and R. E. Kearney, "Dynamics of human ankle stiffness: variation with mean ankle torque," *J Biomech,* vol. 15, pp. 747-52, 1982.

[19] R. R. Carter, P. E. Crago, and M. W. Keith, "Stiffness regulation by reflex action in the normal human hand," *J Neurophysiol,* vol. 64, pp. 105-18, Jul 1990.

[20] E. P. Zehr and R. B. Stein, "What functions do reflexes serve during human locomotion?," *Prog Neurobiol,* vol. 58, pp. 185-205, Jun 1999.

[21] S. H. Duenas and P. Rudomin, "Excitability changes of ankle extensor group Ia and Ib fibers during fictive locomotion in the cat," *Exp Brain Res,* vol. 70, pp. 15-25, 1988.

[22] J. P. Gossard, J. M. Cabelguen, and S. Rossignol, "An intracellular study of muscle primary afferents during fictive locomotion in the cat," *J Neurophysiol,* vol. 65, pp. 914-26, Apr 1991.

[23] E. Bizzi, F. A. Mussa-Ivaldi, and S. Giszter, "Computations underlying the execution of movement: a biological perspective," *Science,* vol. 253, pp. 287-91, Jul 19 1991.

[24] S. V. Adamovich, M. F. Levin, and A. G. Feldman, "Central modifications of reflex parameters may underlie the fastest arm movements," *J Neurophysiol,* vol. 77, pp. 1460-9, Mar 1997.

[25] P. L. Weiss, R. E. Kearney, and I. W. Hunter, "Position dependence of ankle joint dynamics--II. Active mechanics," *J Biomech,* vol. 19, pp. 737-51, 1986.

[26] R. E. Kearney and I. W. Hunter, "Dynamics of human ankle stiffness: variation with displacement amplitude," *J Biomech,* vol. 15, pp. 753-6, 1982.

[27] T. R. Nichols and J. C. Houk, "Improvement in linearity and regulation of stiffness that results from actions of stretch reflex," *J Neurophysiol,* vol. 39, pp. 119-42, Jan 1976.

[28] J. A. Hoffer and S. Andreassen, "Regulation of soleus muscle stiffness in premammillary cats: intrinsic and reflex components," *J Neurophysiol,* vol. 45, pp. 267-85, Feb 1981.

[29] R. Herman, W. Freedman, and N. Mayer, "Neurophysiological mechanisms of hemiplegic and paraplegic spasticity: implications for therapy," *Arch Phys Med Rehabil,* vol. 55, pp. 338-343, 1974.

[30] J. Noth, H. R. Matthews, and H. H. Friedemann, "Long latency reflex force of human finger muscles in response to imposed sinusoidal movements," *Exp Brain Res,* vol. 55, pp. 317-324, 1984.

[31] T. Sinkjaer, E. Toft, S. Andreassen, and B. C. Hornemann, "Muscle stiffness in human ankle dorsiflexors: intrinsic and reflex components," *J Neurophysiol,* vol. 60, pp. 1110-1121, 1988.

[32] P. E. Crago, J. C. Houk, and Z. Hasan, "Regulatory actions of human stretch reflex," *J Neurophysiol,* vol. 39, pp. 925-35, Sep 1976.

[33] R. E. Kearney and I. W. Hunter, "Nonlinear identification of stretch reflex dynamics," *Ann Biomed Eng,* vol. 16, pp. 79-94, 1988.

[34] R. B. Stein and R. E. Kearney, "Nonlinear behavior of muscle reflexes at the human ankle joint," *J Neurophysiol,* vol. 73, pp. 65-72, Jan 1995.

[35] M. Meinders, R. Price, J. F. Lehmann, and K. A. Questad, "The stretch reflex response in the normal and spastic ankle: effect of ankle position," *Arch Phys Med Rehabil,* vol. 77, pp. 487-92, May 1996.

[36] P. L. Weiss, R. E. Kearney, and I. W. Hunter, "Position dependence of stretch reflex dynamics at the human ankle," *Exp Brain Res,* vol. 63, pp. 49-59, 1986.

[37] L. Q. Zhang and W. Z. Rymer, "Simultaneous and nonlinear identification of mechanical and reflex properties of human elbow joint muscles," *IEEE Trans Biomed Eng,* vol. 44, pp. 1192-209, Dec 1997.

[38] T. Kimura, D. Nozaki, K. Nakazawa, M. Akai, and T. Ohtsuki, "Gradual increment/decrement of isometric force modulates soleus stretch reflex response in humans," *Neurosci Lett,* vol. 347, pp. 25-8, Aug 14 2003.

[39] C. Capaday and R. B. Stein, "Difference in the amplitude of the human soleus H reflex during walking and running," *J Physiol,* vol. 392, pp. 513-22, Nov 1987.

[40] J. F. Yang, R. B. Stein, and K. B. James, "Contribution of peripheral afferents to the activation of the soleus muscle during walking in humans," *Exp Brain Res,* vol. 87, pp. 679-687, 1991.

[41] J. B. Andersen and T. Sinkjaer, "Stretch reflex and H-reflex during human walking," in *Annual International Conference of the IEEE Engineering in Medicine and Biology Society*, Amsterdam, 1996, pp. 589-590.

[42] C. Capaday and R. B. Stein, "Amplitude modulation of the soleus H-reflex in the human during walking and standing," *J Neurosci,* vol. 6, pp. 1308-13, May 1986.

[43] J. D. Brooke, D. F. Collins, S. Boucher, and W. E. McIlroy, "Modulation of human short latency reflexes between standing and walking," *Brain Res,* vol. 548, pp. 172-8, May 10 1991.

[44] M. Llewellyn, J. F. Yang, and A. Prochazka, "Human H-reflexes are smaller in difficult beam walking than in normal treadmill walking," *Exp Brain Res,* vol. 83, pp. 22-8, 1990.

[45] M. J. Grey, C. W. Pierce, T. E. Milner, and T. Sinkjaer, "Soleus stretch reflex during cycling," *Motor Control,* vol. 5, pp. 36-49, Jan 2001.

[46] J. D. Brooke, W. E. McIlroy, and D. F. Collins, "Movement features and H-reflex modulation. I. Pedalling versus matched controls," *Brain Res,* vol. 582, pp. 78-84, Jun 5 1992.

[47] W. E. McIlroy, D. F. Collins, and J. D. Brooke, "Movement features and H-reflex modulation. II. Passive rotation, movement velocity and single leg movement," *Brain Res,* vol. 582, pp. 85-93, Jun 5 1992.

[48] J. D. Brooke, W. E. McIlroy, D. F. Collins, and J. E. Misiaszek, "Mechanisms within the human spinal cord suppress fast reflexes to control the movement of the legs," *Brain Res,* vol. 679, pp. 255-60, May 15 1995.

[49] J. D. Brooke, J. Cheng, D. F. Collins, W. E. McIlroy, J. E. Misiaszek, and W. R. Staines, "Sensori-sensory afferent conditioning with leg movement: gain control in spinal reflex and ascending paths," *Prog Neurobiol,* vol. 51, pp. 393-421, Mar 1997.

[50] J. D. Brooke and E. P. Zehr, "Limits to fast-conducting somatosensory feedback in movement control," *Exercise & Sport Sciences Reviews,* vol. 34, pp. 22-8, Jan 2006.

[51] J. B. Andersen and T. Sinkjaer, "Afferent input from the human ankle extensors during walking," in *20th Annual International Conference of the IEEE Engineering in Medicine and Biology Society*, Hong Kong, 1998, pp. 2332-2335.

[52] R. E. Kearney, M. Lortie, and R. B. Stein, "Modulation of stretch reflexes during imposed walking movements of the human ankle," *J Neurophysiol,* vol. 81, pp. 2893-902, Jun 1999.

[53] F. Lacquaniti, F. Licata, and J. F. Soechting, "The mechanical behavior of the human forearm in response to transient perturbations," *Biol Cybern,* vol. 44, pp. 35-46, 1982.

[54] D. J. Bennett, J. M. Hollerbach, Y. Xu, and I. W. Hunter, "Time-varying stiffness of human elbow joint during cyclic voluntary movement," *Exp Brain Res,* vol. 88, pp. 433-42, 1992.

[55] Y. Xu and J. M. Hollerbach, "A robust ensemble data method for identification of human joint mechanical properties during movement," *IEEE Trans Biomed Eng,* vol. 46, pp. 409-19, Apr 1999.

[56] F. Lacquaniti, N. A. Borghese, and M. Carrozzo, "Transient reversal of the stretch reflex in human arm muscles," *J Neurophysiol,* vol. 66, pp. 939-54, Sep 1991.

[57] R. F. Kirsch and R. E. Kearney, "Identification of time-varying dynamics of the human triceps surae stretch reflex. II. Rapid imposed movement," *Exp Brain Res,* vol. 97, pp. 128-38, 1993.

[58] R. F. Kirsch and R. E. Kearney, "Identification of time-varying stiffness dynamics of the human ankle joint during an imposed movement," *Exp Brain Res,* vol. 114, pp. 71-85, Mar 1997.

[59] R. E. Kearney and I. W. Hunter, "System identification of human joint dynamics," *Crit Rev Biomed Eng,* vol. 18, pp. 55-87, 1990.

[60] R. E. Kearney and I. W. Hunter, "System identification of human stretch reflex dynamics: tibialis anterior," *Exp Brain Res,* vol. 56, pp. 40-9, 1984.

[61] J. F. Soechting, J. R. Dufresne, and F. Lacquaniti, "Time-varying properties of myotatic response in man during some simple motor tasks," *J Neurophysiol,* vol. 46, pp. 1226-43, Dec 1981.

[62] F. Lacquaniti, N. A. Borghese, and M. Carrozzo, "Internal models of limb geometry in the control of hand compliance," *J Neurosci,* vol. 12, pp. 1750-62, May 1992.

[63] R. F. Kirsch, R. E. Kearney, and J. B. MacNeil, "Identification of time-varying dynamics of the human triceps surae stretch reflex. I. Rapid isometric contraction," *Exp Brain Res,* vol. 97, pp. 115-27, 1993.

[64] I. W. Hunter and M. J. Korenberg, "The identification of nonlinear biological systems: Wiener and Hammerstein cascade models," *Biol Cybern,* vol. 55, pp. 135-44, 1986.

[65] J. B. Andersen, B. Larsen, and T. Sinkjaer, "Modulation of the human soleus stretch reflex during gait," in *16th Annual International Conference of the IEEE Engineering in Medicine and Biology Society*, Denmark, 1994, pp. 432-433.

[66] J. F. Lehmann, R. Price, B. J. deLateur, S. Hinderer, and C. Traynor, "Spasticity: quantitative measurements as a basis for assessing effectiveness of therapeutic intervention," *Arch Phys Med Rehabil,* vol. 70, pp. 6-15, Jan 1989.

[67] M. M. Mirbagheri, M. Ladouceur, R. E. Kearney, and H. Barbeau, "The effects of long term FES-assisted walking on intrinsic and reflex dynamic stiffness in spinal cord injured patients," in *19th Annual International Conference of the IEEE Engineering in Medicine and Biology Society*, Chicago, 1997, pp. 1768-1769.

[68] N. Hogan, "Stable execution of contact tasks using impedance control," 1987, pp. 1047-1054.

[69] R. E. Isman and V. T. Inman, "Anthropometric studies of the human foot and ankle," *Bulletin of Prosthetics Research,* pp. 97-129, Spring, 1969 1969.

[70] http://www.bmed.mcgill.ca/REKLAB/manual/, "REKLAB on-line Manual," Accessed: June 30, 2006.

[71] J. Tung, "Task-Dependent Modulation of Stretch Reflex Stiffness in the Ankle," Master's Thesis, McGill University, Department of Biomedical Engineering, 2002.

[72] T. Sinkjaer, J. B. Andersen, and B. Larsen, "Soleus stretch reflex modulation during gait in humans," *J Neurophysiol,* vol. 76, pp. 1112-20, Aug 1996.

[73] P. B. S. Matthews and R. B. Stein, "The sensitivity of muscle spindle afferents to small sinusoidal changes in length.," *J. Physiol.,* vol. 200, pp. 723-743, 1969.

[74] B. Bigland-Ritchie and J. J. Woods, "Changes in muscle contractile properties and neural control during human muscular fatigue," *Muscle Nerve,* vol. 7, pp. 513-525, 1984.

[75] R. B. Stein and C. Capaday, "The modulation of human reflexes during functional motor tasks," *Trends Neurosci,* vol. 11, pp. 328-332, 1988.

[76] J. R. Dufresne, J. F. Soechting, and C. A. Terzuolo, "Modulation of the myotatic reflex gain in man during intentional movements," *Brain Res,* vol. 193, pp. 67-84, Jul 7 1980.

[77] F. Pisano, G. Miscio, R. Colombo, and P. Pinelli, "Quantitative evaluation of normal muscle tone," *J Neurol Sci,* vol. 135, pp. 168-72, Feb 1996.

Appendix A. Ethics Certificate

Please find attached our Ethics Certificate, approved by the McGill University Research Ethics Board. Certificate is dated May 8, 2006 and valid until May 7, 2007.

Appendix B. Servo Controller

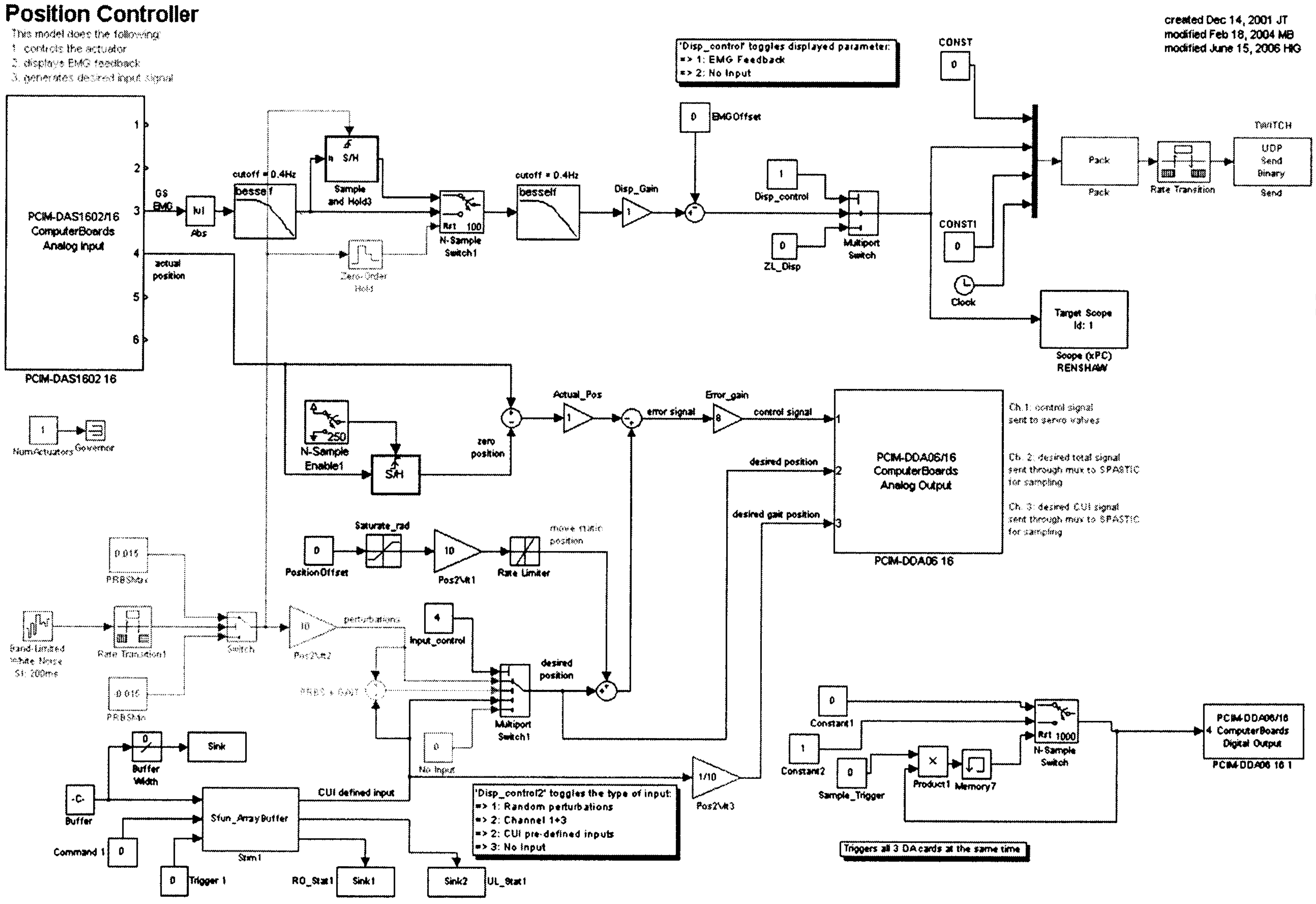

Position Controller

This model does the following:
1. controls the actuator
2. displays EMG feedback
3. generates desired input signal

created Dec 14, 2001 JT
modified Feb 18, 2004 MB
modified June 15, 2006 HIG

'Disp_control' toggles displayed parameter:
=> 1: EMG Feedback
=> 2: No Input

'Disp_control2' toggles the type of input:
=> 1: Random perturbations
=> 2: Channel 1+3
=> 2: CUI pre-defined inputs
=> 3: No Input

Ch. 1: control signal sent to servo valves

Ch. 2: desired total signal sent through mux to SPASTIC for sampling

Ch. 3: desired CUI signal sent through mux to SPASTIC for sampling

Triggers all 3 DA cards at the same time